이학박사 학위논문

Decadal changes in transports and characteristics of the deep waters in the Ulleung Interplain Gap, East Sea

동해 울릉해저간극
심층 해수 특성과 수송량의 십년 규모 변화

2023년 8월

서울대학교 대학원

지구환경과학부

이호준

Decadal changes in transports and characteristics of the deep waters in the Ulleung Interplain Gap, East Sea

지도 교수 남 성 현

이 논문을 이학박사 학위논문으로 제출함

2023년 5월

서울대학교 대학원

지구환경과학부

이 호 준

이호준의 이학박사 학위논문을 인준함

2023년 7월

위 원 장 조 양 기 (인)

부위원장 남 성 현 (인)

위 원 나 한 나 (인)

위 원 윤 승 태 (인)

위 원 박 재 형 (인)

Abstract

Decadal changes in transports and characteristics of the deep waters in the Ulleung Interplain Gap, East Sea

Hojun Lee
School of Earth and Environmental Sciences
The Graduate School
Seoul National University

Long-term changes in the physical characteristics of the deep waters and the volume transports of the deep waters through the Ulleung Interplain Gap (UIG), which is a unique passageway for exchanges in deep waters (>1500 m) between the Japan Basin to Ulleung Basin, are crucial for understanding long-term changes in the East Sea meridional overturning circulation. In particular, the western part of the UIG is very suitable for examining the change in the deep water transports from the Japan Basin to the Ulleung Basin considering the path of the deep and abyssal circulation due to the bottom topographic effect. The boundary depth and physical characteristics of the deep water masses in the Ulleung Interplain Gap (UIG), the Ulleung Basin, and the Japan Basin, as well as the meridional volume transports of the deep waters from 1500 m to 2300 m, were all examined in this study.

The data used in this study are surface moored current meter data collected at the UIG from 1997 to 2019 and hydrographic data collected from the Japan Basin, Ulleung Basin, and the UIG from 1993 to 2019. The volume transports of the deep

waters from 1500 m to 2300 m through the western UIG from 1997 to 2019 were obtained by correlating the along-channel current component at 1800 m at EC1 from 1997 to 2019 with the volume transports of the deep waters from 1500 m to 2300 m through the western UIG from November 2002 to April 2004 obtained from five subsurface moored current meter data.

The equatorward volume transports of the deep waters from 1500 m to 2300 m through the western UIG continued to increase from the late 1990s to the 2010s. In addition, it was revealed that the deep water transported from 1500 m to 2300 m through the western UIG was composed of the Deep Water until 2000s, but the portion of the Central Water was increasing in the 2010s based on the changes in deep salinity minimum (boundary between CW and DW) and upper boundary homogeneous layer (boundary between DW and BW). Considering that the portion of the CW increases not only in UIG but also in the Japan Basin, it is believed to related to the increase in CW formation and the increase in equatorward volume transports of the deep waters from 1500 m to 2300 m through the western UIG. However, it is necessary to compare the relationship with the volume transports of the deep waters from 1500 m to 2300 m through the western UIG through additional studies such as quantitative CW formation estimation.

Deep water warming has recently intensified, as evidenced by the potential temperature of the deep waters in the Japan Basin, Ulleung Basin, and the UIG being twice as high from the 2000s to the 2010s as it was from the 1990s to the 2000s. On the other hand, it was established that the potential density of the deep waters increased in the 2000s due to the salinity effect and reduced once more in the 2010s, as well as that the salinity of the deep water increased from the 1990s to the 2000s and decreased again.

Not only from the Japan Basin to the Ulleung Basin, but also from the Ulleung Basin to the Yamato Basin and from the Yamato Basin to the Japan Basin, the deep and abyssal circulation can be strengthened from 1500 m to 2300 m form the 1990s to the 2010s, which suggests that the amount of the Deep Water in the depth range may have decreased and the amount of the Central Water may have increased. The fact that CW formation is strengthening independently of BW development further indicates that the future East Sea meridional overturning circulation may evolve into a double circulation or a more complicated circulation than a single circulation.

Keyword: East Sea, deep waters, deep transports, abyssal circulation, meridional overturning circulation, decadal changes

Student Number: 2018-30103

Table of Contents

List of Figures

List of Tables

1. Introduction

1.1. Background

The East Sea (Japan Sea) has been regarded as a “miniature ocean” because it has self-contained thermohaline convection and meridional overturning circulation (MOC) system similar to the ocean (Kim et al., 2004; Talley et al., 2006). The East Sea, surrounded by Korea, Japan, and Russia, is a deep marginal sea with maximum and mean depths of 4036 and 1667 m, respectively, which has three basins deeper than 2000 m: the Japan Basin (JB) in the northern half with a water depth of nearly 4000 m, the Ulleung Basin (UB) in the southwest with a water depth of 2000 m, and the Yamato Basin (YB) in the southeast with a water depth of 2000 m (Tsunogai et al., 2003; Chang et al., 2004; Kim et al., 2004) (Figure 1.1). Since the East Sea is connected to the North Pacific Ocean through relatively narrow and shallow (<150 m in bottom depth) four straits such as the Korea/Tsushima Strait, Tsugaru Strait, Soya Strait, and Tatarsky Strait, the East Sea is a semi-enclosed sea with minimal seawater exchange with the ocean (Yanagimoto and Taira, 2003; Min and Warner, 2005; Gamo et al., 2014). Therefore, deep waters form and circulate on the inside rather than inflowing or outflowing from the outside. Since the turnover time of the East Sea MOC is much shorter than that of the ocean due to the relatively small size of the East Sea, the East Sea is filled with deep waters with lower temperatures and higher dissolved oxygen concentration compared to the deep waters in the ocean.

Deep waters below 400 m, which had been considered a single water mass called Japan Sea Proper Water until the 1990s, were found to consist of three different water masses: Central Water (CW), Deep Water (DW), and Bottom Water (BW) in the 1990s, depending on vertical structures with physical characteristics

resembling those of the ocean (Uda, 1934; Kim et al., 1996; Kim and Kim, 1996). As found in the ocean, the deep salinity minimum (DSM) layer is found at a depth of ca. 1500 m, the deep oxygen minimum layer is found at a depth of ca. 2000 m, and the benthic homogeneous layer is found at a depth of ca. 2500 m (Kim et al., 2004; Talley et al., 2006; Yoon et al., 2018) (Figure 1.2). Accordingly, CW was defined as seawater with a potential temperature of 0.12-0.60 ℃ and a salinity higher than 34.067 psu at a depth of 400-1500 m, and DW was defined as seawater with a potential temperature lower than 0.12 ℃ and salinity of 34.067-34.070 psu at a depth of 1500-2500 m. BW was defined as seawater with a potential temperature lower than 0.073 ℃ and a salinity of about 34.070 psu below 2500 m (Kim et al., 2004).

Deep waters (CW, DW, and BW) in the East Sea are known to be formed by two different deep convection processes: an open-ocean deep convection and a slope deep convection. Open-ocean deep convection is known to occur south of Vladivostok to depths of more than 700 m due to strong surface cooling (Talley et al., 2003; Kim et al., 2022). Therefore, low temperature, high dissolved oxygen, and high salinity surface water can be supplied to the CW, reducing the temperature and increasing the salinity and dissolved oxygen of the CW (Talley et al., 2003). On the other hand, deep slope convection is known to occur along the continental shelf on the northern coast off Peter the Great Bay to depths of more than 2000 m due to surface cooling, sea-ice formation, and brine rejection (Talley et al., 2003, 2006; Yoon et al., 2018; Lee and Nam, 2023). Through the slope deep convection process, low temperature, high dissolved oxygen, and high salinity surface water can be supplied to the DW and BW, reducing the temperature and increasing the salinity and dissolved oxygen of the DW and BW (Talley et al., 2003). The supply of low temperature and high salinity surface waters into the deep layers was constrained

from the 1950s to the 1990s as deep slope convection weakened and open-ocean deep convection prevailed, leading to a steep rise in the boundary depth between CW and DW, and DW and BW (Yoon et al., 2018). However, the trend of increasing boundary depths has slowed from the 2000s to 2015 and the tendency of reducing the dissolved oxygen concentration in BW has slowed by about twice since the deep slope convection began again in the winter of 2000/2001 (Yoon et al., 2018).

Deep waters formed by deep convection in the northern East Sea circulate horizontally counterclockwise along the periphery of the three deep basins from the JB to UB (and YB), from the UB to YB, and from the YB to JB (Senjyu et al., 2005; Choi and Yoon, 2010) (Figure 1.1). In the northern hemisphere, it is believed that deep mean current flows cyclonically in the direction of shallower water on the right due to topographic control, essentially following ambient potential vorticity contours (fH^{-1}), where f is the Coriolis parameter, and H is the depth (Choi and Yoon, 2010; Shin et al., 2020). Deep waters formed in the JB flow into the UB through the western Ulleung Interplain Gap (UIG), which is a unique passageway for exchanges in deep waters (>1500 m) between the JB to UB (Talley et al., 2003; Clayson and Luneva, 2004; Senjyu et al., 2005; Teague et al., 2005). Deep waters circulate counterclockwise in the UB and flow out of the UB through the eastern UIG, with the same volume transport of deep waters passing narrower and more robust in the eastern UIG than in the western UIG (Chang et al., 2002). Accordingly, the solid and narrow northward outflow in the eastern UIG was named Dokdo Abyssal Current (DAC) (Chang et al., 2009; Shin et al., 2020). Deep waters from UB circulate clockwise with the Yamato Rise to the right, and flow into the YB (Senjyu et al., 2005). In YB, deep waters circulate counterclockwise, move northward along the continental slope of the eastern part of the YB, and flow into the JB (Senjyu et al.,

2005).

It was proposed that zonally and vertically integrated horizontal deep flows of the East Sea have two MOC structures based on Hybrid Coordinate Ocean Model (HYCOM) reanalysis data: single full-depth overturning circulation and two counterrotating overturning circulations (Han et al., 2020, 2021) (Figure 1.3). Full-depth overturning circulation has a single-cell structure in which deep water sinks more than 2000 m in the northern East Sea by the slope deep convection, upwells in the southern East Sea, and moves north at the upper layer. On the other hand, two counterrotating overturning circulation cell has a two-cell structure in which deep water sinks to a depth of ca. 1000 m in the northern East Sea, moves south, upwells, and downwells in the southern East Sea, and moves north at the upper and lower layers completing upper and lower circulations, respectively. It was suggested that the variation of the East Sea MOC was two-cell structures in the late 1990s and early 2010s, while it was a single-cell structure in the 2000s (Han et al., 2020). In addition, the turnover time of the East Sea MOC was estimated to be about 60 years, which is much smaller than previous estimations of about 100 years (Han et al., 2021). Thus, it is crucial to understand the changes in the path and strength of the East Sea MOC for a better understanding of the exchanges of dissolved oxygen, heat, salt, and materials from the surface to the deep waters and between the deep basins (Kang et al., 2003; Yoon et al., 2018; Han et al., 2020, 2021).

However, based on current observation data, research has yet to be conducted on the long-term transport of deep waters concerning the abyssal circulation and the East Sea MOC. Understanding the changes in abyssal circulation and East Sea MOC, in particular, depends on changing the volume transport in the deep water exchange passage between deep basins. From this point of view, the UIG

is a suitable place to examine the fluctuations in volume transport of deep waters between the JB and the UB. Since deep waters flowing from the JB to the UB mainly pass through the western UIG, it is essential to understand the East Sea MOC to investigate long-term changes in the volume transport of deep waters at western UIG. Nevertheless, this topic has yet to be researched due to the scant availability of long-term deep current observation data at the UIG.

1.2. Purpose of study

The objectives of this study are to address long-term (multi-decade-long) variations of

1) volume transports of the deep waters through the western UIG,

2) the volume of deep water masses in the East Sea,

3) physical characteristics of the deep waters in the East Sea,

and finally to analyze how changes in volume transports of the deep waters through the western UIG and changes in the volume of deep water masses are related to changes in the deep and abyssal circulation of the East Sea.

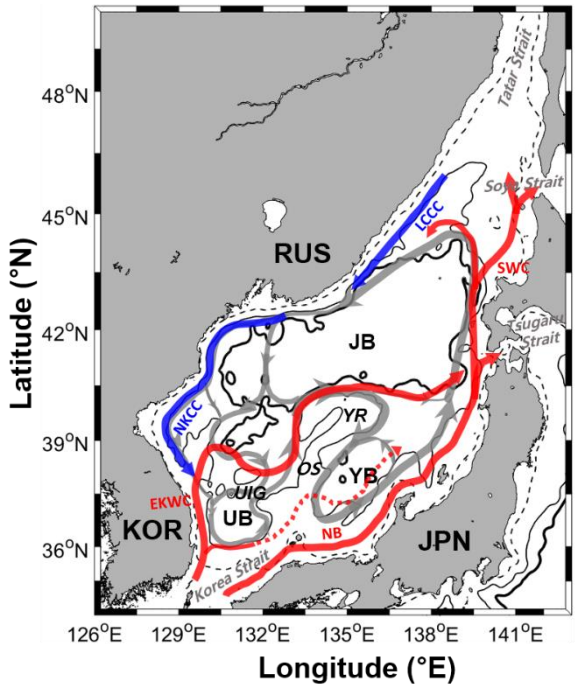

Figure 1.1. Schematic of upper ocean circulation (red and blue arrows), deep and abyssal circulation (gray arrows) in the East Sea. Most widely recognized currents and geographical features are highlighted. Isobaths are indicated by thick solid (3000 m), thin solid (1500 m), and thin broken (150 m) lines. KOR, RUS, and JPN indicate Korea, Russia, and Japan, respectively. JB, UB, YB, UIG, YR, and OS indicate the Japan Basin, Ulleung Basin, Yamato Basin, Ulleung Interplain Gap, Yamato Rise, and Oki Spur, respectively. Surface warm and cold currents are marked by red and blue arrows, respectively: LCCC, NKCC, EKWC, NB, and SWC indicate Liman Coastal Cool Current, North Korea Cold Current, East Korea Warm Current, Nearshore Branch, and Soya Warm Current, respectively. Modified from original figures in Senjyu et al. (2005). Figure from Lee and Nam (2023).

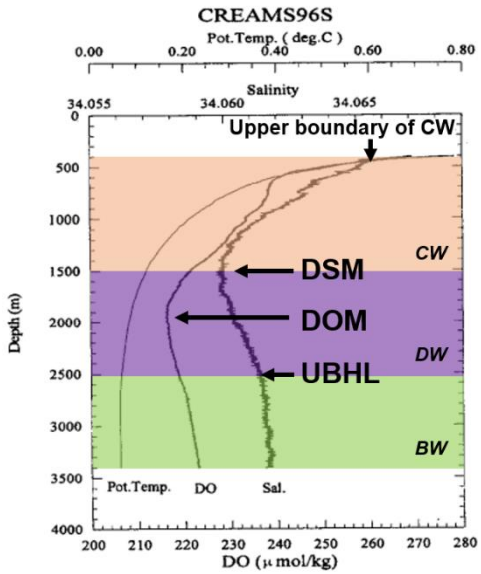

Figure 1.2. Vertical profiles of potential temperature, practical salinity, and dissolved oxygen concentration at a station in the western Japan Basin during the summer of 1996. DSM, DOM, UBHL denote the deep salinity minimum, dissolved oxygen minimum, and upper boundary homogeneous layer, respectively. CW, DW, and BW represent the Central Water, Deep Water, and Bottom Water, respectively. Modified from Kim and Kim (1996).

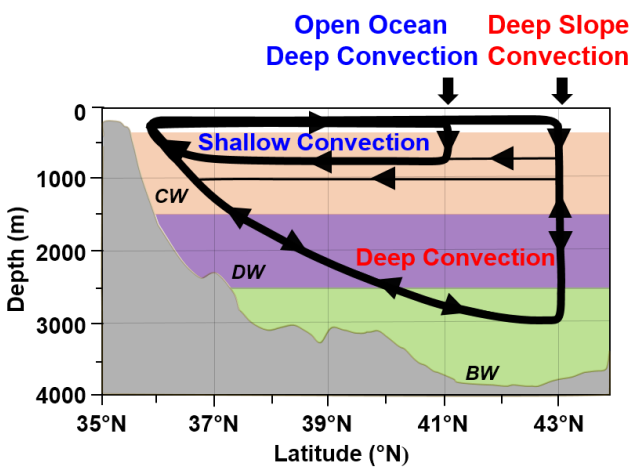

Figure 1.3. Schematic of meridional overturning circulation (MOC) in the East Sea. Double cells with shallow convection (open-ocean deep convection) vs single cell with deep convection (deep slope convection). Note that the upper cell still exists even when the deep slope convection is active although the mid-depth equatorward flow becomes weak and abyssal poleward flow reverses to equatorward. Modified from Han et al. (2020). Figure from Lee and Nam (2023).

2. Data and processing

2.1. Data

2.1.1. Subsurface moored current meter data

Time-series data of horizontal current speed and direction were obtained using single-depth current-meters (Aanderaa rotary-type recording current-meters RCM-7 and RCM-8; rRCMs) mounted on five subsurface moorings of U1, U2, U3 (same location as EC1), U4, and U5 across the UIG from November 2002 to April 2004 (Figure 2.1a and Table 2.1). Two rRCMs were mounted on each mooring line: one between 1685 and 1830 m and the other 20 m above the bottom. At mooring U3 and U4, two rRCMs at 20 m above the bottom failed to record the full time-series data but only for 187 and 325 days, respectively. One rRCM attached at 1800 m of U5 could not record the data for the entire measurement period due to a data storage unit failure. The sampling time interval of all rRCM current measurements is 30 minutes. This study used data recorded from the nine current-meters attached on the five subsurface moorings.

At the U3 (EC1) mooring location in the center of UIG, longer-term time-series data were collected using current-meters of rRCMs, Aanderaa Doppler-type recording current-meters of RCM-9 and RCM-11; dRCMs, Nortek Aquadopp current-meters; ACMs, and Vector Averaging Current Meters; VACMs attached at three nominal depths of 400, 1400, and 2200 m from November 1996 to November 2020 (twenty-three deployments in total; from Leg-1 to Leg-23) (Table 2.2). The sampling time intervals are 10 minutes for ACMs, 30 or 60 minutes for rRCMs and dRCMs, and 15 minutes for VACMs. This study used current-meter data at two nominal depths of 1400 m (1300–1700 m) and 2200 m (1900–2400 m) except for

Leg-2 current-meter data of 900 m and 1375 m.

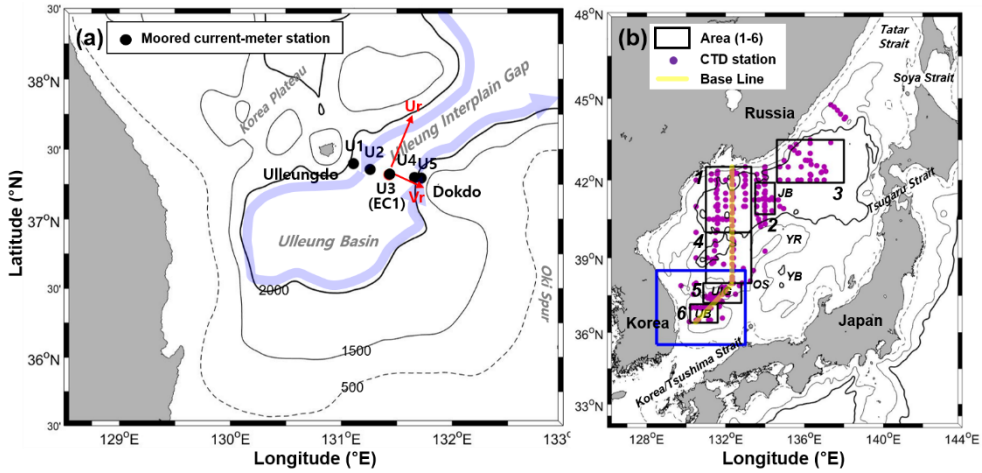

Figure 2.1. Geographical location of subsurface mooring observations at the Ulleung Interplain Gap (UIG) and shipboard hydrographic observations in the East Sea. (a) Bottom topography and abyssal current (represented by thick pale purple arrows) of the southwestern ES, and subsurface mooring stations of U1, U2, U3 (same as EC1), U4, and U5 marked by black circles across the Ulleung Interplain Gap (UIG). Red arrows denote along-channel (Ur, 12° from the north in a clockwise direction) and cross-channel (Vr, 102° from the north in a clockwise direction) directions. (b) Geographical locations of the East Sea and the vicinity of the East Sea, shipboard CTD observation stations (magenta dots), and six areas (black boxes) denoted by black numbers 1–6: 1 is western Japan Basin; WJB, 2 is central Japan Basin; CJB, 3 is eastern Japan Basin; EJB, 4 is between WJB and UIG, 5 is the Ulleung Interplain Gap; UIG, and 6 is Ulleung Basin; UB. Bold, thin, and thin broken lines indicate 3000, 1500, and 150 m depth contours, respectively. Thick pale yellow line represents the baseline of hydrographic observations. Abbreviations in black italic indicate the bottom topography: JB, UB, YB, UIG, YR, and OS represent the Japan Basin, Ulleung Basin, Yamato Basin, Ulleung Interplain Gap, Yamato Rise, and Oki Spur, respectively.

Table 2.1. Details on subsurface mooring current-meter data collected at the Ulleung Interplain Gap between November 2002 and April 2004. The locations of U1–U5 are represented in Figure 2.1a.

Station	Location (mooring depth)	Instrument	Instrument depth (m)	Observation period	Sampling interval (min.)
U1	37°23.876'N 131°06.732'E (2110 m)	RCM-7 or RCM-8	1760	Nov. 30, 2002 – Apr. 7, 2004	30
			2090		
U2	37°21.394'N 131°15.649'E (2270 m)		1830		
			2250		
U3 (EC1)	37°19.136'N 131°25.625'E (2255 m)		1365	Nov. 29, 2002 – Apr. 7, 2004	
			1685		
			2235	Nov. 29, 2002 – Jun. 14, 2003	
U4	37°17.932'N 131°39.486'E (2150 m)		1750	Nov. 29, 2002 – Apr. 7, 2004	
			2130	Nov. 29, 2002 – Oct. 20, 2003	
U5	37°17.681'N 131°43.229'E (2060 m)		2040	Nov. 28, 2002 – Apr. 7, 2004	

Table 2.2. Details on subsurface mooring current-meter data collected at the U3 (EC1) station between November 1996 and November 2020.

Leg	Location (mooring depth)	Instrument	Instrument depth (m)	Observation period	Sampling interval (min.)
1	37°20.65'N 131°24.36'E (2320 m)	RCM-7	1305	Nov. 3, 1996 – Jul. 2, 1997	120
		VACM	1910		15
2	37°21.98'N 131°24.48'E (2330 m)	VACM	900	Oct. 15, 1997 – Oct. 18, 1998	15
		RCM-7	1375		30
3	37°21.774'N 131°24.283'E (2340 m)	RCM-8	1385	Oct. 20, 1998 – May 24, 1999	30
			1890		
4	37°22.686'N 131°23.626'E (2250 m)	RCM-8	1355	May 24, 1999 – Oct. 21, 1999	30
			2230		
5	37°21.627'N 131°24.278'E (2275 m)	RCM-8	1340	Oct. 21, 1999 – May 19, 2000	30
			2255		
6	37°21.56'N 131°24.145'E (2305 m)	RCM-8	1420	May 19, 2000 – Apr. 13, 2001	30
			2285		
7	37°19.77'N 131°25.40'E (2265 m)	RCM-7	1335	Apr. 13, 2001 – Oct. 13, 2001	30
		RCM-8	2245		
8	37°19.208'N 131°25.518'E (2255 m)	RCM-8	1360	Oct. 14, 2001 – May 22, 2002	30
			2235		
9	37°19.136'N 131°25.625'E (2255 m)	RCM-8	1365	Nov. 29, 2002 – Apr. 7, 2004	30
			1685		
			2235	Nov. 29, 2002 – Jun. 14, 2003	
10	37°19.383'N 131°24.490'E (2270 m)	RCM-8	1425	Apr. 8, 2004 – Feb. 24, 2005	30
		RCM-11	2250		60

11	37°19.370’N 131°24.558'E (2345 m)	RCM-8	1405	Jun. 17, 2005 – May 24, 2006	30
		RCM-11	2325		
12	37°19.370’N 131°24.586'E (2287 m)	RCM-9	1380	May 25, 2006 – Sept. 12, 2007	60
		RCM-11	2055		
13	37°19.789’N 131°25.299'E (2340 m)	RCM-9	1450	Sept. 12, 2007 – Nov. 4, 2008	30
		RCM-11	2130		
14	37°20.816’N 131°26.893'E (2300 m)	RCM-9	1380	Nov. 05, 2008 – Feb. 22, 2010	60
		RCM-11	2180		
15	37°20.959’N 131°26.644'E (2353 m)	RCM-9	1400	Feb. 22, 2010 – Mar. 12, 2011	30
		RCM-11	2200		
16	37°19.693’N 131°26.943'E (2354 m)	RCM-9	1400	Mar. 12, 2011 – Jul. 28, 2012	30
		RCM-11	2200		
17	37°20.166’N 131°27.318'E (2337 m)	RCM-11	2200	Jul. 28, 2012 – Aug. 29, 2014	30
18	37°19.942’N 131°27.340'E (2245 m)	Aquadopp	2200	Aug. 29, 2014 – Sept. 13, 2015	10
19	37°19.575’N 131°25.866'E (2340 m)	Aquadopp	1400	Sept. 13, 2015 – Apr. 1, 2017	10
		RCM-11	2200	Sept. 13, 2015 – May 17, 2017	30
20	37°20.359’N 131°27.243'E (2317 m)	RCM-11	1400	May 18, 2017 – May 29, 2017	30
		Aquadopp	2200		10
21	37°20.644’N 131°22.99'E	RCM-11	1400	Jul. 21, 2017 – Jul. 19, 2018	30
		Aquadopp	2200		10
22	37°20.631’N 131°22.782'E (2320 m)	RCM-11	1400	Jul. 20, 2018 – Dec. 9, 2019	30
		Aquadopp	2200		10
23	37°20.365’N 131°22.012'E (2240 m)	RCM-11	1400	Dec. 9, 2019 – Nov. 11, 2020	30
		Aquadopp	2200	Dec. 10, 2019 – Nov. 11, 2020	10

2.1.2. Hydrographic data

Hydrographic observation data were collected in western ES using a standard 24 Hz Sea-Bird Electronics 9 plus Conductivity-Temperature-Depth (CTD) unit and Sea-Bird Electronics 11 deck unit (SBE9/11plus CTD) and 1 Hz Neil Brown Instrument Systems MKIIIB CTD unit via 42 research cruises between 1993 and 2019: 21 cruises were occupied over the western ES from August 1993 to November 2019 whereas the other 21 cruises were conducted only covering the southwestern ES across the UIG from November 2002 to October 2019 (Figure 2.1b and Table 2.3). Vertical profiles of water temperature, conductivity, and pressure data were collected using full-depth CTD casts (down to 5 m above the bottom) at each station during all the cruises except for some cruises across the UIG. In this study, potential temperature, conductivity, and pressure data collected deeper than 1000 m from 42 research cruises were used, except for selected cruises (excluding unreliable conductivity data collected in the other cruises marked as asterisks (*) on the variable S in the Table 2.3).

Hydrographic and subsurface moored current-meter time-series data used in this study are summarized in Figure 2.2.

Table 2.3. Details on hydrographic observation data occupied in the western ES (Japan Sea) from August 1993 to November 2019. Asterisk (*) on the variables S refers that the salinity data were not used in this study. [a]Sea-Bird Electronics 9 CTD unit and Sea-Bird Electronics 11 deck unit. [b]Neil Brown Instrument Systems MKIIIB CTD unit. [c]Sea-Bird Electronics 9 plus CTD unit and Sea-Bird Electronics 11 plus V2 deck unit. Numbers in area coverage represent area numbers in Figure 2.1b.

No.	Cruise year and date	Instrument	Total number of stations	Variables	Area coverage
1	August 12–19, 1993	SBE911[a]	69	θ, S	1-6
2	July 10–21, 1994	SBE911	51	θ, S	
3	March 1–7, 1995	SBE911	35	θ, S	
4	July 24–August 8, 1995	SBE911	45	θ, S	
5	February 17–24, 1996	SBE911	26	θ, S	
6	August 1–11, 1996	SBE911	35	θ, S, DO	
7	March 20–April 8, 1997	SBE911	67	θ, S, DO	
8	February 22–March 8, 1999	SBE911	43	θ, S	
9	June 14–August 13, 1999	NBMK[b]	203	θ, S, DO	
10	February 2–March 17, 2000	NBMK	81	θ, S*	
11	April 16–20, 2001	NBMK	19	θ, S	
12	April 7–26, 2002	SBE911p[c]	15	θ, S*	
13	October 15-27, 2005	SBE911p	43	θ, S, DO	
14	May 10–20, 2007	SBE911p	23	θ, S, DO	
15	July 8–19, 2009	SBE911p	38	θ, S*, DO	
16	October 13–27, 2012	SBE911p	42	θ, S*, DO	
17	April 15–29, 2014	SBE911p	28	θ, S*, DO	
18	April 6–May 3, 2015	SBE911p	36	θ, S, DO	
19	April 5–15, 2016	SBE911p	23	θ, S	
20	November 30–December 15, 2018	SBE911p	20	θ, S*, DO	
21	October 27–November 22, 2019	SBE911p	42	θ, S, DO	
1	November 28–29, 2002	SBE911p	8	θ, S	5
2	June 25–26, 2003	SBE911p	4	θ, S	
3	April 7, 2004	SBE911p	6	θ, S	
4	March 8–15, 2007	SBE911p	3	θ, S	
5	December 2–7, 2007	SBE911p	3	θ, S	
6	March 27–30, 2008	SBE911p	3	θ, S*	
7	August 9–15, 2008	SBE911p	6	θ, S	
8	August 13–18, 2009	SBE911p	6	θ, S*	
9	February 7–9, 2010	SBE911p	3	θ, S*	
10	July 15–21, 2010	SBE911p	7	θ, S	
11	November 3–7, 2010	SBE911p	3	θ, S	
12	July 6–12, 2011	SBE911p	3	θ, S	

13	May 28–June 3, 2012	SBE911p	6	θ, S*	
14	August 5–11, 2012	SBE911p	4	θ, S	
15	May 1–2, 2014	SBE911p	3	θ, S*	
16	September 2–5, 2015	SBE911p	3	θ, S*	
17	May 16–18, 2017	SBE911p	7	θ, S*	
18	May 27–31, 2017	SBE911p	5	θ, S	
19	July 20–21, 2018	SBE911p	5	θ, S	
20	August 19–22, 2018	SBE911p	11	θ, S*	
21	October 21–24, 2019	SBE911p	5	θ, S*	

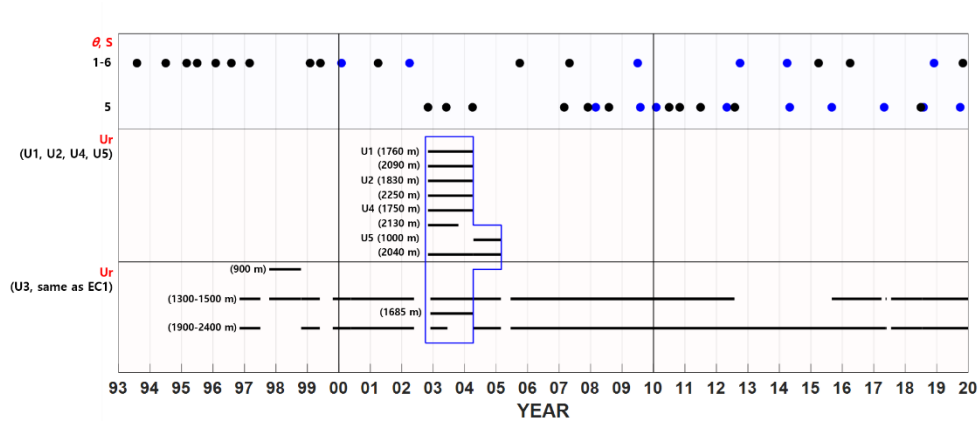

Figure 2.2. Timetable of the hydrographic and subsurface moored current-meter time-series data used in this study. θ, S, and numbers 1–6 in upper left side represent CTD observation parameters of potential temperature, salinity, and CTD observation areas in Figure 2.1b, respectively. The subsurface moored current-meter data (Ur) from November 2002 to April 2004 (inside the solid blue lines) are used to find the correlation between the along-channel currents (Ur) at 1800 m at U3 (EC1) and the volume transports of the deep waters below 1500 m in western UIG. The blue closed circles represent the salinity data excluded from this study because the salinity value is found to be strange through the local range test.

2.2. Data processing

Standard quality controls (e.g., time and location tests, global and regional range tests, and spike and gradient tests) based on protocols and procedures for the Ocean Observatories Initiative data products (Consortium for Ocean Leadership, 2013) were applied to time-series data obtained from rRCMs, dRCMs, VACMs and ACMs at U1–U5 subsurface moorings, and unreasonable outliers were removed manually. The rRCMs records the minimum current speed of 1.1 cm s^{-1}, which is considered as a current stall (i.e., zero speed) (Teague et al., 2005); current speed equal or below 1.1 cm s^{-1} are treated as zero and discarded. Considering the resolution of the rRCMs (~0.3 cm s^{-1}), the minimum resolvable current speed is 1.4 cm s^{-1} (Teague et al., 2005). Horizontal current vector is decomposed into along-channel (defined as Ur, 12^{o} rotated clockwise from the north) and cross-channel (Vr, orthogonal to the along-channel direction) components (Figure 2.1a). Spline fits were applied to the Ur and Vr time-series data for stall periods less than 5 h, and zero values were entered for longer periods. Ur and Vr time-series data were 40-h low-pass filtered and then subsampled every 12 h (Chang et al., 2009; Kim et al., 2013; Shin et al., 2020). Processing of horizontal current-meter data obtained from U1-U5 moorings is illustrated in Figure 2.3. Basic statistics for low-pass filtered currents subsampled at 12 h intervals at U1–U5 subsurface moorings across the UIG are summarized in Table 2.4.

All CTD data were processed by standard quality control and quality assurance procedures (Kim et al., 2000; Choi et al., 2009; Lee et al., 2019) (Figure 2.4). In the process of removing abnormal values (Wild edit), CTD data that exceeds twice the standard deviation included in 1000 consecutive data intervals from each

vertical profile were eliminated, after which the standard deviation was computed again and data that is 20 times more than the standard deviation were removed again, and the procedure was carried out three times. Then, for smoothing the pressure data occurred due to ship movements (Low-pass filter), 0.15 second was applied to the low-pass filter of the pressure data. For correcting the time off-sets of the temperature and conductivity sensors (Align CTD), the optimal correction time for each profile was calculated and applied (minimum -0.01 s, max 0.07 s) using the delay correlation. To correct the effect of thermal mass that occurs when the CTD passes through a thermocline layer with a large change in water temperature (Cell Thermal Mass), optimal correction coefficients (α: 0.01–0.06, τ: 1.0–11.0) for each profile were calculated and applied (Morison et al., 1994; Mensah et al., 2009; Lee et al., 2019). Here, water temperature and salinity are in potential temperature (°C) and practical salinity (psu), respectively, and potential density (kg m^{-3}) was calculated using the Thermodynamic Equation of Sea Water 2010 (TEOS-10) (McDougall & Barker, 2011).

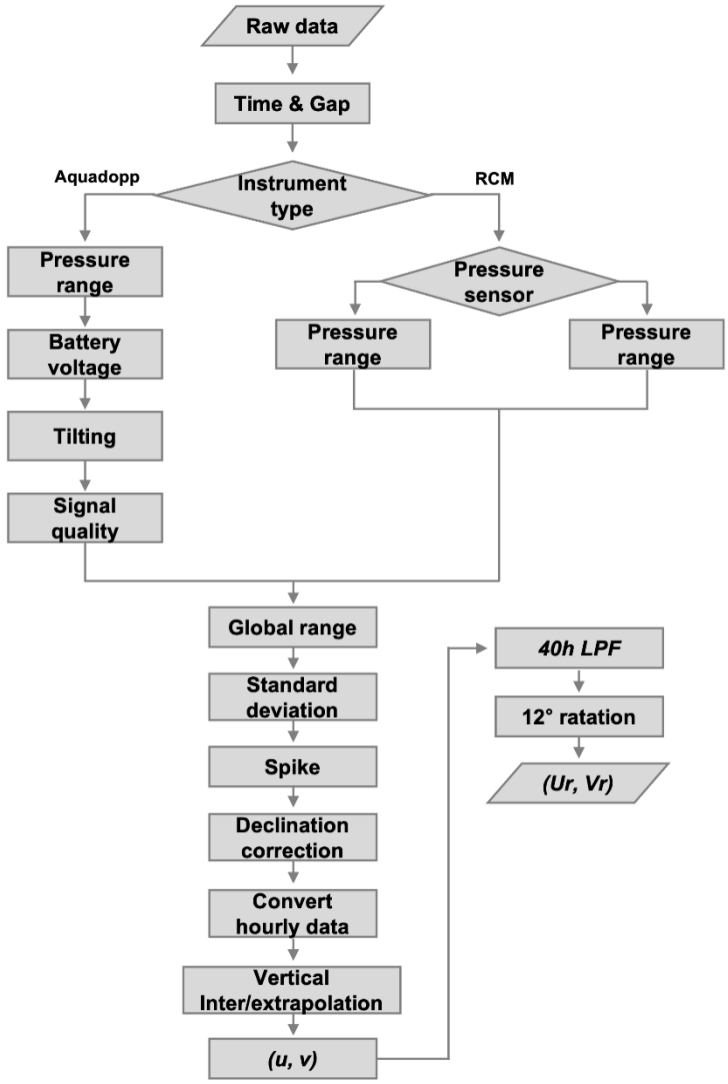

Figure. 2.3. A flow chart for processing of horizontal currents data obtained from U1-U5 moorings.

Table 2.4. Basic statistics for the low pass filtered currents subsampled at 12 h intervals at five subsurface moorings in the Ulleung Interplain Gap (UIG). Asterisk (*) on the mooring depths of 1400 and 2200 m in EC1 represent the nominal depth and actual mooring depths range from 1320 to 1685 m and from 1910 to 2388 m, respectively. [a]All directions are measured clockwise from north.

Station	Mooring depth (m)	Period (year/month)	Sampling time interval (min.)	Velocity components	Mean (cm s^{-1})	STD (cm s^{-1})	Vector mean			MKE (cm^2 s^{-2})	EKE (cm^2 s^{-2})	EKE/MKE
							Speed (cm s^{-1})	[a]Heading (°)	Max Speed (cm s^{-1})			
EC1	1400*	00/01–20/12	10, 30 or 60	Ur	–0.48	2.88	1.27	206.4	16.42	0.80	7.85	9.8
				Vr	–1.17	2.72						
	2200*	00/01–20/12	10, 30 or 60	Ur	–0.61	3.51	1.37	218.4	19.93	0.93	10.65	11.4
				Vr	–1.22	3.00						
U1	1760	02/11–04/04	30	Ur	–0.16	1.84	0.20	245.5	13.82	0.02	5.37	276.6
				Vr	–0.12	2.71						
	2090	02/11–04/04	30	Ur	–0.21	1.76	0.27	323.4	14.05	0.04	4.66	124.0
				Vr	0.18	2.50						
U2	1830	02/11–04/04	30	Ur	–0.98	2.00	1.19	247.3	12.10	0.71	5.24	7.4
				Vr	–0.68	2.55						
	2250	02/11–04/04	30	Ur	–0.88	2.14	0.94	261.1	12.10	0.45	5.59	12.5
				Vr	–0.34	2.57						
U3 (EC1)	1685	02/11–04/04	30	Ur	–0.93	2.49	1.08	251.6	9.68	0.58	5.31	9.1
				Vr	–0.54	2.10						
	2235	02/11–03/06	30	Ur	–1.01	2.57	1.01	286.8	9.35	0.51	4.41	8.6
				Vr	0.09	1.49						
U4	1750	02/11–04/04	30	Ur	1.36	4.20	1.49	77.8	15.47	1.11	14.60	13.17
				Vr	0.61	3.40						
	2130	02/11–03/10	30	Ur	0.48	2.80	0.70	55.8	11.08	0.24	5.84	24.2
				Vr	0.50	1.97						
U5	2040	02/11–04/04	30	Ur	2.16	5.01	2.91	59.8	28.71	4.25	25.28	6.0
				Vr	1.96	5.05						

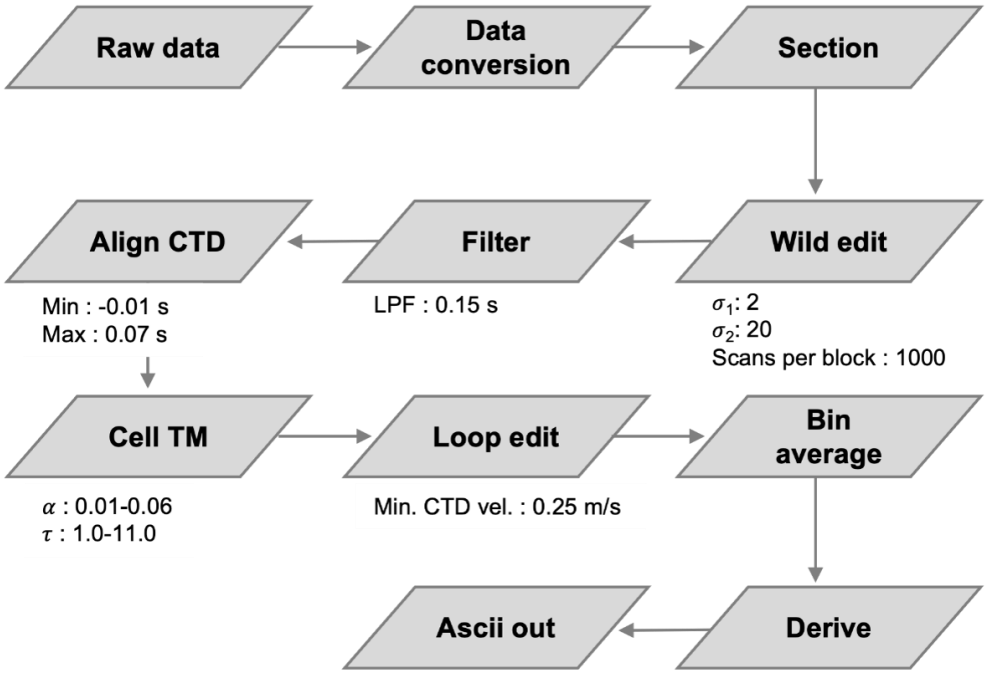

Figure. 2.4. A flow chart for CTD data processing.

2.3. Estimation of annual-mean volume transports of the deep waters below 1500 m through the western UIG from 1997 to 2019

Volume transports of the deep water below 1500 m depth across the UIG from November 2002 to April 2004 are obtained using current-meters (rRCMs) data from five subsurface moorings (U1–U5) at depths greater than 1600 m (Figure 2.5). The area below 1500 m across the UIG was divided into 7 areas: 5 rectangles centered on each mooring line from U1 to U5, and 2 right-angled triangles located to the west of the U1 rectangle and to the east of the U5 rectangle. Time-series data of Ur velocity at a depth of 1800 m at U1–U5 subsurface mooring stations were determined using the linear interpolation or extrapolation, and application of mean shears at two depth levels of current data at each mooring (Chang et al., 2009). Since the current data at U5 were only available at 20 m above the bottom from November 2002 to April 2004, mean shear of the Ur components between 1020 and 2000 m from April 2004 to February 2005 ($-2.97 \pm 2.77 \times 10^{-5}\ s^{-1}$) were applied to Ur time-series at 2000 m to estimate the Ur time-series at a depth of 1800 m (Chang et al., 2009). The negative shear shows that the flow at 2000 m is stronger than the flow at 1020m, indicating the bottom intensification at U5 in association with the DAC (Chang et al., 2009; Shin et al., 2020). Each area of 5 rectangles for U1 to U5 was multiplied by the Ur at 1800 m depth of each mooring station, and the areas of the right-angled triangles at both ends were multiplied by the Ur at 1800 m depth of adjacent U1 and U5 moorings.

The volume transport of the deep waters below 1500 m passing through the four western (three eastern) areas of U1–U3 (U4–U5) was defined as the volume transport across the western (eastern) UIG (Figures 2.5 and 2.6a). The sum of western and eastern volume transports was defined as net transport (Figure 2.6a).

The positive (negative) sign of the volume transport means the poleward (equatorward) flow from UB (JB) to JB (UB). From November 2002 to April 2004, the volume transports of the deep waters below 1500 m depth was -0.259 Sv (1 Sv = 10^6 m^3 s^{-1}) through western UIG and 0.313 Sv through eastern UIG, and the net transport of the deep waters below 1500 m depth through the UIG was about 0.054 ± 0.011 Sv, which is one order larger than the volume transport of the deep water below 1800 m across the UIG (0.005 ± 0.025 Sv) reported by Chang et al. (2009) (Figure 2.6a).

A regression between the volume transports of the deep waters below 1500 m depth through the western UIG (VT_{15} hereafter) and 40-h low-passed Ur at 1800 m depth of U3 (EC1) (Ur_1800 hereafter) obtained by linear interpolation of Ur at 1685 and 2235 m depth of U3 (EC1) (Ur_1685 and Ur_2235 hereafter, respectively) from November 2002 to April 2004 was calculated (Figure 2.6b). To fill the gap in Ur_2235 from June 2003 to April 2004, the Ur_1365 and Ur_1685 were extrapolated (Figure 2.7). VT_{15} (blue line in Figure 2.6a) were correlated with Ur_1800 yielding a relationship below between them obtained by the least square method (R=0.78).

$$Transport\ (Sv) = 0.1302 \times Ur\ (cm\ s^{-1}) - 0.1307 \quad \text{……(Eqn. 1)}$$

Here, the slope and intercept are approximately doubled the values obtained from the regression between the volume transport of the deep waters below 1800 m depth through the western UIG (VT_{18} hereafter) and 40-h low-passed Ur at 2200 m depth at U3 (EC1) (Ur_2200 hereafter), e.g., $Transport\ (Sv) = 0.078 \times Ur\ (cm\ s^{-1}) - 0.068$ (R=0.80) (Chang, 2016).

The slopes, intercepts, and R values according to the correlation between

VT_{15} and Ur components at various depths (1500, 1800, 2000, 2200, 1500–1800, 1500–2000, 1800–2000, 2000–2200 m) range from 0.1275 to 0.1312, –0.1421 to –0.0994, and 0.77 to 0.78, respectively (Figure 2.8). Considering that 1800 m depth is an intermediate level in the depth ranges of 1500–2300 m at U3 (EC1), and the correlation coefficient between VT_{15} and Ur_1800 is the largest, in this study, VT_{15} from 2000 to 2020 was derived by applying Ur_1800 to Eqn. 1. The slopes, intercepts, and R values according to the correlation between VT_{15} and Ur_1800 at three month intervals range from 0.0862 to 0.1951, –0.0253 to –0.3729, and 0.56 to 0.93, respectively (Figure 2.9).

The 40-h low-passed VT_{15} from 2000 to 2020 was obtained by applying the Eqn. (1) and averaged to yield annual-mean time series (VT_{15_annual} hereafter). Here, Ur_1800 were obtained by linear interpolation of Ur observed at depths above (1300–1500 m) and below (1900–2400 m) the depth. To fill the data gap from July 2012 to September 2015, Ur_1800 during the period were estimated using mean vertical shear of -7.53×10^{-4} s^{-1} (negative shear means stronger current at deeper depth) between 1400 and 2200 m obtained for the period from January 2010 to December 2017 (excluding the data gap period). Since the purpose of this study is to examine long-term (multi-decadal-long) variations, 3-year low-pass filter was applied to the time series of VT_{15}, then the VT_{15_annual} was obtained by averaging the volume transports annually.

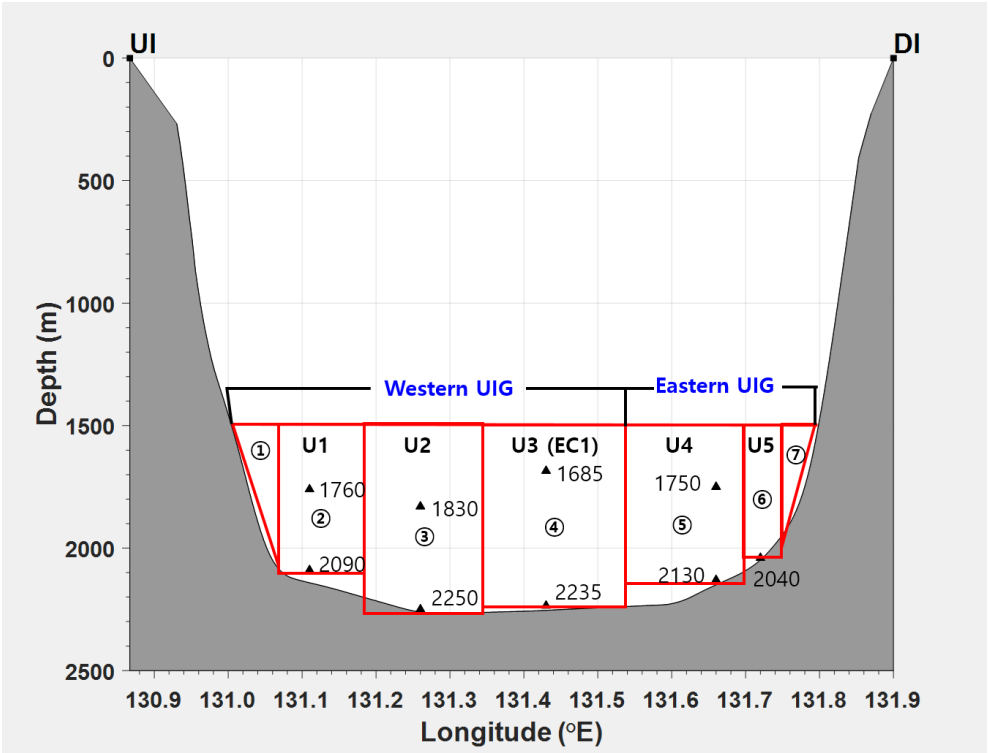

Figure 2.5. Vertical sections across the Ulleung Interplain Gap (UIG). U1–U5 indicate the subsurface mooring stations, and closed triangles and numbers next to them represent the locations of Aanderaa rotary-type recording current-meters (rRCMs) and their mounted depth, respectively. Open circle number 1–7 indicate cross-sectional area used for estimation of volume transports below 1500 m across the UIG. The four western areas (①–④) were defined as the western UIG and the three eastern areas (⑤–⑦) were defined as the eastern UIG. UI and DI stand for the Ulleung Island and Dok Island, respectively.

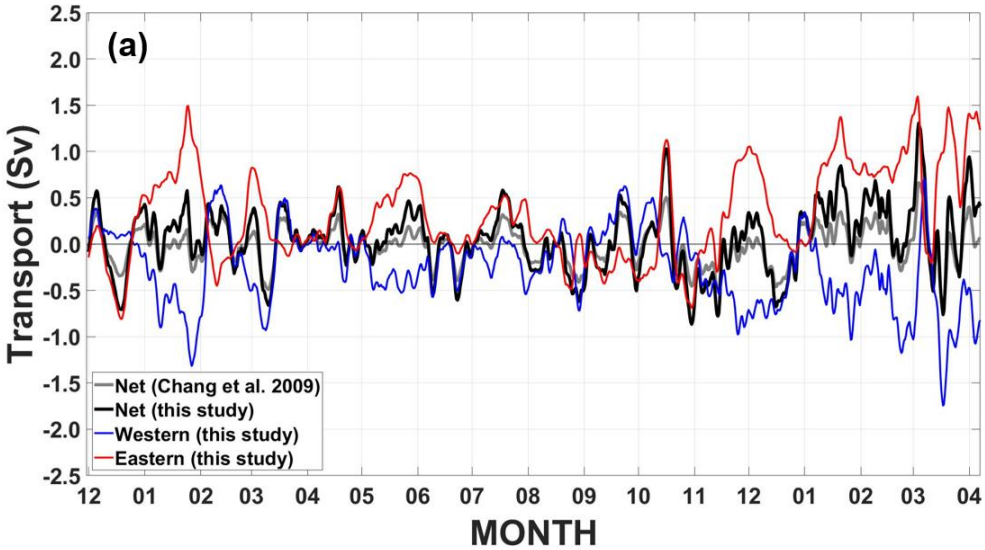

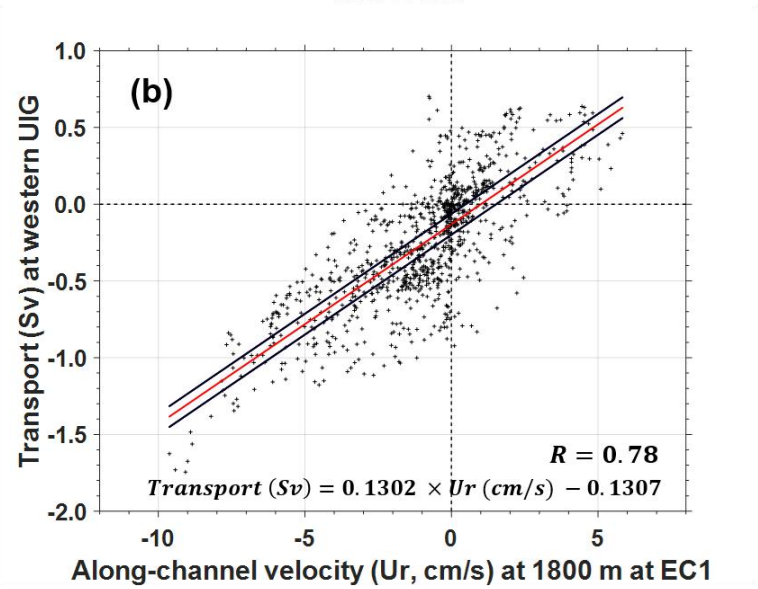

Figure 2.6. (a) Volume transports of the deep water below 1500 m in the UIG from November 2002 to April to 2004. Net (thick black line), western (thin bl ue line), and eastern (thin red line) transports are drawn together with net (thic k gray line) transports below 1800 m across the UIG drawn in Figure 6 of Ch ang et al. (2009). (b) Linear regression between the volume transport below 15 00 m in western UIG and the along-channel velocity (Ur, cm/s) at 1800 m of EC1 using 40-h low-pass filtering and subsampled data every 12 h. The thick r ed and black lines represent the linear regression and the standard error bounds of the regression.

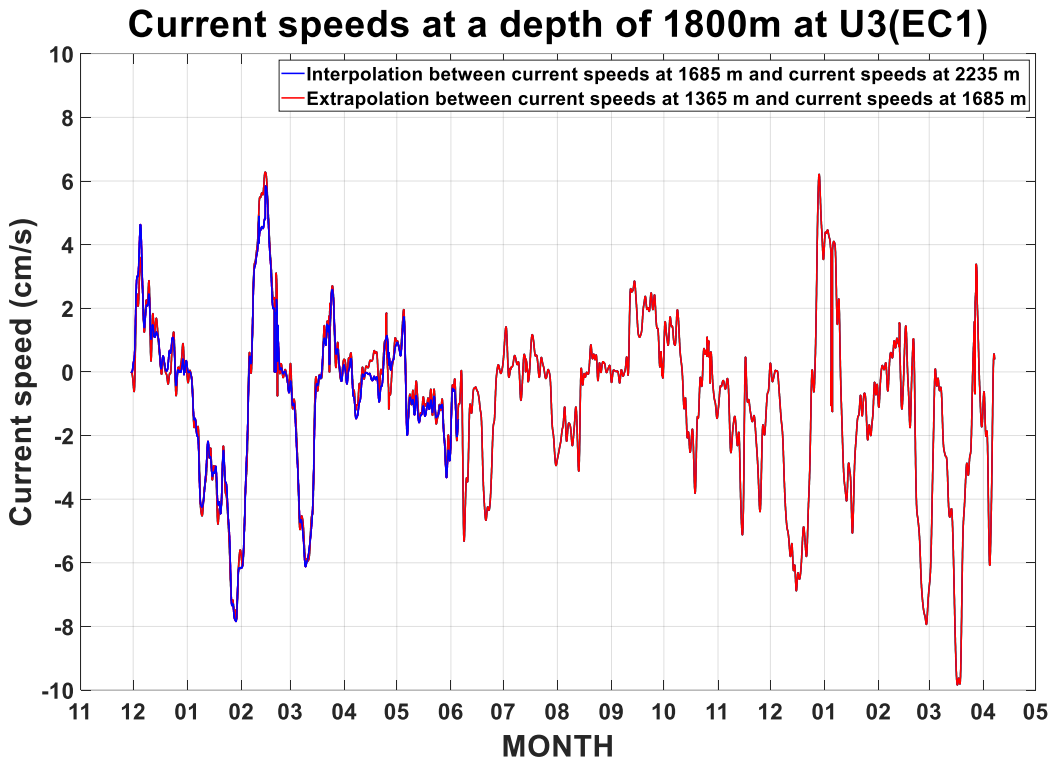

Figure 2.7. Current speeds at a depth of 1800 m at U3 (EC1) from November 2002 to April 2004. Current speeds at a depth of 1800 m at U3(EC1) were obtained from interpolation between current speeds at 1685 m and current speeds at 2235 m (blue lines) and extrapolation between current speeds at 1365 m and current speeds at 1685 m (red lines) from November 2002 to June 2003. From June 2003 to April 2004, current speeds at a depth of 1800 m at U3(EC1) were obtained from extrapolation between current speeds at 1365 m and current speeds at 1685 m.

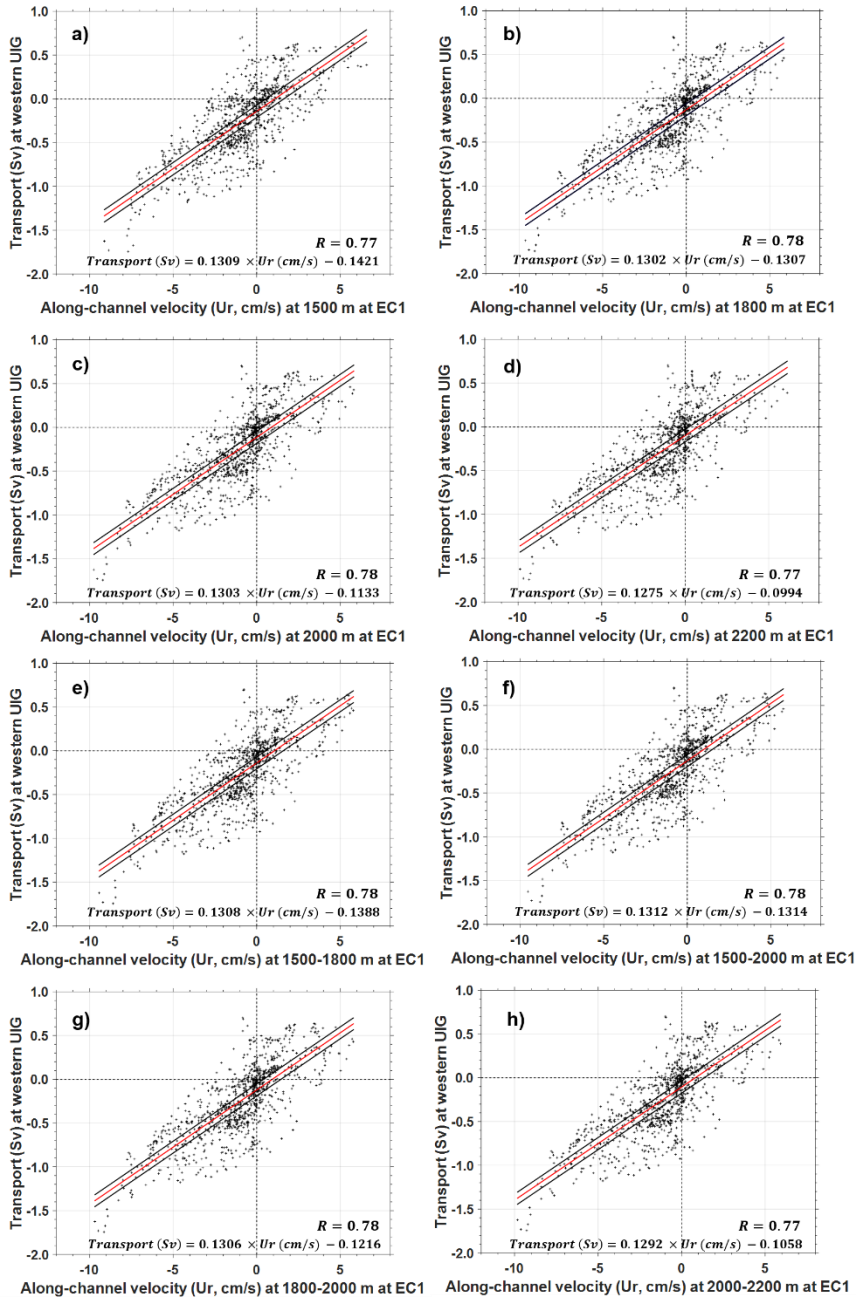

Figure 2.8. Linear regressions between the volume transports of the deep waters below 1500 m depth through the western UIG (VT_{15}) and 40-h low-passed Ur at various depths (1500, 1800, 2000, 2200, 1500–1800, 1500–2000, 1800–2000, and 2000–2200 m) of U3 (EC1). The thick red and black lines represent the linear re gression and the standard error bounds of the regression.

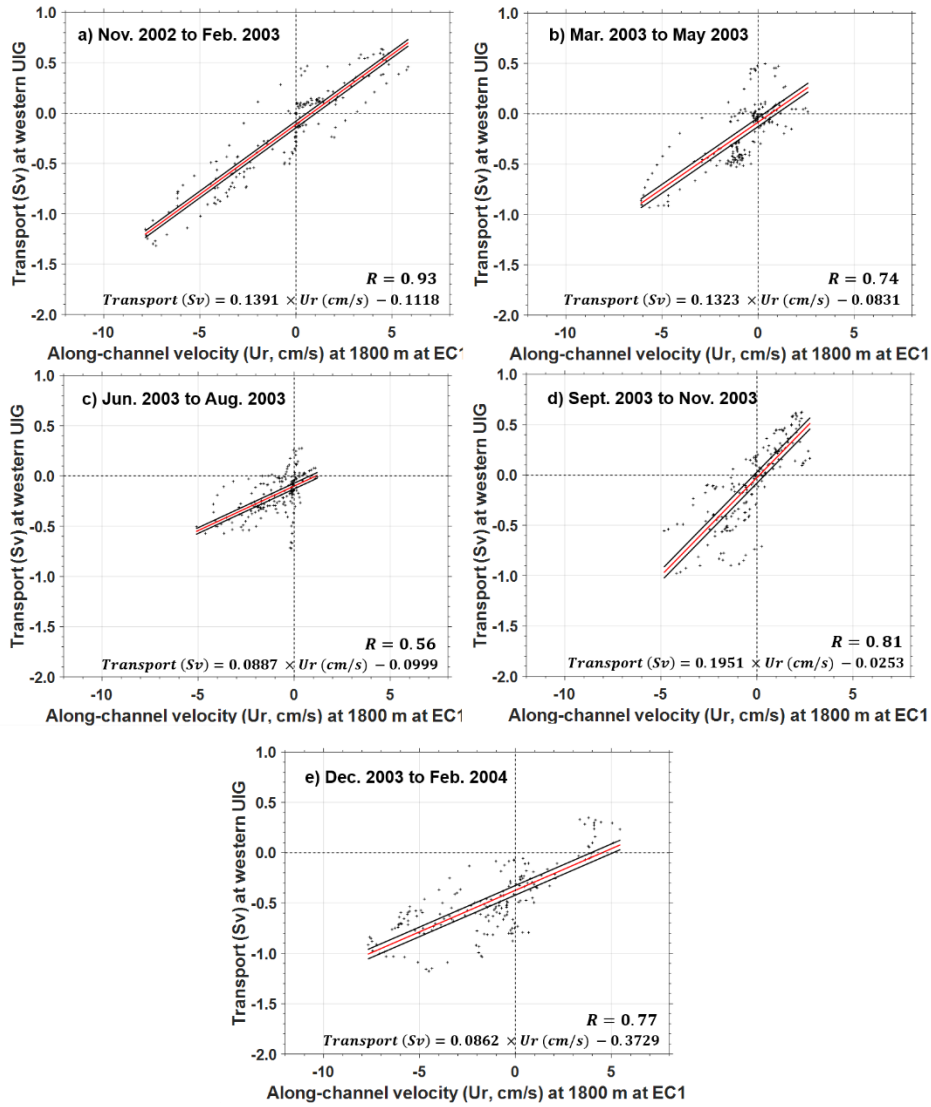

Figure 2.9. Linear regressions between the volume transports of the deep waters below 1500 m depth through the western UIG (VT_{15}) and 40-h low-passed Ur at time intervals of three months at 1800 m of U3 (EC1). The thick red and black lines re present the linear regression and the standard error bounds of the regression.

2.4. Estimation of boundaries between the deep waters (CW/DW/BW)

Isotherm depth of 0.6 ℃ , deep salinity minimum (DSM hereafter) and upper boundary homogeneous layer (UBHL hereafter) were used as the upper boundary of CW, boundary depth between CW and DW, and DW and BW (Kim et al., 1996; Kim et al., 2004; Yoon et al., 2018), respectively (Figure 1.2). The upper boundary depth of CW (UBD_{CW} hereafter) was defined as a isotherm depth of 0.6 ℃. In order to remove the wiggle of the vertical salinity profiles, a 200 m-moving-average was applied to the vertical salinity profiles (Figure 2.10). Then, the depth of the DSM (D_{DSM} hereafter) was defined as a depth between 600 and 3000 m where salinity reaches its local minimum (Yoon et al., 2018). A vertical θ gradient of less than 0.001 ℃ (temperature accuracy) per 100-m range was determined for the depth of the UBHL (D_{UBHL} hereafter) as a DW-BW boundary (Figure 2.11). Potential temperatures at D_{DSM} and D_{UBHL} were defined as θ_{DSM} and θ_{UBHL}, respectively.

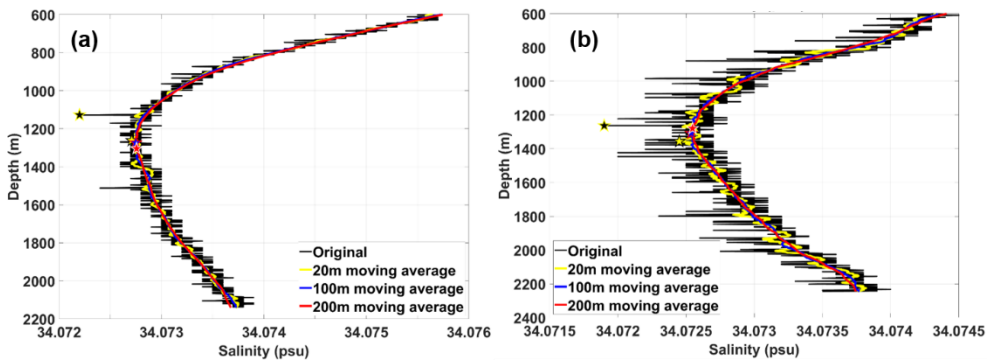

Figure 2.10. Various depths (20, 100, and 200 m)-moving-averaged vertical salinity profiles at the western Japan Basin (number 1 area in Figure 2.1b) in February 1996. To determine the DSM depth (D_{DSM}), a vertical salinity profile with a 200 m-moving-averaged was used.

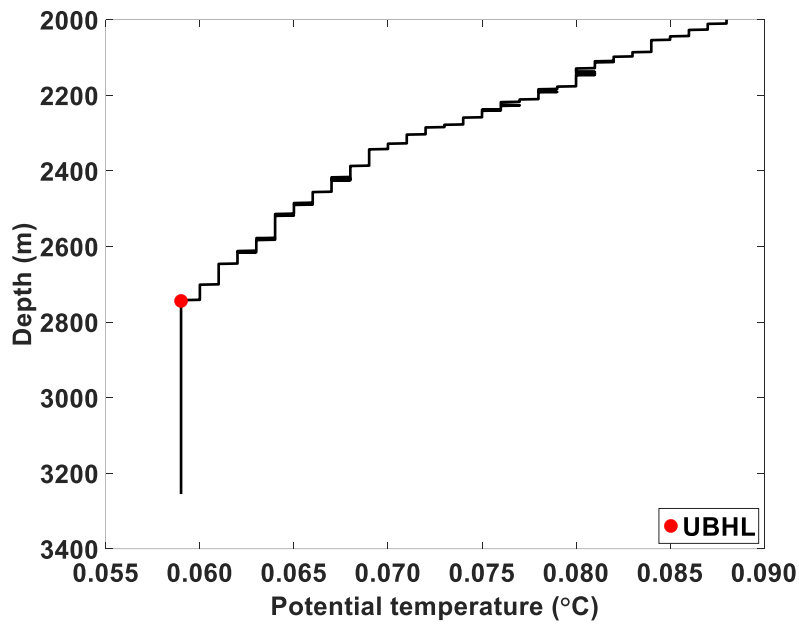

Figure 2.11. A vertical θ profiles at the western Japan Basin (number 1 area in Figure 2.1b) in February 1996. A vertical θ gradient of less than 0.001 °C (temperature accuracy) per 100-m range was determined for the depth of the UBHL (D_{UBHL}) as a DW-BW boundary.

3. Results

3.1. Interannual to decadal variation of the volume transports of the deep waters below 1500 m through the western UIG from 1997 to 2019

Long-term (1997–2019) mean VT_{15_annual} is equatorward (volume transport from the JB to UB) with the time mean and standard error of VT_{15_annual} = -0.20 ± 0.01 Sv and their interannual and decadal variations are significant (Figure 3.1). Equatorward VT_{15_annual} was the largest in 2015 and 2019 with 0.31 Sv, followed by 0.28 Sv in 2010 and 2019 and then 0.27 Sv in 2016, and was the smallest in 1998 with 0.11 Sv, followed by 0.13 in 2002 and 2014 and then 0.14 Sv in 2005. Decadal-mean equatorward VT_{15_annual} (represented by blue thick horizontal dotted lines in Figure 3.1) was about 0.04 ± 0.02 Sv larger in the 2000s (0.18 ± 0.01 Sv) than in the late 1990s (0.14 ± 0.02 Sv) and about 0.05 ± 0.02 Sv larger in the 2010s (0.23 ± 0.02 Sv) than in the 2000s (0.18 ± 0.01 Sv). Linear trend of equatorward VT_{15_annual} from 1997 to 2019 was 0.0050 Sv yr^{-1}, meaning an increasing trend of inflow transport from JB to UB. The mean standard error of VT_{15_annaul} is less than 2 %.

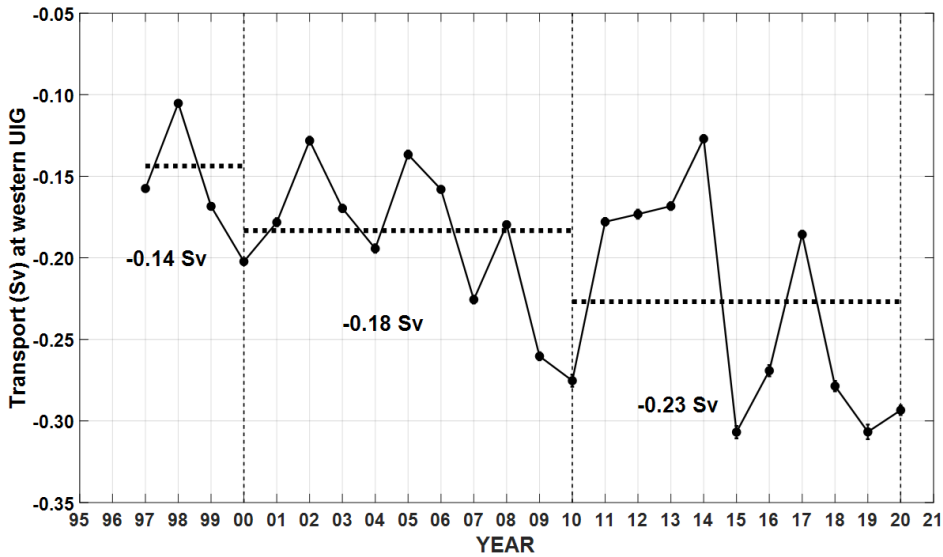

Figure. 3.1. Time-series of the annual-mean volume transports of the deep water s below 1500 m through the western UIG from 1997 to 2019. The closed circl es indicate the annual-mean volume transports of the deep waters below 1500 m through the western UIG. The dotted lines represent the decadal-mean volu me transports of the late 1990s (-0.14 ± 0.02 Sv), 2000s (-0.18 ± 0.01 Sv), and 2010s (-0.23 ± 0.01 Sv).

3.2. Decadal variation in the depth and the potential temperature of DSM, UBHL and the upper boundary depth of CW from the 1990s to 2010s

The D_{DSM} and D_{UBHL}, and UBD_{CW} in the East Sea show decadal variations from the 1990s to the 2010s (Figures 3.2, 3.3, and 3.4). The decadal-mean depths of DSM gradually became deeper from the 1990s to the 2010s at WJB, between WJB and UIG, UB, and UIG (Figures 3.2a, 3.3a, 3.3c, and 3.3d), whereas the decadal-mean depths of DSM became deeper (shallower) from the 1990s to the 2000s at CJB (EJB), and became unchanged (deeper) from the 2000s to the 2010s at CJB (EJB) (Figures 3.2c and 3.2e). Meanwhile, the decadal-mean depths of UBHL became shallowed from the 1990s to the 2000s, and became deeper from the 2000s to the 2010s at WJB, CJB, and between WJB and UIG (Figures 3.2a, 3.2d, and 3.3b), whereas the decadal-mean depths of UBHL remained unchanged significantly from the 1990s to the 2010s at EJB (Figure 3.2f). In the WJB, the UBD_{CW} became shallow from the 1990s to the 2000s and then deepened again from the 2000s to the 2010s, while the rest of the area gradually deepened from the 1990s to the 2010s (Figure 3.4).

θ_{DSM} and θ_{UBHL} have both increased from the 1990s to the 2010s, while changes in D_{DSM} determine the θ_{DSM}, while D_{UBHL} has continued to rise regardless of changes in D_{UBHL} (Figures 3.2 and 3.3). The θ_{DSM} averaged in all areas increased by 0.0399 ± 0.0068 ℃ from the 1990s (0.1196 ± 0.0010 ℃) to the 2000s (0.1595 ± 0.0067 ℃), while it increased by 0.0287 ± 0.0187 ℃ from the 2000s (0.1595 ± 0.0067 ℃) to the 2010s (0.1882 ± 0.0175 ℃) (Table 3.1). On the other hand, the θ_{UBHL} averaged in all areas increased by 0.0123 ± 0.0018 ℃ from the 1990s (0.0625 ± 0.0006 ℃) to the 2000s (0.0748 ± 0.0017 ℃), while it increased by 0.0196 ± 0.0024 ℃ from the 2000s (0.0748 ± 0.0017 ℃) to the 2010s (0.0944 ± 0.0016 ℃).

The θ_{DSM} follows changes in D_{DSM} because the effect of potential temperature variation as the water depth itself changes is greater than overall potential temperature rise effect in the D_{DSM} range (Figure 3.5). However, The θ_{UBHL} have continuously increased from the 1990s to the 2010s regardless of changes in D_{UBHL} because overall potential temperature rise effect in the DUBHL range is greater than the effect of potential temperature variation as the water depth itself changes (Figure 3.5). Basic statistics of decadal-mean of the UBD_{CW}, D_{DSM}, θ_{DSM}, D_{UBHL}, and θ_{UBHL} with standard errors in the East Sea in the 1990s, 2000s, 2010s, and their differences (2000s–1990s and 2010s–2000s) are summarized in the Tabl e 3.1.

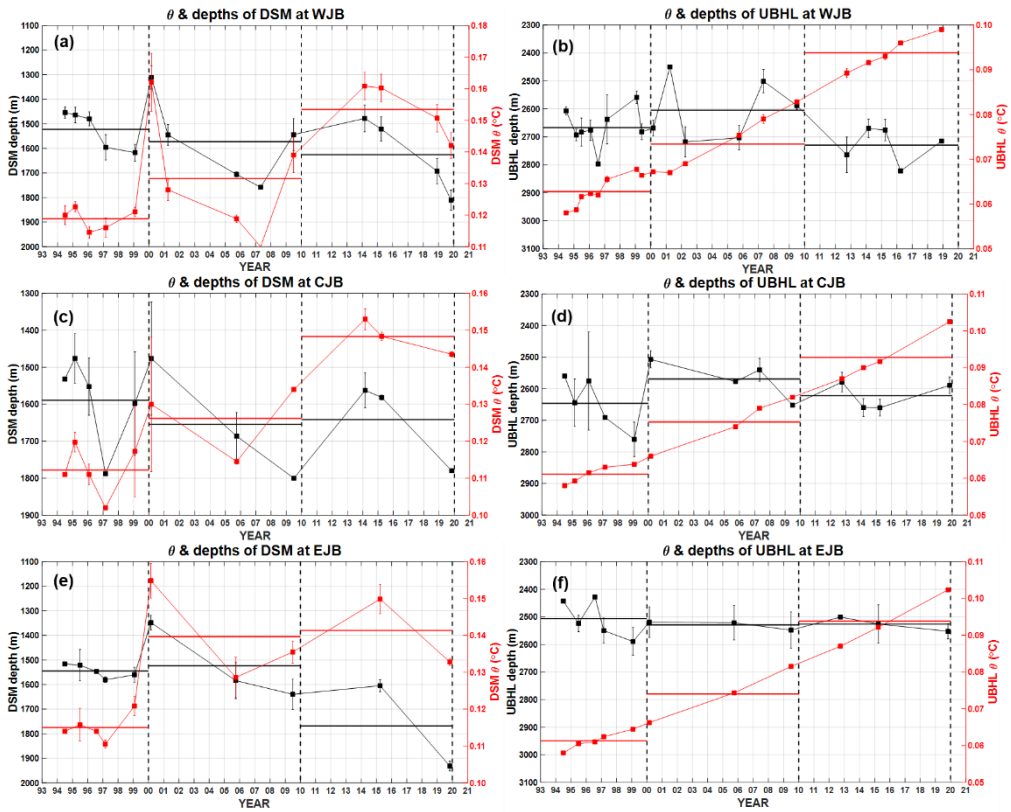

Figure. 3.2. Annual-mean depth and potential temperature of DSM and UBHL at (a, b) WJB, (c, d) CJB, and (e, f) EJB from 1994 to 2019. Black and red closed circles indicate depths and potential temperatures of DSM and UBHL, respectively. Black and Red horizontal thick lines indicate decadal-mean depths and potential temperatures of DSM and UBHL in the 1990s, 2000s, and 2010s, respectively. The vertical bars represent the standard error. Note that vertical scale varies from panel to panel.

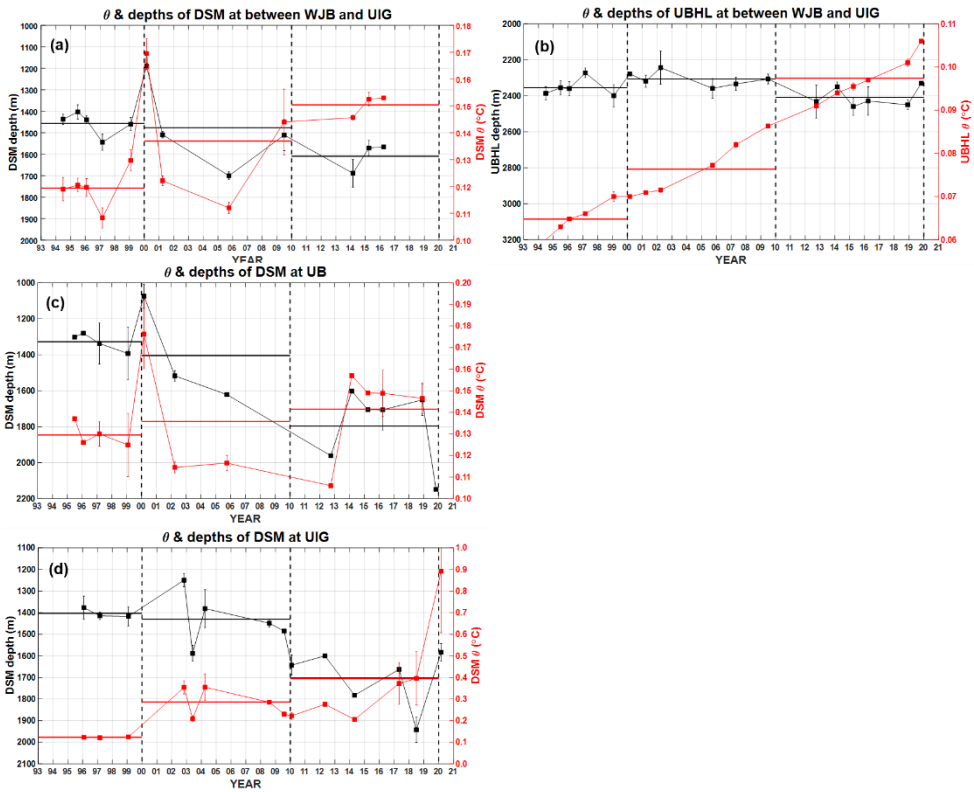

Figure. 3.3. Annual-mean depth and potential temperature of DSM and UBHL at (a, b) between the WJB and UIG, and annual-mean depth of DSM at (c) UB and (d) UIG from 1994 to 2019. Black and red closed circles indicate depths and potential temperatures of DSM and UBHL, respectively. Black and Red horizontal thick lines indicate decadal-mean depths and potential temperatures of DSM and UBHL in the 1990s, 2000s, and 2010s, respectively. The vertical bars represent the standard error. Note that vertical scale varies from panel to panel.

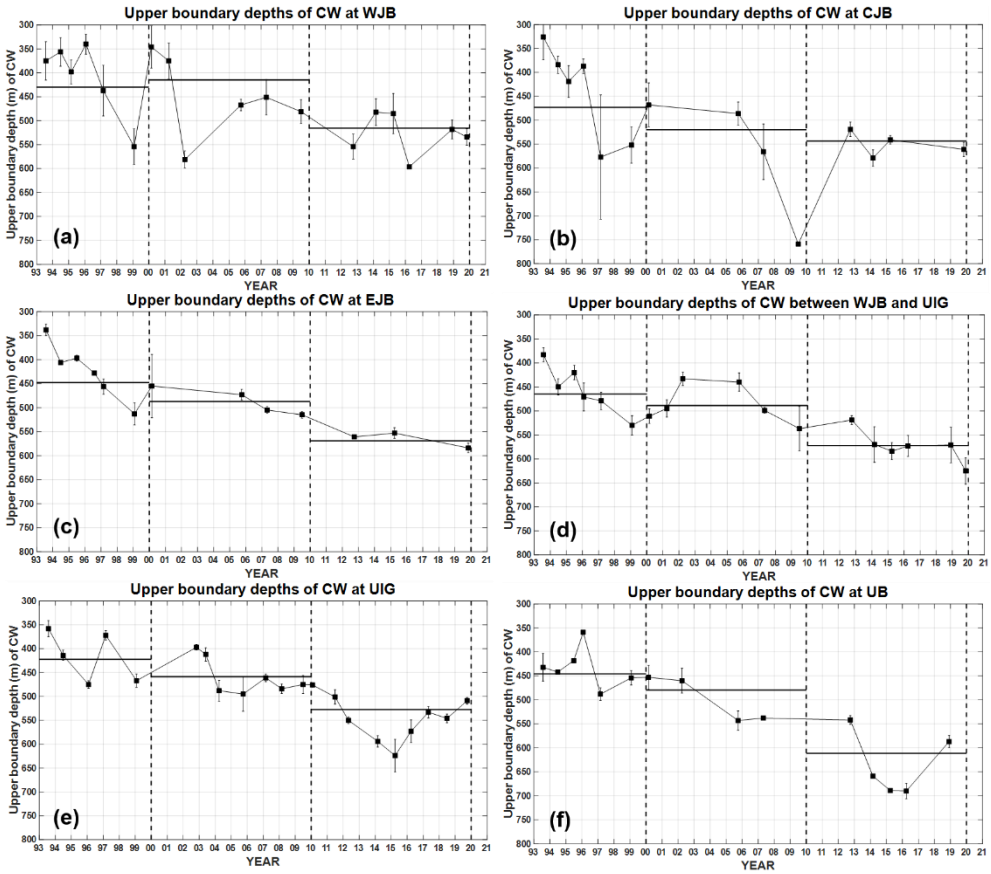

Figure. 3.4. Annual-mean upper boundary depth of CW at (a) WJB, (b) CJB, (c) EJB, (d) between WJB and UIG, (e) UIG, and (f) UB from 1993 to 2019. Black closed circles and vertical bars indicate annual-mean upper boundary depths of CW and the standard errors, respectively. The horizontal thick lines indicate decadal-mean upper boundary depths of CW in the 1990s, 2000s, and 2010s.

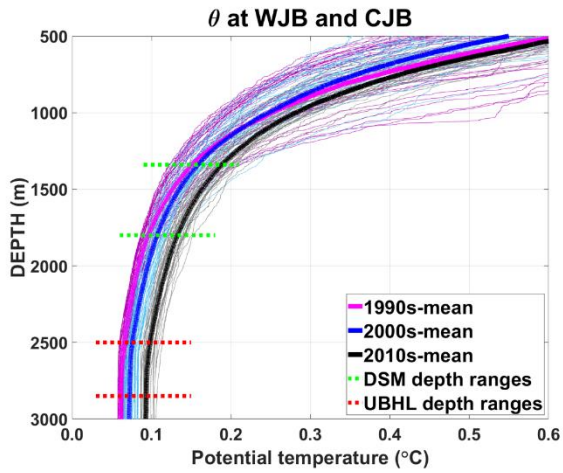

Figure. 3.5. Vertical potential temperature profiles at WJB and CJB from 1993 to 2019. Thin magenta, blue, and black lines represent the salinity profiles in the 1990s, 2000s, and the 2010s, respectively. Thick magenta, blue, and black lines indicate the decadal-mean of the 1990s, 2000s, and the 2010s, respectively. The horizontal dotted green and red lines represent depth ranges of DSM and UBHL from 1993 to 2019, respectively.

Table 3.1. Basic statistics of decadal-mean of upper boundary depth of CW, depth of DSM (D_{DSM}), potential temperature at DSM depth (θ_{DSM}), depth of UBHL (D_{UBHL}), potential temperature at UBHL depth (θ_{UBHL}) with standard errors in the East Sea in the 1990s, 2000s, 2010s, and their differences (2000s–1990s and 2010s–2000s). sWJB indicate the area between WJB and UIG.

Parameter	Area	1990s	2000s	2010s	2000s–1990s	2010s–2000s
Upper boundary depth of CW	WJB	430 ± 17	415 ± 20	516 ± 13	-15 ± 26	101 ± 24
	CJB	473 ± 25	520 ± 38	543 ± 10	47 ± 45	23 ± 39
	EJB	448 ± 15	487 ± 17	569 ± 8	39 ± 23	82 ± 19
	sWJB	465 ± 11	489 ± 11	572 ± 11	24 ± 16	83 ± 16
	UIG	422 ± 11	459 ± 7	528 ± 5	37 ± 13	69 ± 9
	UB	446 ± 11	480 ± 17	611 ± 16	34 ± 20	131 ± 23
	Total	**447 ± 6**	**475 ± 8**	**557 ± 5**	**28 ± 10**	**82 ± 9**
D_{DSM}	WJB	1522 ± 35	1573 ± 71	1626 ± 69	51 ± 79	53 ± 99
	CJB	1589 ± 53	1654 ± 95	1641 ± 60	65 ± 109	-13 ± 112
	EJB	1545 ± 12	1524 ± 89	1768 ± 133	-21 ± 90	244 ± 160
	sWJB	1457 ± 24	1477 ± 95	1609 ± 35	20 ± 98	132 ± 101
	UIG	1403 ± 13	1431 ± 56	1702 ± 56	28 ± 57	271 ± 79
	UB	1328 ± 22	1404 ± 168	1795 ± 87	76 ± 169	391 ± 189
	Total	**1474 ± 12**	**1511 ± 42**	**1690 ± 32**	**37 ± 44**	**179 ± 53**
θ_{DSM}	WJB	0.1189±0.0015	0.1316±0.0082	0.1534±0.0040	0.0127±0.0083	0.0218±0.0091
	CJB	0.1122±0.0031	0.1262±0.0059	0.1483±0.0024	0.0140±0.0067	0.0221±0.0064
	EJB	0.1150±0.0017	0.1396±0.0079	0.1413±0.0070	0.0246±0.0081	0.0017±0.0106
	sWJB	0.1194±0.0034	0.1369±0.0114	0.1504±0.0020	0.0175±0.0119	0.0135±0.0116
	UIG	0.1228±0.0011	0.2866±0.0304	0.3940±0.1046	0.1638±0.0304	0.1074±0.1089
	UB	0.1295±0.0024	0.1358±0.0203	0.1415±0.0083	0.0063±0.0204	0.0057±0.0219
	Total	**0.1196±0.0010**	**0.1595±0.0067**	**0.1882±0.0175**	**0.0399±0.0068**	**0.0287±0.0187**
D_{UBHL}	WJB	2667 ± 23	2605 ± 45	2729 ± 29	-62 ± 51	124 ± 54
	CJB	2646 ± 37	2569 ± 31	2622 ± 22	-77 ± 48	53 ± 38
	EJB	2507 ± 31	2530 ± 9	2527 ± 15	23 ± 32	-3 ± 17
	sWJB	2355 ± 31	2307 ± 17	2408 ± 22	-48 ± 35	101 ± 28
	Total	**2544 ± 14**	**2503 ± 14**	**2572 ± 11**	**-41 ± 20**	**69 ± 18**
θ_{UBHL}	WJB	0.0628±0.0012	0.0734±0.0027	0.0938±0.0017	0.0106±0.0030	0.0204±0.0038
	CJB	0.0611±0.0011	0.0753±0.0035	0.0928±0.0034	0.0142±0.0037	0.0175±0.0049
	EJB	0.0613±0.0011	0.0740±0.0044	0.0938±0.0045	0.0127±0.0045	0.0198±0.0062
	sWJB	0.0648±0.0017	0.0763±0.0027	0.0974±0.0022	0.0115±0.0032	0.0211±0.0038
	Total	**0.0625±0.0006**	**0.0748±0.0017**	**0.0944±0.0016**	**0.0123±0.0018**	**0.0196±0.0024**

3.3. Decadal variation of physical characteristics of the deep waters from 1993 to 2019

The physical characteristics of the deep waters at a depth of over 1000 m in the study area show clear decadal changes (Figure 3.6). The potential temperature increased by about 0.01 ℃ from the 1990s to the 2000s, while it increased by about 0.02 ℃ from about 1500 m to about 3000 m, and the potential temperature increased by about 0.04 ℃ as the water depth decreased from 1500 m to 1000 m from the 2000s to the 2010s (Figure 3.6c). The salinity increased by about 0.002 psu from 1000 m to the bottom from the 1990s to the 2000s, but the salinity in the 2010s do not show a significant difference from the 2000s (Figure 3.6f). The potential density increased by about 0.0018 kg m^{-3} from 1000 m to the bottom from the 1990s to the 2000s, while the potential density in the 2010s decreased by about 0.001 kg m^{-3} from 1500 m to 1000 m, and the potential density in the 2010s decreased by about 0.0025 kg m^{-3} from 1500 m to 1000 m from the 2000s (Figure 3.6i).

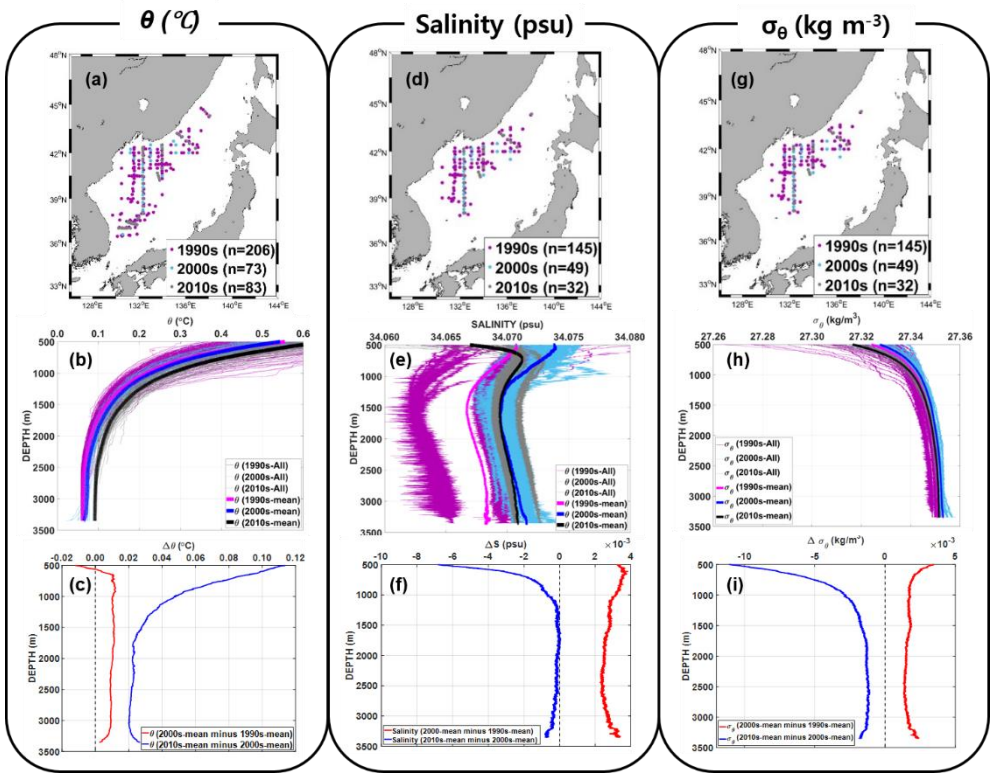

Figure. 3.6. Vertical distributions of potential temperature, salinity, and potential density in the areas including JB, between WJB and UIG, UIG, and UB. (a, d, g) Station maps of potential temperature, salinity, and potential density. Magenta, cyan, and gray colored closed circles indicate stations occupied in the 1990s, 2000s, and 2010s. The value of n in parentheses indicate sample numbers. (b, e, h) Vertical distributions of potential temperature, salinity, and potential density. Magenta, cyan, and gray thin and thick lines represent each profiles at each station and decadal-mean profiles in the 1990s, 2000s, and 2010s. (c, f, i) Differences of decadal-mean vertical profiles of potential temperature, salinity, and potential density. Red and blue thick lines indicate 2000s-mean minus 1990s-mean and 2010s-mean minus 2000s-mean, respectively.

4. Discussion

4.1. Comparison between the quatorward volume transports of the deep waters below 1500 m in western UIG (VT_{15}) and zonal geostrophic flows below 1500 m in the latitude of 38–39 °N along the baseline

The variation of VT_{15} can be explained by the deep transports obtained through the zonal-directional geostrophic flow below 1500 m in the latitude of 38–39 °N along the meridional baseline (represented by a thick pale yellow line in Figure 2.1). The amount of geostrophic flow in the zonal direction passing through the depth below 1500 m in the 38–39 °N latitude range obtained at five observation periods (Feb. 1999, Apr. 2001, Oct. 2005, Apr. 2015, and Apr. 2016) was -0.150 Sv, 0.210 Sv, -0.090 Sv, -0.250 Sv, and 0.014 Sv for the level of no motion with 1000 m, and 0.020 Sv, -0.150 Sv, 0.005 Sv, 0.050 Sv, and 0.002 Sv for the level of no motion with maximum depth (Figures 4.1, 4.2, and 4.3). The VT_{15} for the same periods was -0.15 Sv, -0.02, -0.07, -0.33, and 0.02, showing a closer correlation (R=0.8) with the zonal geostrophic flows with a level of no motion at 1000 m rather than the zonal geostrophic flows with a level of no motion at the maximum depth (R=-0.6). This means that when isopycnal over 27.349 kg m^{-3} sloped up equatorward below 1500 m in the 38–39 °N latitude, eastward zonal geostrophic flows are dominant, resulting in an increase of equatorward VT_{15}. However, it is essential to find the long-term average to know the long-term fluctuation of VT_{15} because it differs significantly from the annual change of the volume transport of the deep waters below 1500 m through the western UIG the six months before and after each observation period. (Figure 4.4).

The range of latitude 38–39 °N is determined because the variation in deep water transports in the zonal direction between these latitudes is closely related to

the amount of VT_{15} considering the deep and abyssal circulation path (Figure 1.1). The level of no motion for the geostrophic flow in the zonal direction passing blow the depth of 1500 m in the range of 38–39 °N along the meridional baseline was set to a depth of 1000 m, and the maximum depth (5 m above the bottom) because the horizontal slope of the isopycnal is the flattest and a no-slip boundary condition for the bottom, respectively.

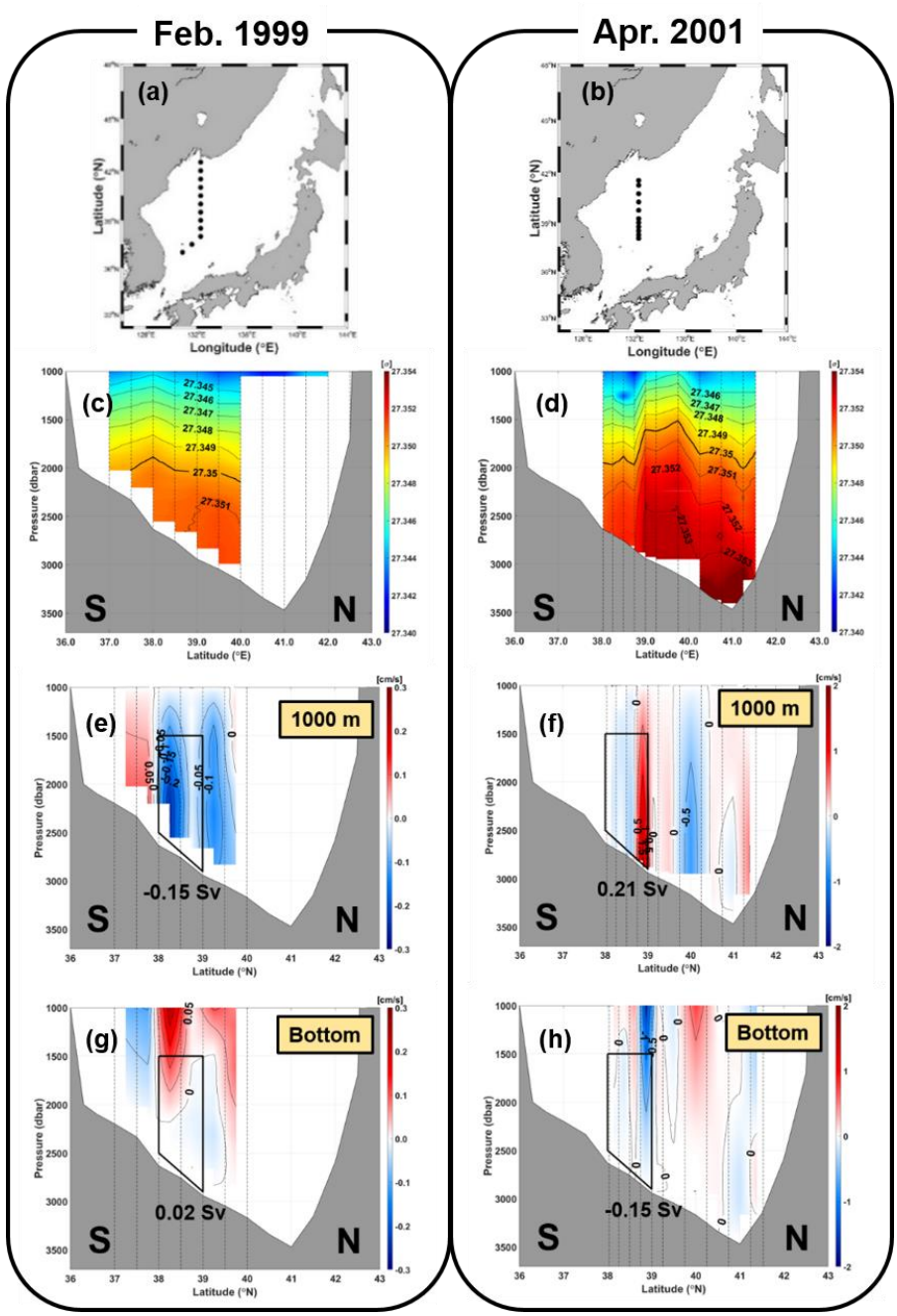

Figure. 4.1. Cross-section of (c, d) potential density (a, b) along the 132.3 °E meridional line and zonal (perpendicular to the cross-section of potential density) geostrophic current with a level of no motion (e, f) at 1000 m and (g, h) bottom depth in February 1999 and April 2001. The areas inside trapezoids in (e)-(h) are used to calculate the geostrophic transport passing through the area. The positive (negative) sign of the geostrophic transport indicates westward (eastward) direction.

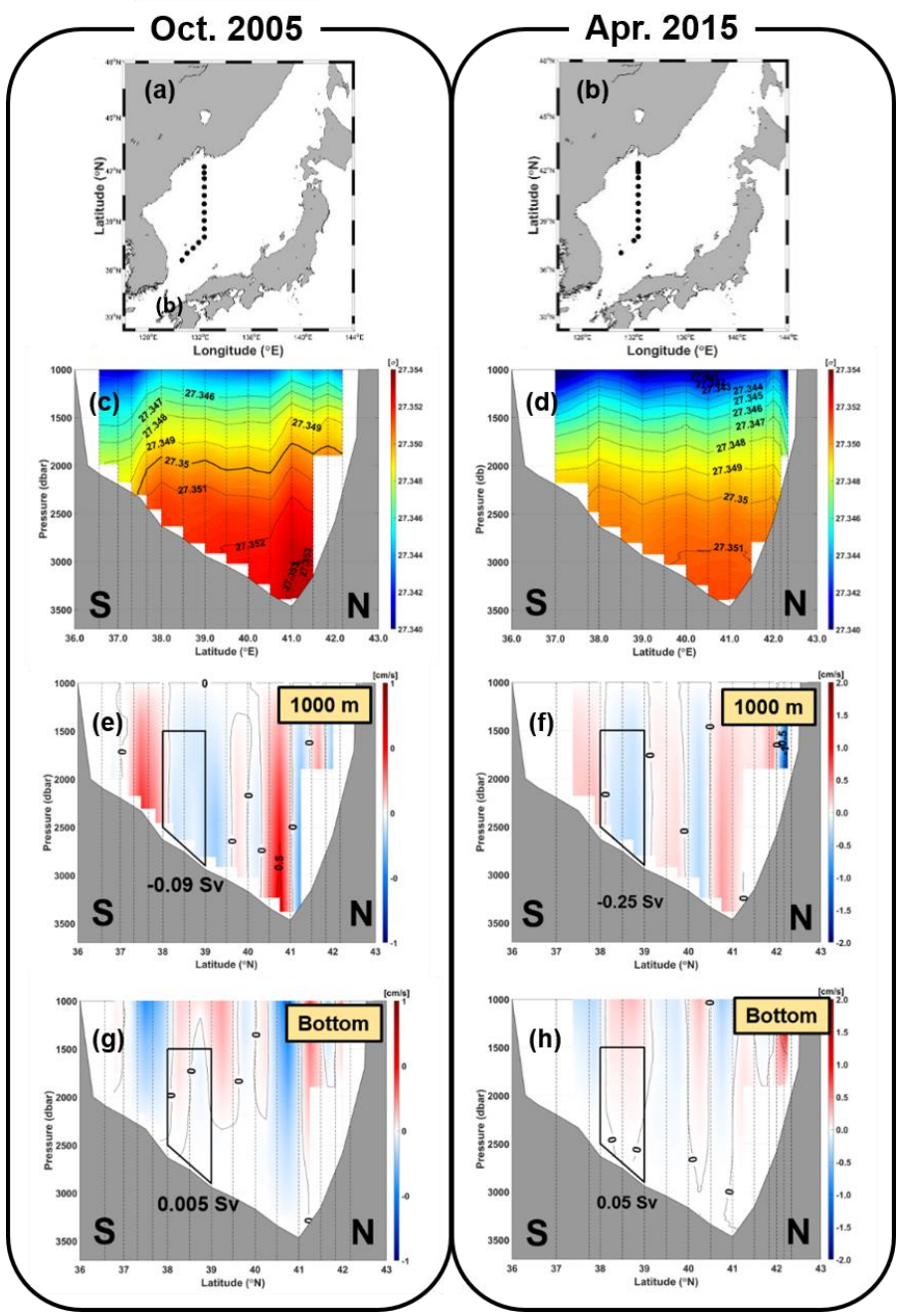

Figure. 4.2. Cross-section of (c, d) potential density (a, b) along the 132.3 °E meridional line and zonal (perpendicular to the cross-section of potential density) geostrophic current with a level of no motion (e, f) at 1000 m and (g, h) bottom depth in October 2005 and April 2015. The areas inside trapezoids in (e)-(h) are used to calculate the geostrophic transport passing through the area. The positive (negative) sign of the geostrophic transport indicates westward (eastward) direction.

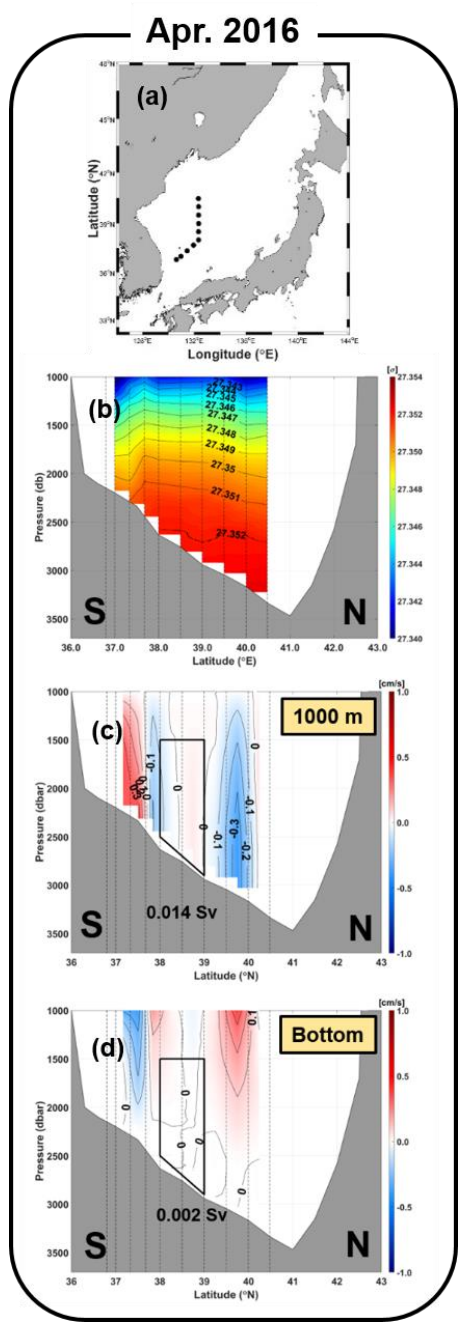

Figure. 4.3. Cross-section of potential density along the 132.3 °E meridional line and zonal (perpendicular to the cross-section of potential density) geostrophic current with a level of no motion at 1000 m and bottom depth in April 2016. The areas inside trapezoids in (e)-(h) are used to calculate the geostrophic transport passing through the area. The positive (negative) sign of the geostrophic transport indicates westward (eastward) direction.

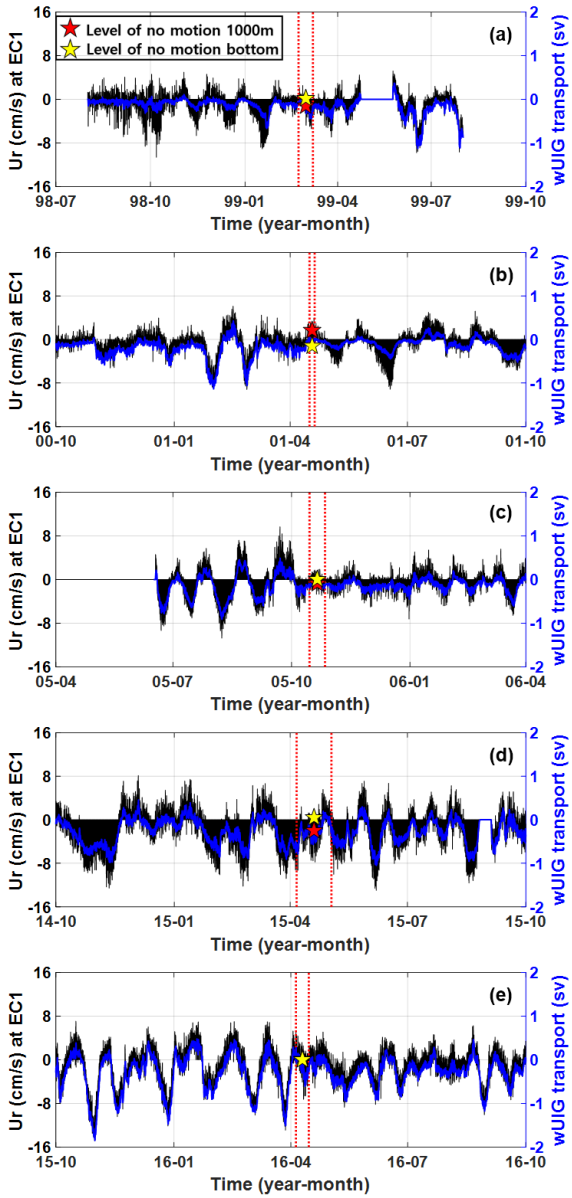

Figure. 4.4. Geostrophic transports passing through the area below 1500 m in the range of 38–39 °N (represented by a trapezoid in Figures 4.1 to 4.3) with a level of no motion at 1000 m (represented by red stars) and bottom depth (represented by yellow stars) in February 1999, April 2001, October 2005, April 2015, and April 2016 together with Ur at EC1 and wUIG transports for a period of 6 months before and after the time of calculating the geostrophic transport. The positive (negative) sign represents equatorward (poleward) direction for Ur at EC1 and wUIG transport, and eastward (westward) direction for the geostrophic transport. Vertical red dotted lines indicate the shipboard hydrographic observation periods.

4.2. Decadal changes of the volume of the deep waters in relation to decadal changes in the quatorward volume transport of the deep waters below 1500 m in western UIG (VT_{15}) from the 1990s to the 2010s

Deep waters transported below 1500 m through the western UIG consisted only of the DW from the late 1990s to the 2000s, whereas the deep waters transported below 1500 m through the western UIG consisted of the CW and DW in the 2010s, resulting from expanding the CW deeply down (Figure 4.5). The increase in the volume transports of the equatorward VT_{15} from 0.14 Sv in the late 1990s to 0.23 Sv in the 2010s is related to the deep expansion of the CW (Figure 3.1). Considering that the DSM, the lower boundary depth of the CW, has deepened from 1474 m in the 1990s to 1511 m in the 2000s and 1690m in the 2010s (Figure 4.6 and Table 3.1), it can be seen that the CW has been expanded in depth throughout the East Sea during this period. Considering that the increase in the upper boundary depth of CW, which averaged the entire observation area, was 110 m (from 447 m in the 1990s to 475 m in the 2000s and 557 m in the 2010s), about half of the increase in DSM depth (216 m) during the period, it can be seen that the vertical volume of the CW continued to increase from the 1990s to the 2010s.

The vertical volume of the CW (DW) continued to increase (decrease) from the 1990s to the 2010s, while the vertical volume of the BW increased slightly in the 2000s and then decreased again in the 2010s (Figure 4.6). This means that the BW formation strengthened from the 1990s to the 2000s and weakened again from the 2000s to the 2010s, while the CW formation continued to strengthen from the 1990s to the 2010s, which is a different result from previous studies. According to Yoon et al. (2018), the BW formation has prevailed, while the CW formation has weakened since the 2000s, and the volume of the deep waters has not changed significantly

from the 2000s to the 2010s. In Kang et al. (2003), the UBHL depth was considered 2900 m in the 2010s, but in this study, the UBHL depth was about 2570 m in the 2010s, and the BW's vertical volume did not decrease significantly. However, as Kang et al. (2003) reported, the CW penetrates deeper from the 1980s to the 2040s; this study also shows that the CW penetrates deeper from the 1990s to the 2010s. Although the vertical volume of the BW may be repeated depending on the BW formation event, the vertical volume of the CW continue to expand deeply in the future, and follow-up studies on the CW and BW formation processes are expected to be needed in the future.

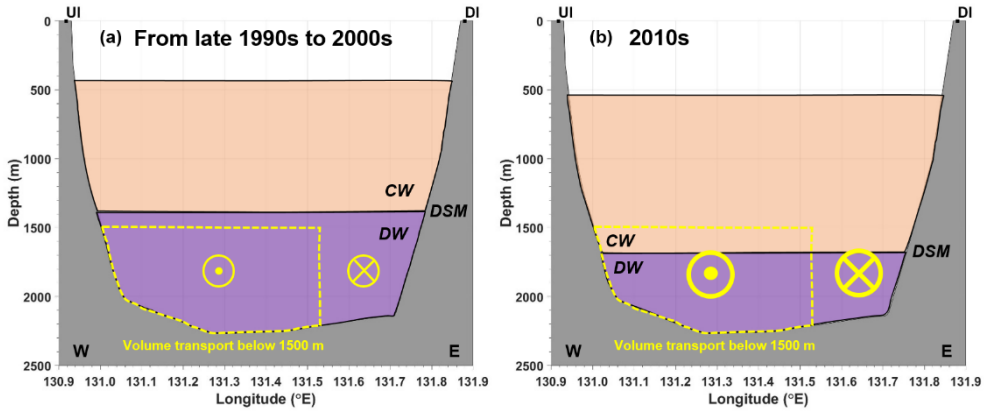

Figure. 4.5. Schematic of the decadal changes in the deep waters occupying the Ulleung Interplain Gap (UIG) and the strength of equatorward and poleward transports in the western and eastern UIG. The amount of transports passing through the cross-sectional area in the yellow dotted line means VT_{15}. The 'W' and 'E' in the lower left and right corners represent the west and the east direction. The yellow open circle with dot (cross) indicate the equatorward (poleward) transport, and the thick open circles with dot and cross in the (b) panel represent the increased volume transport.

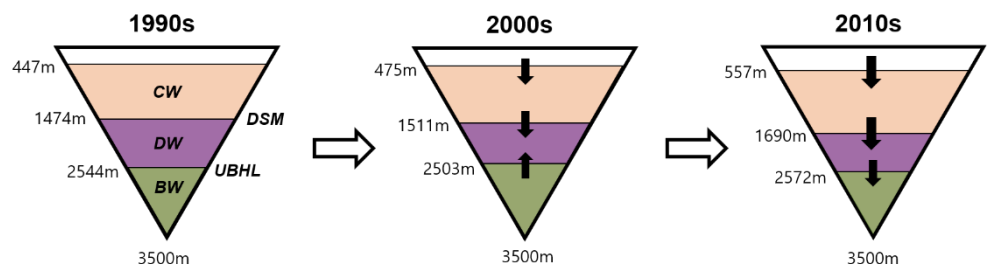

Figure. 4.6. Schematic of decadal changes in the volume of the deep water masses (CW, DW, and BW) from the 1990s to the 2000s and from the 2000s to the 2010s. Upward and downward black closed arrows at the boundary between the deep water masses indicate the shallowing and deepening of the boundary depth.

4.3. Decadal changes in the physical characteristics of the deep waters from the 1990s to the 2010s

The increase rate of the decadal-mean potential temperature at the UBHL of the East Sea overall shows a rapid increase in the 2010s than the rate before the 2000s. The increase in potential temperature of the deep waters deeper than 2500 m in EJB has increased by about 0.011–0.012 ℃ per decade from the 1970s to the 2000s (Gamo et al., 2014), and in this study, the increase rate of the decadal-mean potential temperature at the UBHL of the EJB from the 1990s to the 2000s was about 0.013 ℃ (Table 3.1). In the results of Chen et al. (1999), the increase in potential temperature at a depth of 3000 m increased by about 0.05 ℃ over the 50 years (0.01 ℃ per decade) from 1950 to 1996. However, this study shows that the decadal-mean potential temperature at the UBHL of the East Sea rose 0.02 ℃ from the 2000s to the 2010s, about 1.6 times higher than the increase rate in potential temperature of the deep waters deeper than 2500 m from the 1950s to the 2000s. The rapid increase in potential temperature of the deep waters in the East Sea in the 2010s seems to be due to the rapid increase in the surface water temperature of the East Sea in the 2010s compared to the 2000s, which is related to climate change in association with abnormal Arctic warming and the heat-dome phenomena in East Asia in recent years (Han and Lee, 2020).

Decadal-mean salinity of the deep waters below 1000 m increased by about 0.002 psu from the 1990s to the 2000s, while there was no significant change in salinity from the 2000s to the 2010s. The rise in decadal-mean salinity of the deep waters in the 2000s seems to be that evaporation occurs more actively than precipitation in deep water formation area, and surface salinity increases due to

horizontal salt flux by the Tsushima Warm Water recirculation and brine rejection by severe surface cooling (Talley et al., 2003; Yoon et al., 2018; Han et al., 2020). However, in the 2010s, precipitation was more dominant than evaporation and warming was more dominant than surface cooling (Yoon et al., 2018), so the supply of high salinity surface water to the deep waters was limited, so there seems to be no significant change in deep salinity. Follow-up studies are needed on the cause of the change in the physical characteristics of the deep waters in the East Sea on decadal timescales.

5. Conclusion

The physical characteristics of the deep waters in the JB, UB, and the UIG from 1993 to 2019 were investigated in this study as well as the decadal changes in the volume transports of the deep waters below 1500 m through the western UIG from 1997 to 2019 using subsurface mooring current data through the UIG from 1997 to 2019 and hydrographic data in the JB, UB, and UIG from 1993 to 2019. The main results of this study are summarized as follows.

(1) Long-term variation of the volume transports of the deep waters below 1500 m through the western UIG (VT_{15}) from 1997 to 2019 were investigated for the first time in this study. It was found that the VT_{15} was on a increasing trend by 0.0050 Sv yr^{-1} in the equatorward direction. Decadal-mean equatorward VT_{15} was about 0.04 ± 0.02 Sv larger in the 2000s (0.18 ± 0.01 Sv) than in the late 1990s (0.14 ± 0.02 Sv) and about 0.05 ± 0.02 Sv larger in the 2010s (0.23 ± 0.02 Sv) than in the 2000s (0.18 ± 0.01 Sv).

(2) It was discovered that the deep waters transported by the equatorward VT_{15} consisted of only DW until the 2000s, but it consisted of CW and DW in the 2010s, based on the fact that the depth of DSM in the UIG extends from 1474 m in the 1990s to 1511 m in the 2000s and 1690 m in the 2010s. The increasing equatorward VT_{15} appears to be related to the CW's expansion to below 1500 m, but a follow-up study is needed for this part.

(3) The boundary depth distribution of the deep waters, which averaged the study sea area, shows that the UBD_{CW} (D_{DSM}) continued to increase from 447m (1474 m) in the 1990s to 475m (1511 m) in the 2000s, and to 557m (1690 m) in the 2010s,

while the D_{UBHL} decreased from 2544 m in the 1990s to 2503m in the 2000s, and again increased to 2572 m in the 2010s. As a result, the vertical range of the CW continued to increase from 1027 m in the 1990s to 1036 m in the 2000s and 1133 m in the 2010s, while the vertical range of the DW gradually decreased from 1070 m in the 1990s to 992 m in the 2000s and 882 m in the 2010s. On the other hand, the vertical range of the BW was expanded from 956 m in the 1990s to 997 m in the 2000s, and then reduced to 928 m in the 2010s. Vertical fluctuations in the volume of the deep waters are attributed to the fact that the BW formation strengthened from the 1990s to the 2000s and weakened again from the 2000s to the 2010s, while the CW formation continued to strengthen from the 1990s to the 2010s

(4) The potential temperature increased by about 0.01 ℃ from the 1990s to the 2000s, while it increased by about 0.02 ℃ from about 1500 m to about 3000 m, and the potential temperature increased by about 0.04 ℃ as the water depth decreased from 1500 m to 1000 m from the 2000s to the 2010s. This study shows that the decadal-mean potential temperature at the UBHL of the East Sea rose 0.02 ℃ from the 2000s to the 2010s, about 1.6 times higher than the increase rate in potential temperature of the deep waters deeper than 2500 m from the 1950s to the 2000s (Chen et al., 1999; Gamo et al., 2014). The rapid increase in potential temperature of the deep waters in the East Sea in the 2010s seems to be due to the rapid increase in the surface water temperature of the East Sea in the 2010s compared to the 2000s, which is related to climate change in association with abnormal Arctic warming and the heat-dome phenomena in East Asia in recent years (Han and Lee, 2020).

(5) The salinity increased by about 0.002 psu from 1000 m to the bottom from the 1990s to the 2000s, but the salinity in the 2010s do not show a significant

difference from the 2000s. The rise in decadal-mean salinity of the deep waters in the 2000s seems to be that evaporation occurs more actively than precipitation in deep water formation area, and surface salinity increases due to horizontal salt flux by the Tsushima Warm Water recirculation and brine rejection by severe surface cooling (Talley et al., 2003; Yoon et al., 2018; Han et al., 2020).

(6) The potential density increased by about 0.0018 kg m^{-3} from 1000 m to the bottom from the 1990s to the 2000s, while the potential density in the 2010s decreased by about 0.001 kg m^{-3} from 1500 m to 1000 m, and the potential density in the 2010s decreased by about 0.0025 kg m^{-3} from 1500 m to 1000 m from the 2000s.

The decadal changes in the volume transports of the deep waters below 1500 m through the western UIG and the physical characteristics of the deep waters in the East Sea are shown in this study. However, many questions still need to be addressed in future research. First, it is necessary to clarify why the CW formation continues to increase from the 1990s to the 2010s regardless of the increase of the BW formation from the 1990s to the 2000s and then decreasing again in the 2010s. Previous studies describe the BW formation and the CW formation as an alternative event: when the BW formation prevails, CW formation weakens, and when the BW formation weakens, CW formation prevails. However, in this study, considering that the CW formation continues to increase regardless of changes in BW formation, it is necessary to modify the concept of dividing the East Sea meridional overturning circulation into one-cell (enhanced BW formation) and two-cell (enhanced CW formation) in the past in consideration of the complex formation of the CW and the BW.

To comprehensively understand the long-term changes in the physical characteristics of the deep waters in the East Sea, it is necessary to study how and why sea surface temperature and sea surface salinity conditions that affect the surface density in the CW and BW formation areas are changing over long times. In particular, a follow-up study is needed on why the increase in the potential temperature of the deep waters from the 2000s to the 2010s has increased about twice as much as that of the deep waters from the 1990s to the 2000s. Since the sea surface salinity changes in deep water formation area have a significant impact on the sea surface density and the resulting deep water formation, follow-up studies are needed on how and why the conditions of the sea surface salinity changes (freshwater and heat fluxes, sea-ice formation, recirculation of the Tsushima Warm Water) vary over long times.

References

Chang, K. I., Hogg, N. G., Suk, M. S., Byun, S. K., Kim, Y. G., & Kim, K. (2002). Mean flow and variability in the southwestern East Sea. *Deep Sea Research Part I: Oceanographic Research Papers*, *49*(12), 2261–2279.

Chang, K. I., Teague, W. J., Lyu, S. J., Perkins, H. T., Lee, D.-K., Watts, D. R., et al. (2004). Circulation and currents in the southwestern East/Japan Se a: Overview and review. *Progress in Oceanography*, *61*(2–4), 105–156.

Chang, K. I., Kim, K., Kim, Y. B., Teague, W. J., Lee, J. C., & Lee, J. H.(20 09). Deep flow and transport through the Ulleung Interplain Gap in the sou thwestern East/Japan Sea. *Deep Sea Research Part I: Oceanographic Resear ch Papers*, *56*(1), 61–72.

Chang, K. I. (2016). Temporal variation of deep water transport in the southwes tern East/Japan Sea. *American Geophysical Union*, *2016*, PO31A-03.

Chen, C. T. A., Bychkov, A. S., Wang, S. L., & Pavlova, G. Y. (1999). An an oxic Sea of Japan by the year 2200?. *Marine Chemistry*, *67*(3-4), 249-265.

Choi, A. R., Park, Y. G., Min, H. S., & Kim, K. H. (2009). The Improvement of CTD Data through Post Processing. *Ocean and Polar Research*, *31*(4), 33 9–347.

Choi, Y. J., & Yoon, J. H. (2010). Structure and seasonal variability of the dee p mean circulation of the East Sea (Sea of Japan). *Journal of oceanography , 66*, 349-361.

Clayson, C. A., & Luneva, M. (2004). Deep convection in the Japan (East). Se a: A modeling perspective. *Geophysical Research Letters*, *31*(17).

Consortium for Ocean Leadership (2013) Protocols and Procedures for OOI. Dat a Products: QA, QC, Calibration, Physical Samples. Version 1.22. Washingt on DC, Consortium for Ocean Leadership for Ocean Observatories Initiative , 32pp. and 43pp. Appendices.

Gamo, T., Nakayama, N., Takahata, N., Sano, Y., Zhang, J., Yamazaki, E., et a l (2014). The Sea of Japan and its unique chemistry revealed by time-serie s observations over the last 30 years. *Monographs on Environment, Earth a nd Planets*, *2*(1), 1–22.

Han, M., Cho, Y. K., Kang, H. W., & Nam, S. (2020). Decadal changes inmeri dional overturning circulation in the East Sea (Sea of Japan). *Journal of Ph ysical Oceanography*, *50*(6), 1773–1791.

Han, M., Chang, Y. S., Kang, H. W., Kang, D. J., & Kim, Y. S. (2021). Turn over time of the East Sea (Sea of Japan) meridional overturning circulation . *Frontiers in Marine Science*, *8*.

Han, I. S., & Lee, J. S. (2020). Change the annual amplitude of sea surface te mperature due to climate change in a recent decade around the Korean Pen insula. *J. Korean Soc. Mar. Environ. Saf*, *26*, 233-241.

Kang, D. J., Park, S., Kim, Y. G., Kim, K., & Kim, K. R. (2003). A moving-boundary box model (MBBM) for oceans in change: An application to the East/Japan Sea. *Geophysical Research Letters*, *30*(6).

Kim, K., Kim, K. R., Kim, Y. G., Cho, Y. K., Chung, J. Y., Choi, B. H., et a

l. (1996). New findings from CREAMS observations: water masses and edd ies in the East Sea. *Journal of the Korean Society of Oceanography*, 31(4), 155-163.

Kim, K. R., & Kim, K. (1996). What is happening in the East Sea (Japan Sea) ?: Recent chemical observations during CREAMS 93-96. *Journal of the Ko rean Society of Oceanography*, 31(4), 164-172.

Kim, K., Cho, Y. K., Ossi, H., & Kim, Y. G. (2000). CTD data processingfor CREAMS expeditions: Thermal-lag correction of Sea-Bird CTD. *Journal of t he Korean Society of Oceanography*, *35*(4), 192–199.

Kim, K., Kim, K. R., Kim, Y. G., Cho, Y. K., Kang, D. J., Takematsu, M., et al. (2004). Water masses and decadal variability in the East Sea (Sea of Ja pan). *Progress in Oceanography*, *61*(2–4), 157–174.

Kim, Y. B., Chang, K. I., Park, J. H., & Park, J. J. (2013). Variability of the dokdo abyssal current observed in the Ulleung Interplain Gap of the East/ Japan Sea. *Acta Oceanologica Sinica*, *32*(1), 12–23.

Kim, B. G., Cho, Y. K., & Noh, Y. (2022). Deep Convection Along the Contin ental Slope in the East/Japan Sea: A Large-Eddy Simulation Study. *Physics and Biogeochemistry of the East Asian Marginal Seas*.

Lee, K., NAM, S., & KIM, Y. G. (2019). Statistical characteristics of east sea mesoscale eddies detected, tracked, and grouped using satellite altimeter da ta from 1993 to 2017. *The Sea: Journal of the Korean Society of Oceano graphy*, *24*(2), 267–281.

LEE, H., & NAM, S. (2023). Studies on Changes in the Hydrography and Circ ulation of the Deep East Sea (Japan Sea) in a Changing Climate: Status a nd Prospectus. *The Sea Journal of the Korean Society of Oceanography*, *28* (1), 1-18.

McDougall, T. J., & Barker, P. M. (2011). Getting started with TEOS-10 and t he Gibbs Seawater (GSW) oceanographic toolbox. Scor/Iapso WG, *127*, 1-28.

Mensah, V., Le Menn, M., & Morel, Y. (2009). Thermal mass correction for th e evaluation of salinity. *Journal of Atmospheric and Oceanic Technology*, *2 6*(3), 665–672.

Morison, J., Andersen, R., Larson, N., D'Asaro, E., & Boyd, T. (1994). The cor rection for thermal-lag effects in Sea-Bird CTD data. *Journal of Atmospher ic and Oceanic Technology*, *11*(4), 1151–1164.

Min, D. H., & Warner, M. J. (2005). Basin-wide circulation and ventilation. stu dy in the East Sea (Sea of Japan) using chlorofluorocarbon tracers. *Deep S ea Research Part II: Topical Studies in Oceanography*, *52*(11–13), 1580–16 16.

Senjyu, T., Shin, H. R., Yoon, J. H., Nagano, Z., An, H. S., Byun, S. K., et al . (2005). Deep flow field in the Japan/East Sea as deduced from direct cu rrent measurements. *Deep Sea Research Part II: Topical Studies in Oceano graphy*, *52*(11–13), 1726–1741.

Shin, J., Noh, S., & Nam, S. (2020). Intraseasonal abyssal current variabilityof bottom-trapped topographic Rossby Waves in the Southwestern East Sea (J

apan Sea). *Frontiers in Marine Science*, *916*.

Talley, L. D., Lobanov, V., Ponomarev, V., Salyuk, A., Tishchenko, P., Zhabin, I., et al. (2003). Deep convection and brine rejection in the Japan Sea. *Ge ophysical Research Letters*, *30*(4).

Talley, L. D., Min, D. H., Lobanov, V., Luchin, V., Ponomarev, V., SalyukA., et al. (2006). Japan/East Sea water masses and their relation to thesea's ci rculation. *Oceanography*, *19*(3), 32–49.

Teague, W. J., Tracey, K. L., Watts, D. R., Book, J. W., Chang, K. I., Hogan, P. J., et al. (2005). Observed deep circulation in the Ulleung Basin. *Deep Sea Research Part II: Topical Studies in Oceanography*, *52*(11–13), 1802–1826.

Tsunogai, S., Kawada, K., Watanabe, S., & Aramaki, T. (2003). CFC indicating renewal of the Japan Sea deep water in winter 2000–2001. *Journal of oce anography*, *59*, 685-693.

Uda, M. (1934). The results of simultaneous oceanographic investigations in. the Japan Sea and its adjacent waters in May and June, 1932. *Journal of Im perial Fishery Experimental Stations*, *5*, 57–190.

Yanagimoto, D., & Taira, K. (2003). Current measurements of the Japan Sea pr oper water and the intermediate water by ALACE floats. *Journal of ocean ography*, *59*, 359-368.

Yoon, S. T., Chang, K. I., Nam, S., Rho, T., Kang, D. J., Lee, T., et al. (2018). Re-initiation of bottom water formation in the East Sea (Japan Sea) in a warming world. *Scientific Reports*, *8*(1), 1–10.

Abstract in Korean

동해 자오면 순환 경로의 주요 길목 중 하나인 독도와 울릉도 사이의 심층 수송 통로인 울릉해저간극에서의 남북 방향 심층 수송량과 심층 해수의 물리적 특성 변화는 동해 전체 자오면 순환의 변화를 이해하는데 있어 매우 중요하다. 특히, 울릉해저간극의 서쪽 해역은 해저지형효과에 의한 심층 순환 경로를 고려했을 때 일분 분지로부터 울릉 분지로 유입하는 심층 수송량의 변화를 살펴보기에 매우 적합한 해역이다. 이 연구에서는 울릉해저간극 서쪽 해역의 1500m부터 2300m 수심 범위에서 심층 해수의 남북 방향 수송량과 일본 분지, 울릉 분지, 울릉해저간극에서 동해 심층 해수의 경계 수심과 물리적 특성의 10년 규모의 변화를 연구하였다.

이 연구에서는 1997년부터 2019년까지 울릉해저간극에서 수집된 아표층 계류 유속 자료와 1993년부터 2019년까지 일본 분지, 울릉 분지, 울릉해저간극에서 수집된 물리적 특성을 관측한 자료를 사용하였다. 1997년부터 2019년까지의 울릉해저간극 서쪽 해역의 수송량은 2002년 11월부터 2004년 4월까지 울릉해저간극에서 5개의 아표층 계류 유속 자료로 구한 울릉해저간극 서쪽 해역의 심층 수송량과 1997년부터 2019년까지 울릉해저간극의 한 가운데 위치한 EC1 정점에서의 수심 1800m 유속과의 상관관계를 통해 계산하였다.

울릉해저간극 서쪽 해역을 통해 일본 분지에서 울릉 분지로 수송되는 심층 해수 수송량은 1990년대 후반부터 2010년대까지 지속적으로 증가하였다. 이와 함께 수송되는 심층 해수는 심층 해수의 경계 수심인 심해염분최소층과 해저균질층상부수심 변화를 통해 2000년대까지는 심층수로만 구성되어 있던 반면, 2010년대는 중앙수의 비율이 증가하고 있음을 확인하였다.

일본 분지, 울릉 분지, 울릉해저간극의 심층 온위는 1990년대에서 2000년대로의 증가보다 2000년대에서 2010년대로의 증가가 2배 높아 심층 해수의 온난화가 최근 더욱 가속화 되었음을 확인하였다. 반면 심층

해수의 염분은 1990년대에서 2000년대에 증가한 후 2010년대에 다시 감소하였고, 염분 효과에 의해 2000년대 심층 해수의 밀도는 증가 후 2010년대 다시 감소하였다.

1990년대부터 2010년대까지 1500m에서 2300m 수심 범위에서의 심층 순환 강화는 일본 분지에서 울릉 분지로 뿐만 아니라 울릉 분지에서 야마토 분지로, 그리고 야마토 분지에서 일본 분지로까지 강화될 수 있고, 해당 수심 범위에서 심층수의 비율은 감소하고 중앙수의 비율은 증가할 수 있음을 시사한다. 또한 저층수 생성과는 별개로 중앙수 생성이 강화되고 있음을 확인하였고, 이는 향후 동해 자오면 순환이 저층수 생성에 의한 단일 순환보다는 이중 순환 또는 그 이상의 복잡한 순환 형태가 될 수 있음을 시사한다.

Appendix

Ⅰ. 기후변화에 따른 동해 심층 해수의 물리적 특성 및 순환 변화 연구: 현황과 전망 (Studies on changes in the hydrography and circulation of the deep East Sea (Japan Sea) in a changing climate: Status and Prospectus)

Abstract

동해는 전 세계적으로 가장 빠른 수준의 온난화를 경험하는 해역 중 하나로서, 기후변화에 민감하게 반응할 뿐 아니라 대양에 비해 월등히 짧은 순환 주기를 가지고 있기 때문에 미래의 대양 환경 변화에도 중요한 시사점을 주는 것으로 알려져 있다. 그러나 동해 심층 해수의 특성과 순환의 변화 과정에 대한 연구는 동해 전역의 심층을 정밀하게 조사하기 위한 국제협력 프로그램이 자리잡고, 측정 장비의 분해능을 포함하는 관측 기술과 수치모델 모의 능력이 크게 향상된 최근(1990년대 이후)에서야 본격화되고 있다. 여기서는 동해 심층 해수의 물리적 특성과 순환의 변화 과정에 대한 그간의 연구 결과를 요약하고, 향후 남은 과제를 제시하고자 한다. 동해는 내부에서 자체적으로 심층 해수가 생성되며 대양과 분리된 독특한 심층 순환 구조를 가진다. 동해의 수백 m 수심 아래에는 수온이 낮고(<1℃) 염분이 거의 일정(34.0-34.1)한 해수가 분포하기 때문에 오랜 기간 이 해수를 일본해고유수(동해고유수)로 명명된 단일 해수로 여겨왔다. 그러나 1990년대 이후 정밀한 관측이 이루어지며, 동해 심층을 채우고 있는 해수가 적어도 3개의 서로 다른 물리적 특성을 가진 해수(중앙수, 심층수, 저층수)로 구성됨이 밝혀졌다. 이들 3개 해수의 물리적 특성과 해수 사이의 경계 수심은 항상 일정한 것이 아니라, 지난 수십 년 동안 유의한 수준의 변화를 겪어왔다. 동해 북부 해역의 대마난류 재순환, 해양-대기 열과 담수의 교환량, 해빙 형성에 영향을 받는 대류(심층사면대류 및 심층외양대류) 과정에 따라 심층 해수 생성에 뚜렷한 차이가 발생 했기 때문이다. 생성된 심층 해수는 수심이 얕은 곳을 오른쪽에 두고 일본 분지에서부터 반시계 방향으로 울릉 분지, 야마토

분지를 차례로 거쳐 다시 일본 분지로 수송되며, 이 수평적인 심층 순환도 변화를 겪어 왔다. 수평적인 심층 순환은 동시에 남북 및 연직 방향의 순환(자오면 순환) 경로와 강도의 변화를 동반한다. 동해는 수천 년 규모의 순환 주기를 가지는 대양에 비해 훨씬 짧은 수백 년 혹은 그 이내의 순환 시간 규모를 가지기 때문에 동해 심층 해수의 물리적 특성과 자오면 순환의 급격한 변화를 더 뚜렷하게 볼 수 있을 것으로 기대 가능하다. 심층 및 자오면 순환 사이의 연계성, 대양과 동해의 유·출입, 해수 수송을 포함하는 동해 상층 순환과 심층 순환 사이의 연계성은 아직까지 잘 밝혀지지 않았다. 동해 심층 해수 수송의 경로와 강도를 지배하는 다양한 과정들에 대한 후속 연구들이 요구된다.

The East Sea, one of the regions where the most rapid warming is occurring, is known to have important implications for the response of the ocean to future climate changes because it not only reacts sensitively to climate change but also has a much shorter turnover time (hundreds of years) than the ocean (thousands of years). However, the processes underlying changes in seawater characteristics at the sea's deep and abyssal layers, and meridional overturning circulation have recently been examined only after international cooperative observation programs for the entire sea allowed in-situ data in a necessary resolution and accuracy along with recent improvement in numerical modeling. In this review, previous studies on the physical characteristics of seawater at deeper parts of the East Sea, and meridional overturning circulation are summarized to identify any remaining issues. The seawater below a depth of several hundreds of meters in the East Sea has been identified as the Japan Sea Proper Water (East Sea Proper Water) due to its homogeneous physical properties of a water temperature below 1°C and practical salinity values ranging from 34.0 to 34.1. However, vertically high-resolution salinity and dissolved oxygen observations since the 1990s enabled us to separate the water into at least three different water masses (central water, CW; deep water, DW; bottom water, BW). Recent studies have shown that the physical characteristics and boundaries between the three water masses are not constant over time, but have significantly varied over the last few decades in association with time-varying water

formation processes, such as convection processes (deep slope convection and open-ocean deep convection) that are linked to the re-circulation of the Tsushima Warm Current, ocean-atmosphere heat and freshwater exchanges, and sea-ice formation in the northern part of the East Sea. The CW, DW, and BW were found to be transported horizontally from the Japan Basin to the Ulleung Basin, from the Ulleung Basin to the Yamato Basin, and from the Yamato Basin to the Japan Basin, respectively, rotating counterclockwise with a shallow depth on the right of its path (consistent with the bottom topographic control of fluid in a rotating Earth). This horizontal deep circulation is a part of the sea's meridional overturning circulation that has undergone changes in the path and intensity. Yet, the linkages between upper and deeper circulation and between the horizontal and meridional overturning circulation are not well understood. Through this review, the remaining issues to be addressed in the future were identified. These issues included a connection between the changing properties of CW, DW, and BW, and their horizontal and overturning circulations; the linkage of deep and abyssal circulations to the upper circulation, including upper water transport from and into the Western Pacific Ocean; and processes underlying the temporal variability in the path and intensity of CW, DW, and BW.

Keywords: Central water, Deep water, Bottom water, Deep circulation, East Sea

1. 서론

전 지구적인 수문 순환(hydrological cycle), 생지화학적 순환(biogeochemical cycle)과 열, 염, 물질 분배 및 재분배에 지대한 영향을 미치며 기후를 조절하는 대양의 자오면 순환(meridional overturning circulation; MOC)은 대양 심층 해수의 온난화(warming), 산성화(acidification), 탈산소화(deoxygenation)와 함께 변화를 겪고 있는 것으로 알려져 있다(Stouffer et al., 2006; Send et al., 2011; Levin and Le Bris, 2015). 특히 대서양 자오면 순환(Atlantic MOC)은 저위도 상층의 고온고염수를 고위도로 수송하고, 고위도에서 생성된 저온고염의 심층 해수를 저위도로 수송하며 남북 및 연

직 방향의 순환을 통해 열, 염, 물질 분배 및 재분배와 지구의 기후 시스템 조절에 중요한 역할을 담당한다(Srokosz et al., 2012). 그러나 대서양 자오면 순환은 기후변화에 따라 변동하는 것으로 확인되었으며, 대서양 심층 해수 수송량에도 유의한 수준의 증감 변동이 여러 시공간 규모로 나타나고 있음이 보고되었다(Bryden et al., 2005; Send et al., 2011; Jamet et al., 2020; Worthington et al., 2021). 기후변화가 심화되며 대양의 자오면 순환이 완전히 멈추지는 않겠지만 향후 100년 동안 지속 변동하며 심층 해수의 물리적 특성에도 지속적인 변화를 가져올 것으로 전망된다(Stouffer et al., 2006).

대양과 유사하게 자체적인 자오면 순환 시스템이 존재하는(Senjyu et al., 2002; Chang et al., 2004; Han et al., 2020) 동해는 '작은 대양(miniature ocean)'이라 불릴 정도로 대양과 유사한 특성을 보인다(Kim et al., 2004; Talley et al., 2006). 동해는 한-일-러로 둘러싸인 평균 수심 1667 m의 깊은 연해로서 북부, 남서부, 남동부 각각에 수심 2000 m 이상으로 깊은 총 3개 – 일본 분지(Japan Basin), 울릉 분지(Ulleung Basin), 야마토 분지(Yamato Basin) – 의 해저 분지가 존재한다. 수심이 150 m 내외로 얕고 폭이 비교적 좁은 4개의 해협(대한해협; Korea Strait, 쓰가루해협; Tsugaru Strait, 소야해협; Soya Strait, 타타르해협; Tatar Strait)을 통해서만 외해와 연결되기 때문에 동해는 대양과의 해수 교환이 매우 제한적인 반폐쇄성 해역(semi-enclosed sea)이다(Mooers et al., 2006; Gamo et al., 2014). 따라서 심층 해수가 외부로부터 유입하거나 외부로 유출되기 보다는, 내부에서 생성되어 순환하는 뚜렷한 자오면 순환 구조를 보인다(Figure I.1). 이러한 이유로 동해는 대양의 심층 해 수에 비해 수온이 낮고, 용존산소 농도가 높은 심층 해수로 채워져 있다(Figure I.2).

동해의 심층 해수는 1) 북서부 대륙붕 해역과 2) 북부 일본 분지 내외양 해역에서 생성되어 심층에서 수평적으로는 반시계 방향으로 회전하며 순환하는 것으로 알려져 있다(Figure I.1a). 동해 북서부 대륙붕 해역의 표층 해수는 겨울철이 되면 대기 냉각으로 수온이 낮아지고 해빙(sea ice) 형성 과정의 염분 방출(brine rejection 또는 brine injection) 등으로 염분이

높아져 밀도가 증가하는 것으로 알려져 있다(Talley et al., 2003; Yoon et al., 2018). 이렇게 생성되는 고밀도의 표층 저온고염수는 대륙붕에서부터 대륙사면을 따라 연결되어 심층 해수를 생성하고 일본 분지 심해를 채우게 되며, 이 과정을 심층사면대류 (deep slope convection)로 부른다(Figure 1b) (Talley et al., 2003). 한편, 동해 북부 일본 분지 내 외양 해역에서는 겨울철에 강한 해상풍과 함께 혼합층이 깊게 발달하며 심층외양대류(open-ocean deep convection) 또는 중층대류(shallow or intermediate convection) 과정을 통해 다른 성격의 심층 해수를 생성한다(Figure I.1b) (Noh et al., 1999; Yoshikawa et al., 1999; Clayson and Luneva, 2004). 생성된 심층 해수는 해저 분지내에서, 그리고 다른 분지로 수송되는 과정에서 수평적으로는 동해 전체를 반시계 방향으로 회전하며 순환한다(Talley et al., 2003; Senjyu et al., 2005; Kim et al., 2022a).

기후변화에 따라 대양의 심층 순환과 해수 특성에 변화가 발생하고 있는 것과 유사하게 동해 심층 순환과 해수 특성에도 뚜렷한 변화가 나타나는 것으로 알려져 있다(Tanaka, 2014; Yoon et al., 2018). 특히, 동해는 전 세계적으로 가장 빠른 수준의 온난화가 진행 중(Belkin, 2009; Lindsey and Dahlman, 2020)일 정도로 기후변화에 매우 민감하게 반응하는 해역 중 하나이다. 변화하는 기후 조건에서 대양 심층 해수 특성과 순환이 어떻게 변화할 것인지 전망하기 위한 '대양 실험실(Laboratory of open ocean)'로서의 동해에 대한 여러 연구가 수행되었는데, 동해 심층 해수의 물리적 특성과 순환에 대한 연구들(Kim et al., 2002; Cui and Senjyu, 2010, 2012; Gamo, 2011; Tanaka, 2014; Yoon et al., 2018; Han et al., 2020, 2021; Kosugi et al., 2021; Jeong et al., 2022; Senjyu, 2022)은 대양에 비해 월등히 짧은 동해의 순환 시간 규모에 특히 주목했다. 선행 연구를 통해 추정된 동해 심층 순환의 시간 규모는 수백 년(Min and Warner, 2005; Postlethwaite et al., 2005; Han et al., 2021; Na et al., 2022)으로 비록 연구에 따라 이 순환 시간 규모를 추정한 방법과 추정 결과의 차이를 보이기는 하지만, 수천 년 이상의 순환 시간 규모를 가지는 대양에 비해 월등히 짧다는 점은 공통적으로 확인할 수 있는 사실이다. 이러한 점을 고려하면, 빠르게 온난화 중인 동해

의 심층 환경 변화는 미래의 대양 환경 변화를 전망함에 있어 매우 중요한 시사점을 제공한다.

따라서 이 논문에서는 기후변화와 함께 나타나고 있는 동해 심층 해수의 물리적 특성과 순환 변화에 대한 그간의 연구 결과를 요약하고 향후 연구 전망을 제시하고자 한다. 이 논문에서 '심층'이란 1990년대 동해 전역 관측을 통해 최초로 명명된 (동해)중앙수(East Sea Central Water; CW), (동해)심층수(East Sea Deep Water; DW), 그리고 (동해)저층수(East Sea Bottom Water; BW)의 정의를 따르며 CW 상부경계 수심(약 400 m) 하부의 해수를 통칭하는 의미로 사용했다(Kim et al., 2004). 2장에서는 동해 심층 해수의 물리적 특성과 변화에 대한 연구 결과를, 3장에서는 동해 심층 순환과 자오면 순환의 변화에 대한 연구 결과를 정리하고, 4장에서는 전체 요약과 향후 연구 전망을 기술했다.

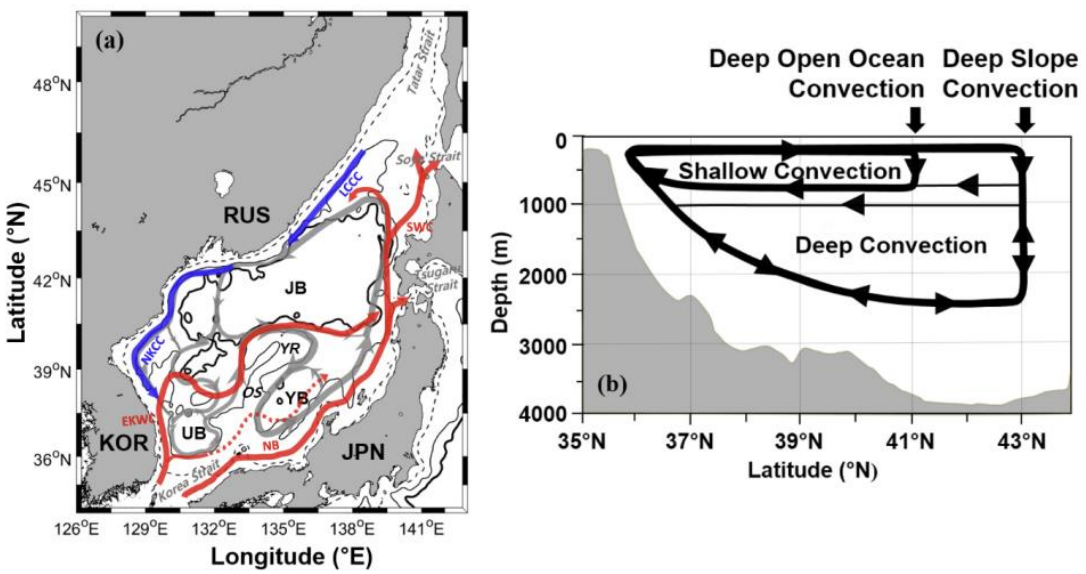

Figure I.1. Schematic of (a) upper ocean circulation (red and blue arrows), dee p and abyssal circulation (gray arrows), and (b) meridional overturning circulati on (MOC) in the East Sea. In (a), most widely recognized currents and geogra phical features are highlighted. Isobaths are indicated by thick solid (3000 m), thin solid (1500 m), and thin broken (150 m) lines. KOR, RUS, and JPN indic ate Korea, Russia, and Japan, respectively. JB, UB, YB, YR, and OS indicate t he Japan Basin, Ulleung Basin, Yamato Basin, Yamato Rise, and Oki Spur, res pectively. Surface warm and cold currents are marked by red and blue arrows,

respectively: LCCC, NKCC, EKWC, NB, and SWC indicate Liman Coastal Co ol Current, North Korea Cold Current, East Korea Warm Current, Nearshore B ranch, and Soya Warm Current, respectively. Two modes of MOC where thick and thin arrows indicate circulation cells with strong and weak flows, respectiv ely: (b) double cells with shallow convection (open-ocean convection) vs single cell with deep convection (deep slope convection). Note that the upper cell sti ll exists even when the deep slope convection is active although the mid-depth equatorward flow becomes weak and abyssal poleward flow reverses to equator ward. Here, (a) and (b) are modified from original figures in Senjyu et al.(200 5) and Han et al.(2020), respectively.

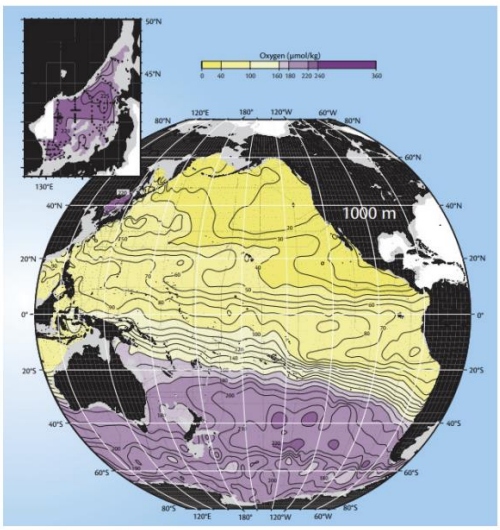

Figure I.2. Oxygen concentrations (μmol/kg) at 1000 m in the Pacific Ocean an d East Sea (upper-left inset with higher horizontal resolution). High oxygen (pu rple) indicates more recent ventilation (surface water penetration). The East Sea exhibits ventilation at depth that is much higher than elsewhere in the Pacific, including the Southern Ocean. This map represents the specialty of the deep (~ 3500 m) East Sea. Data are from the World Ocean Circulation Experiment, the National Oceanographic Data Center, summer 1999 surveys from the R/V Reve lle and R/V Professor Khromov in the East Sea, and a 2000 dataset from the Okhotsk Sea. Modified from Talley et al.(2006).

2. 동해 심층 해수의 물리적 특성과 변화

2.1 동해 심층 해수의 물리적 특성

동해 심층 해수의 물리적 특성은 1932년 일본 학자들에 의해 수행된 동해 전역 관측 결과로부터 정의되었고(Kim and Yi, 2017), 이후 1990년대

이전까지 서로 다른 기준으로 구분되었다. 1932년 동해 내 3개 분지를 포함하는 전역에서 수집한 관측 자료를 분석하여 Uda(1934)에서는 수심 수백 m 아래에 분포하는 잠재수온(온위, potential temperature) 0–1℃, 염분 34.0 –34.1 범위의 매우 균질한 해수를 일본해고유수(Japan Sea Proper Water)로 명명했다(이후 동해고유수; East Sea Proper Water로도 명명). 이렇게 정의된 일본해고유수는 1990년대 이전까지 오랜 기간 동안 동해 심층 해수가 단일 해수로 구성되어 있다는 패러다임을 뒷받침하는 핵심 근거로 사용되어 왔다(Kim and Yi, 2017). 그러나 일본해고유수는 1990년대 이전까지 연구자에 따라 서로 다른 기준으로 세분되었는데, 수온의 연직 기울기(Nitani, 1972), 용존산소 농도와 성층 정도(Sudo, 1986; Senjyu and Sudo, 1993, 1994), 수온, 용존산소, 그리고 규소의 불연속면(Gamo and Horibe, 1983) 등에 따라 심층수 (Deep Water), 상부 저층수(Upper Bottom Water), 하부 저층수(Lower Bottom Water)로 구분하거나(Nitani, 1972), 상부 고 유수(Upper portion of the Proper Water) (Sudo, 1986; Senjyu and Sudo, 1993, 1994) 및 심층수(Deep Water)와 저층수(Bottom Water) (Gamo and Horibe, 1983)로 구분되기도 했다.

동해 심층 해수의 수온과 염분을 정밀하게 측정할 수 있는 장비(SBE-9, Yoon et al., 2018)와 용존산소 농도를 보다 정확하게 측정하는 방법(Pai et al., 1993)이 1990년대부터 본격적으로 활용되면서 동해 심층 해수의 물리적 특성이 구체화됨에 따라 일본해고유수라는 단일 해수 패러다임은 중앙수(CW), 심층수(DW), 저층수(BW)의 3개 해수 패러다임으로 발전했다. 특히, 동해 심층 해수의 특성과 순환 경로를 밝히기 위해 1993년부터 1999년까지 동해 전역에서 수행된 동아시아 연해순환연구(Circulation Research of the East Asian Marginal Seas; CREAMS) 관측 프로그램을 통해 기존에 알려지지 않았던 동해 심층 해수의 정밀한 물리적 특성과 세밀한 구조가 최초로 발견되었다. 대양 심층 해수에 비해 동해 심층 해수의 수온은 월등히 낮고 용존산소 농도는 3-4배가 높으며, 해수 특성의 연직 변화폭이 매우 작지만, 그럼에도 불구하고 대양 심층에서와 유사한 연직 변화(수층 내에서 최대 및 최소를 보이는 구조)가 존재함이 알려졌다

(Kim and Kim, 1996; Kim et al., 1996). 예를 들면, 수심 약 1500 m 부근의 염분 최소로부터 알 수 있는 심해염분최소층(Deep Salinity Minimum), 수심 약 2000 m 부근의 용존산소 최소로부터 알 수 있는 심해용존산소최소층(Deep Oxygen Minimum), 그리고 수심 약 2500 m 아래에서 수온, 염분, 그리고 용존산소 농도가 매우 일정한 균질층이 존재한다(Figure I.3) (Kim et al., 1996; Kim et al., 2004). 대양에 비해 매우 작은 변화폭이므로 정밀한 측정이 불가능했던 1990년대 이전에는 확인할 수 없었지만, 수심 1500 m 부근의 심해염분최소층과 수심 2500 m 부근을 기준으로 동해 심층 해수를 CW, DW, 그리고 BW의 3개 해수로 구분한 결과, CW는 수심 400–1500 m에서 잠재수온 0.12–0.60℃ 범위와 염분 34.067 이상, DW는 수심 1500–2500 m에서 잠재수온 0.12℃ 미만과 염분 34.067– 34.070 범위, 그리고 BW는 수심 2500 m 아래 해저면까지 분포하며 잠재수온 0.073℃ 미만과 염분 34.070 내외의 물리적 특성을 갖는 해수로 정의할 수 있었다(Kim et al., 2004). 대양의 심층 해수에서도 종종 발견되는 심해용존산소최소층이 DW 내에서 발견되므로 DW가 동해 심층 해수 중 생성된 지 가장 오래된 해수라고 볼 수 있다(Kim et al., 2001; Yoon et al., 2018).

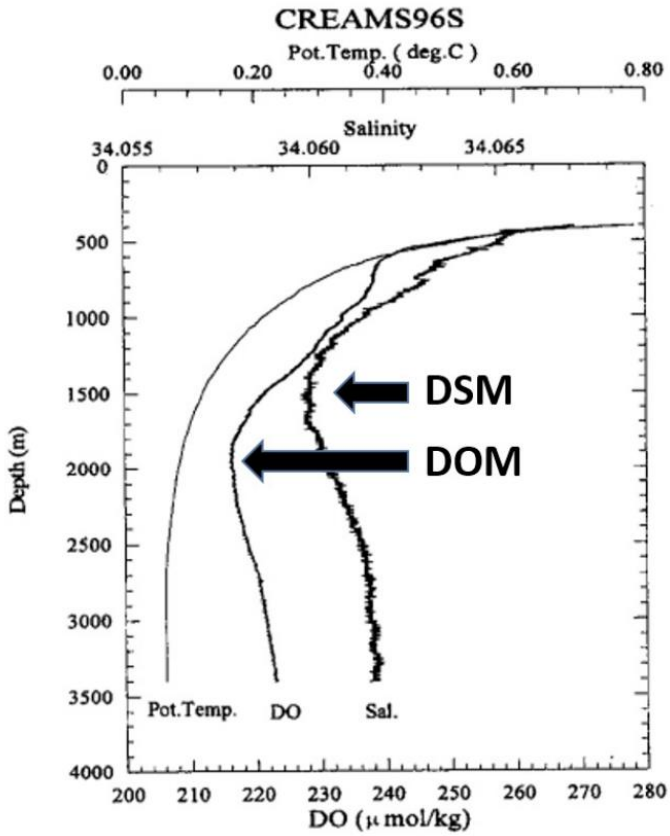

Figure I.3. Vertical profiles of potential temperature, practical salinity, and diss olved oxygen concentration at a station in the western Japan Basin during the summer of 1996. DSM and DOM denote the deep salinity minimum and dissol ved oxygen minimum, respectively. Modified from Kim and Kim(1996).

2.2 물리적 특성의 변화

동해 심층 해수(CW, DW, BW)의 물리적 특성은 서로 다른 심층 해수 생성 기작(심층사면대류 및 심층외양대류)과 생성 과정에 따라 유의한 변화를 겪은 것으로 해석된다. 심층사면대류는 동해 북부 해역에서 냉각과 함께 해빙 형성 시 염분방출 과정에서 발생하며, 북서부에 위치한 표트르 대제만(Peter the Great Bay) 등 수심이 얕은 대륙붕 해역에서 밀도가 증가한 저온고염 특성의 표층 해수가 대륙사면을 따라 수심 2000 m 이상 침강하여 BW를 생성하므로 BW가 위치하는 수심 2500 m 아래에서 수온을 낮게, 염분과 용존산소 농도는 비교적 높게 유지할 수 있다(Figure I.4)

(Kim et al., 2002; Senjyu et al., 2002; Talley et al., 2003; Tanaka, 2014; Kim et al., 2022a). 한편, 심층외양대류(또는 중층대류)는 수심이 깊은 일본 분지 내 외양 해역에서 발생하는데, 겨울철 강한 해표면 냉각 작용에 따라 대류가 강화하고 혼합층이 깊어지며, 전선 부근에서는 섭입과 침강도 발생하기 때문에 CW 생성이 활발하게 나타난다(Marshall and Schott, 1999; Clayson and Luneva, 2004). 수온이 낮고 염분과 용존산소 농도가 높은 해수가 심해염분최소층 상부에 새로 공급되면서 해당 수심의 심층 해수(CW) 수온이 감소하고 염분과 용존산소 농도가 증가한다(Figure I.4) (Talley et al., 2003). 대륙붕 해역 내 해표면 냉각과 염분방출이 충분하지 않아 BW 생성이 활발하지 않았던 반면, 심층외양대류 방식의 CW 생성은 활발했던 1990년대 중반에는, 용존산소 농도가 심해염분최소층 상부에서는 증가하고, 하부에서는 감소하는 독특한 연직 구조의 변화를 보였다(Kim et al., 1996; Gamo et al., 2001). 동해에서 전반적인 심층사면대류의 약화는 1965년부터 1995년까지 야마토 분지의 DW와 BW 수심 범위에서 염분과 용존산소 농도를 지속적으로 감소시켰고(Kwon et al., 2004), 그 결과 심해용존산소최소층 수심은 1960년대 후반 1000 m 이내에서 1990년대 중반 약 2000 m로 약 1000 m 이상 더 깊어지게 되었다(Gamo et al., 1986; Kim and Kim, 1996; Kim et al., 2004). 그러나 2000년대부터는 다시 심층사면대류가 재활성되면서 CW 생성보다 BW 생성이 우세해지고, 그 결과 심해염분최소층 하부에서보다 상부에서 더 큰 폭으로 용존산소 농도가 감소했다(Figures I.4a, I.5b, and I.5c) (Senjyu et al., 2002; Talley et al., 2003; Yoon et al., 2018).

심층사면대류는 1932년부터 줄곧 우세한 BW 생성 기작으로 작용했을 것이라 추정되지만, 해표면에서부터 심층 해수에 이르기까지 전반적인 동해 내 해수의 수온 상승과 함께 그 생성 과정은 뚜렷한 변화를 겪고 있는 것으로 해석된다. 1950년부 터 1990년대 중반까지 심층사면대류를 통한 BW 생성은 지속적으로 약화되어 왔고, 심층외양대류를 통한 CW 생성은 상대적으로 강화되어 왔다. 이에 따라 수심 3000 m에서의 용존산소 농도는 지속적으로 감소하였고, 이 감소 추세로부터 동해 심층의 용

존산소는 180–530년 혹은 300년 이내에 완전히 고갈되어 동해 심층이 무산소 환경으로 변화될 것이라는 전망이 제시되기도 했다(Chen et al., 1999; Gamo, 1999; Minami et al., 1999). 그러나 이동경계상자모델(Moving Boundary Box Model)을 이용하여, 1980년대 중반과 1990년대 후반 사이에 동해 심층 해수의 주요 생성 방식이 심층사면대류에서 심층외양대류로 변화하며 감소한 BW만큼 CW가 더 많이 생성되어 대체할 뿐, 심층 해수 생성을 통한 심층으로의 산소 공급은 멈추지 않고 지속되어 2040년경 BW는 완전히 사라지지만 CW와 DW로 대체되며 동해 심층이 무산소 환경으로 변하지는 않을 것이라 새롭게 전망되었다(Kang et al., 2003, 2004). 그러나 동해 심층 해수의 생성 방식은 2000/2001년 겨울 심층사면대류를 통한 BW 생성이 재활성하면서 다시 변화를 겪게 된다(Figure I.4a) (Kim et al., 2002; Senjyu et al., 2002; Talley et al., 2003; Tanaka, 2014; Kim et al., 2022a). BW 생성이 재개되면서 동일본 분지에서 BW 용존산소의 감소률은 1977–1999년 기간 0.76 μmol/kg/yr에서 1996–2015년 기간 0.38 μmol/kg/yr로 50% 둔화되었고, 과거부터 뚜렷하게 깊어지는 경향을 보였던 BW 상부의 DW-BW 경계 수심은 최근(1995–2015년) 거의 일정하게 유지되고 있음이 새롭게 확인되었다(Figure I.5) (Yoon et al., 2018). 따라서 선행 연구들을 통해 제시된 동해 심층의 무산소 환경 전망과 BW의 소멸(다른 심층 해수로 대체) 전망은 더 이상 유효하지 않으며, 2060년까지도 대양에 비해 높은 용존산소 농도를 유지하며 BW가 존재할 것으로 전망할 수 있다.

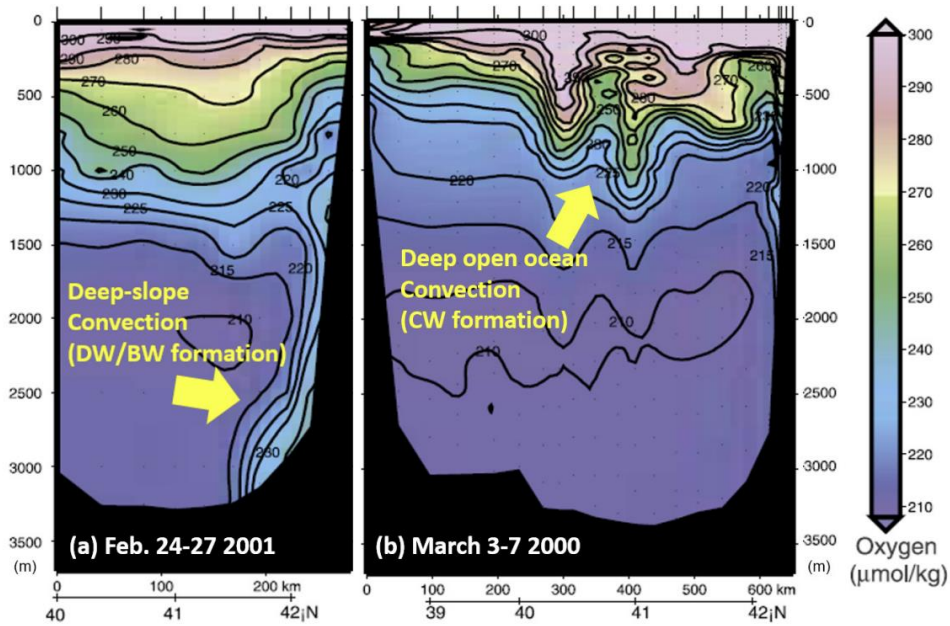

Figure I.4. Cross-section of dissolved oxygen (DO) concentrations (µmol/kg) al ong 131.30°E during (a) February 24–27, 2001 (deep slope convection occurre d) and (b) March 3–7, 2000 (open-ocean deep convection dominant). Deep slo pe convection occurred along the continental slope north of 41.5°N, resulting i n deep water (DW) and bottom water (BW) formation, whereas open-ocean de ep convection occurred south of Vladivostok, resulting in central water (CW) f ormation. Modified from Talley et al.(2003).

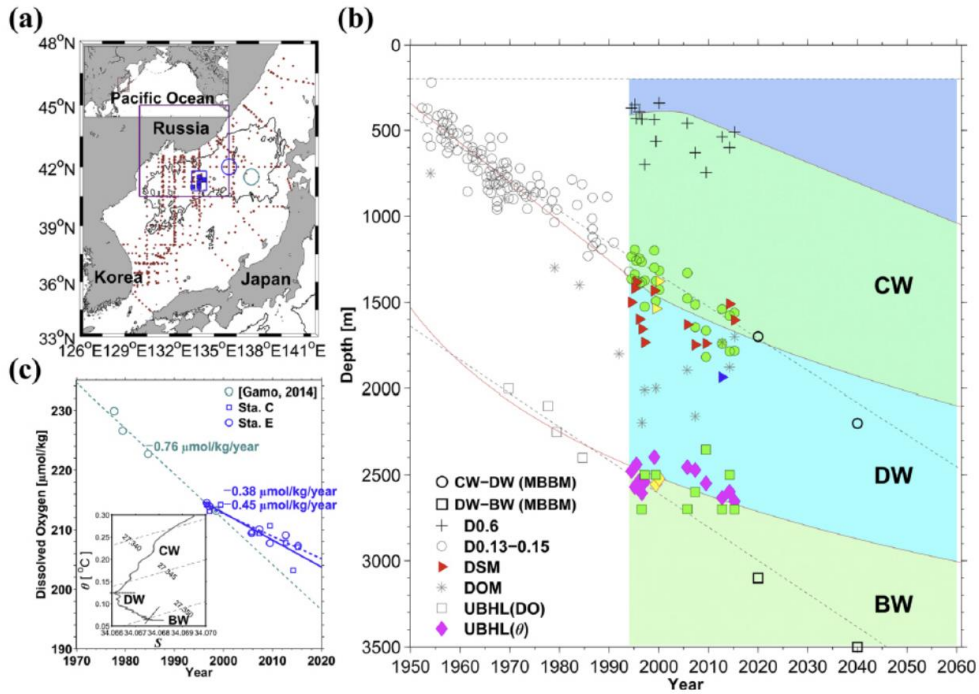

Figure I.5. Deep structural changes in the East Sea (Japan Sea). (a) Locations o f the East Sea (brown box in upper-left panel) and hydrographic stations where data were collected during research cruises (brown dots). The Japan Basin (JB) is deeper than 3,000 m (thick black contour), and data collected in the central JB (centered around 41.3°N, 134°E, blue squares) were mainly used. (b) Time series of the boundaries between central water (CW) and deep water (DW) ma sses defined by 0.13–0.15℃ isotherms (open and filled green circles) or deep s alinity minimum (DSM, red triangles), and between the DW and bottom water (BW) masses by upper limit of the benthic homogeneous layer (UBHL, derive d from potential temperature: magenta diamonds or dissolved oxygen: open and filled green squares), and depth of dissolved oxygen minimum (DOM, gray ast erisk) for 67 years (1950–2016). Isotherms of 0.6℃ used for the upper CW bo undary are shown with crosses. Data collected in 1999, 2000, and 2001 using different conductivity-temperature-depth (CTD) instruments are shown with yell ow triangles and diamonds. The DSM observed in 2012 is denoted by a blue t riangle. Three black dashed lines denote the upper CW boundary fixed at 200 m, and linear fits to the observed CW–DW and DW–BW boundaries from top to bottom, which were previously reported using data from 1950 to 1996 (not shaded). Red solid lines indicate new fits to the updated boundaries. (c) Time series of BW DO observed from 1977 to 2015 in the eastern JB (green open c ircles in Figure I.5a) at Stations C (blue squares in Figure I.5a) and E (blue ci rcles in Figure I.5a). Green dashed line indicates the linear declining BW DO i n the eastern JB between 1970 and 2020, which was obtained using data colle cted from 1977 to 1999. Blue dashed (solid) line indicates the same linear tren

d between 1996 and 2020, but using data collected from Station E (Station C) from 1996 to 2015. A potential temperature–salinity diagram of data collected from Station C in June 1999 is shown in the bottom-left inset. Modified from Yoon et al.(2018).

3. 동해 심층 순환과 자오면 순환

3.1 심층 순환

동해 북서부 대륙붕 해역과 북부 외양 해역에서 생성된 심층 해수는 일본 분지에서부터 울릉 분지, 야마토 분지를 차례대로 거쳐 다시 일본 분지로 복귀하는 경로로 심층에서 동해 전체를 반시계 방향으로 순환한다(Senjyu et al., 2005; Choi and Yoon, 2010). 이론적인 지형 효과에 따르면 북반구에서는 심층 해수가 수심이 얕은 해역을 오른쪽에 두고 등수심선을 따라 수송되는 특징을 보인다. 선행 연구결과들을 통해 알려진 동해의 심층 순환은 이러한 이론적인 지형효과와 일관된 특징을 보인다. 동해 전체적으로나 동해의 3개 분지 각각 내에서도 대체로 반시계 방향의 순환이 우세하기 때문이다. 일본 분지에서 생성된 심층 해수가 반시계 방향으로 순환하며 남쪽으로 수송되는 과정에서 울릉도와 독도 사이의 울릉해저간극(Ulleung Interplain Gap) 서측 수로를 통과해 울릉 분지로 유입된다(Teague et al., 2005). 울릉 분지 내에서도 반시계 방향으로 순환 후 울릉해저간극 동측 수로를 통과해 울릉 분지로부터 유출되는데, 동일한 수송량이 서측 수로보다 동측 수로에서 더 좁은 폭으로 빠르게 통과한다(Chang et al., 2002). 그에 따라 울릉해저간극 서측 수로의 남향류에 비해 동측 수로의 북향류는 상대적으로 폭이 더 좁고 강하며 뚜렷하게 관측되기 때문에 이 북향류를 독도심층해류(Dokdo Abyssal Current)로 명명했다(Figure I.6) (Chang et al., 2009; Shin et al., 2020). 울릉 분지를 빠져나온 심층 해수는 수심이 얕은 오키 해산(Oki spur)과 야마토 해령(Yamato Rise)을 오른쪽으로 두고 시계 방향으로 회전 후 다시 남쪽으로 수송되어 야마토 분지로 유입된다. 야마토 분지 내에서도 반시계 방향으로 순환 후 야마토 분지 동부의 대륙사면을 따라 북상하여 야마토 분지로부터 유출되어 일본 분지로 유입된다(Senjyu et al., 2005).

그러나 계류 관측을 통해 파악된 심층 유속의 시간 평균은 수 cm/s로서 그 시간 변동폭 수십 cm/s에 비해 작으며, 동해 심층 순환도 항상 일정하게 유지되는 것이 아니라 심층 대류를 통한 심층 해수 생성 과정 등의 변화와 함께 유의한 수준의 변화를 겪는다. 동해 심층 해수 생성 과정은 동해 북서부 대륙붕 해역과 북부 외양 해역의 표층 해수 밀도 변화에 민감한 영향을 받으므로 표층 해수 밀도 변화를 좌우하는 아래 3가지 요인들과 관련하여 심층 순환의 변동을 해석할 수 있다.

1) 동해 북동부 해역에서 대마난류(Tsushima Warm Current)의 재순환(recirculation)과 관련된 북서부 해역으로의 열과 염 공급(Park, 2007; Han et al., 2020),

2) 동해 북부 해역에서 해양-대기 열 교환(냉각과 가열) 및 담수 교환(증발과 강수) (Noh et al., 1999; Yoon et al.,2018; Han et al., 2020; Kim et al., 2022a), 그리고

3) 타타르해협, 동해 북부 러시아 연안, 북서부 표트르 대제만 등에 형성되는 해빙과 염분방출 정도(Talley et al., 2003; Yoon et al., 2018)

동해를 4개의 구역으로 구분하여 단순화 한 상자 모델(Box Model)을 이용한 연구 결과는 동해로 유입되는 고온고염의 대마난류수 수송량이 증가할수록 북부 해역으로의 염분 공급이 증가함을 보였다(Park, 2007). 북부 해역으로의 고염수 수송량 증가는 냉각 및 증발에 의한 염분 증가와 함께 표층 해수 밀도 증가를 통한 심층사면대류 강화에 기여할 수 있다. 동해 북부 해역에서의 대마난류수 재순환은 해양-대기 사이의 열과 담수 교환뿐만 아니라 해상풍의 변화에 의해서도 조절되므로 상층 에 크만 수송(Ekman transport) 변화도 심층 순환 변화에 영향을 미칠 수 있다. 또, 현장 관측 자료를 통해 2000/2001년 겨울철에 심층사면대류를 통한 BW 생성이 활발함을 제시한 연구 결과는 표트르 대제만의 해빙 형성 시 염분 방출로 인한 표층 해수 밀도 증가로 해석되었다(Talley et al., 2003). 최근의 수치모델 연구 결과는 심층사면대류(최대 수심 2700 m 아래까지 영향을 미칠 수 있음)를 통해서만 BW가 생성될 수 있으며, 외양

중층대류(수심 700 m까지 영향을 미칠 수 있음) 과정을 통해 생성될 수 있는 심층 해수는 CW에 해당함을 보였다(Kim et al., 2022a). 따라서, 2000년대 이후 심층사면대류를 통한 BW 생성 과정의 재활성화는 동해 북부 해역의 해표면 냉각 증가, 강수량 대비 증발량의 증가, 북동부 해역에서 북풍 강화에 따른 서향의 에크만 수송량 증가, 북부 해역의 해빙 농도 감소율의 둔화 등이 복합적으로 작용한 결과로 해석할 수 있으며, 필연적으로 심층 순환의 변화를 야기했다고 볼 수 있다(Yoon et al., 2018; Han et al., 2020).

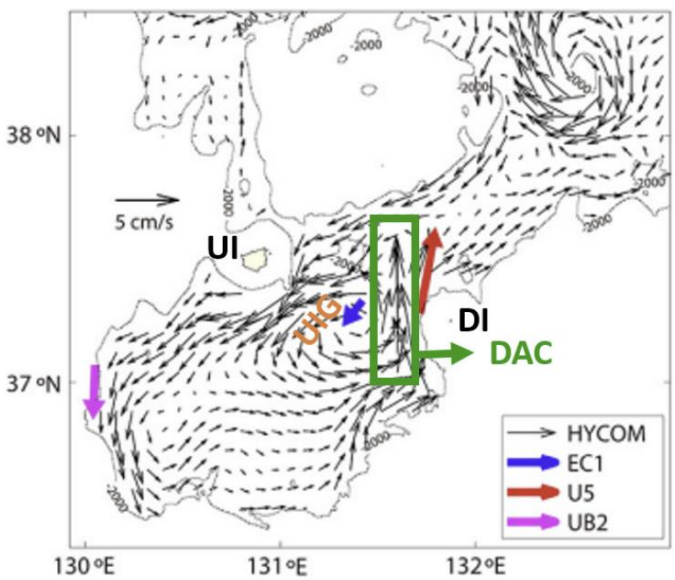

Figure I.6. Mean velocity field obtained using Hybrid Coordinate Ocean Model re-analysis data and mooring observational data collected at sites EC1, U5, and UB2 (blue, red, and purple arrows, respectively). UIG, DAC, UI, and DI denote the Ulleung Inter-plain Gap, Dokdo Abyssal Current, Ulleung Island, and Dokdo Island, respectively. Modified from Shin et al.(2020).

3.2 자오면 순환

대양과 유사한 특성으로 인해 '작은 대양'이라 불리는 동해의 자오면 순환(East Sea MOC, ESMOC)에 대한 연구는 비교적 최근까지도 잘 이루어지기 어려웠으나 최근 연구를 통해 2가지 형태의 ESMOC 순환 구조가 존재하는 것으로 알려졌다 (Han et al., 2020, 2021). 동해 심층에서 시공간

적으로 제한된 관측 자료를 수집하여 심층 해수의 물리적 특성이 장기간에 걸쳐 큰 폭으로 변화함이 밝혀졌고, 여러 관측 및 모델 연구를 통해 이러한 변화가 심층 해수 생성 과정의 변화와 밀접히 관련된 것으로 해석되고 있으나, 여기에 필연적으로 동반되는 ESMOC 순환 구조의 변화에 대해서는 오랜 기간 조사되지 못하였다. 동해 중층 및 심층의 순환 구조를 현실적으로 모의하기 위한 수치모델의 모의 능력 한계점과 함께 수집된 현장 관측 자료의 시공간적인 제약이 존재하기 때문이다. 그러나 수치모의 능력의 향상과 함께 자료동화 기술의 발달로 관측 결과와 일관된 동해 심층의 순환 구조를 나타내는 재분석장 자료들이 생산되며, 최근에는 현실성이 크게 개선된 ESMOC 순환 구조가 조사되고 있다. 최근 연구 결과는 심층사면대류와 심층외양대류의 상대적인 우세 정도에 따라 BW 생성이 우세하여 수심 2000 m 이상의 깊은 대류를 통해 북부 해역에서 생성된 심층 해수가 남부에서 용승하고 상층에서 북상하는 '단일 순환' 셀(cell) 구조와 CW 생성이 우세하여 수심 약 1000 m를 기준으로 상부와 하부에 각각의 순환 셀 구조를 가지는 '이중 순환' 형태의 2가지 ESMOC 순환 구조가 교대로 나타남을 밝혔다(Figures I.7a and I.7b) (Han et al., 2020, 2021; Kim et al., 2022a). 상부 순환 셀은 지속되나 심층사면대류가 우세한 경우 중층의 남향 수송이 약화하고, 심층의 북향 수송은 남향으로 그 방향이 바뀌어 하부 순환 셀의 변화와 함께 ESMOC 순환 구조를 바꾼다(Figures I.1b, I.7a, I.7b, I.7c, and I.7d). 여기서 순환 셀을 따라 흐르는 해수의 순환 주기는 대양 MOC에 비해 월등히 짧은 약 100년 내외로 추정된다(Han et al., 2020, 2021). 특히 수치모델 재분석장으로부터 추정된 중층 순환과 심층 순환 주기는 각각 8.68–45.44년과 26.41–37.28년, 최대 순환 주기가 58.59년으로 조사되어(Figures I.7c and I.7d), 관측된 심층 해수 내 화학적 추적자들(C-14, chlorofluorocarbon, tritium)의 농도 분포로부터 추정된 기존 선행 연구의 순환 주기 약 30–300년(Tsunogai et al., 1993; Kumamoto et al., 1998; Gamo et al., 2014)에 비해 더 짧을 가능성도 제기되었다(Han et al., 2021). 관련된 여러 후속 연구가 진행될 필요가 있다.

심층 해수의 순환 주기와 무관하게 ESMOC 순환 구조 자체가 단일 순

환과 이중 순환으로 변화하는 시간 규모는 약 10년 내외로 제시되었는데 (Han et al., 2020, 2021; Kim et al., 2022a), 앞에서 언급한 심층 해수 생성에 영향을 미치는 요인들의 변동과도 밀접한 관련이 있다. 특히, 2000년 전후로 나타난 중층 및 심층 순환의 유의한 변화에 주목하면, 심층사면대류를 통한 BW 생성 재활성은 2000년대에 우세했던 단일 순환 형태로의 ESMOC 구조 변화를 잘 설명하며, 심층사면대류 이후 비교적 강한(유속 8 cm/s 이상) 심층 해류가 3개월 이상 유지되며 ESMOC를 강화했던 가능성을 뒷받침한다(Figure I.7b) (Senjyu et al., 2002; Yoon et al., 2018; Han et al., 2020, 2021; Kim et al., 2022a). 이와 대조적으로 1990년대 후반과 2010년대 초반에는 심층외양대류를 통한 CW 생성이 심층사면대류를 통한 BW 생성보다 더 우세하며 이중 순환 형태의 ESMOC 구조를 보이고(Figure I.7a) (Han et al., 2020), 중층(수심 700 m)에서 연안을 따라 남하하는 북한 한류(North Korean Cold Current; NKCC)와 심층(수심 2000 m)에서 북상하는 울릉분지의 DAC 및 야마토 분지의 동야마토심층해류(Eastern Yamato Basin Abyssal Current; EYBAC)가 강화된 특징을 보였다(Figures I.7e, I.7f, I.7g, and 7h).

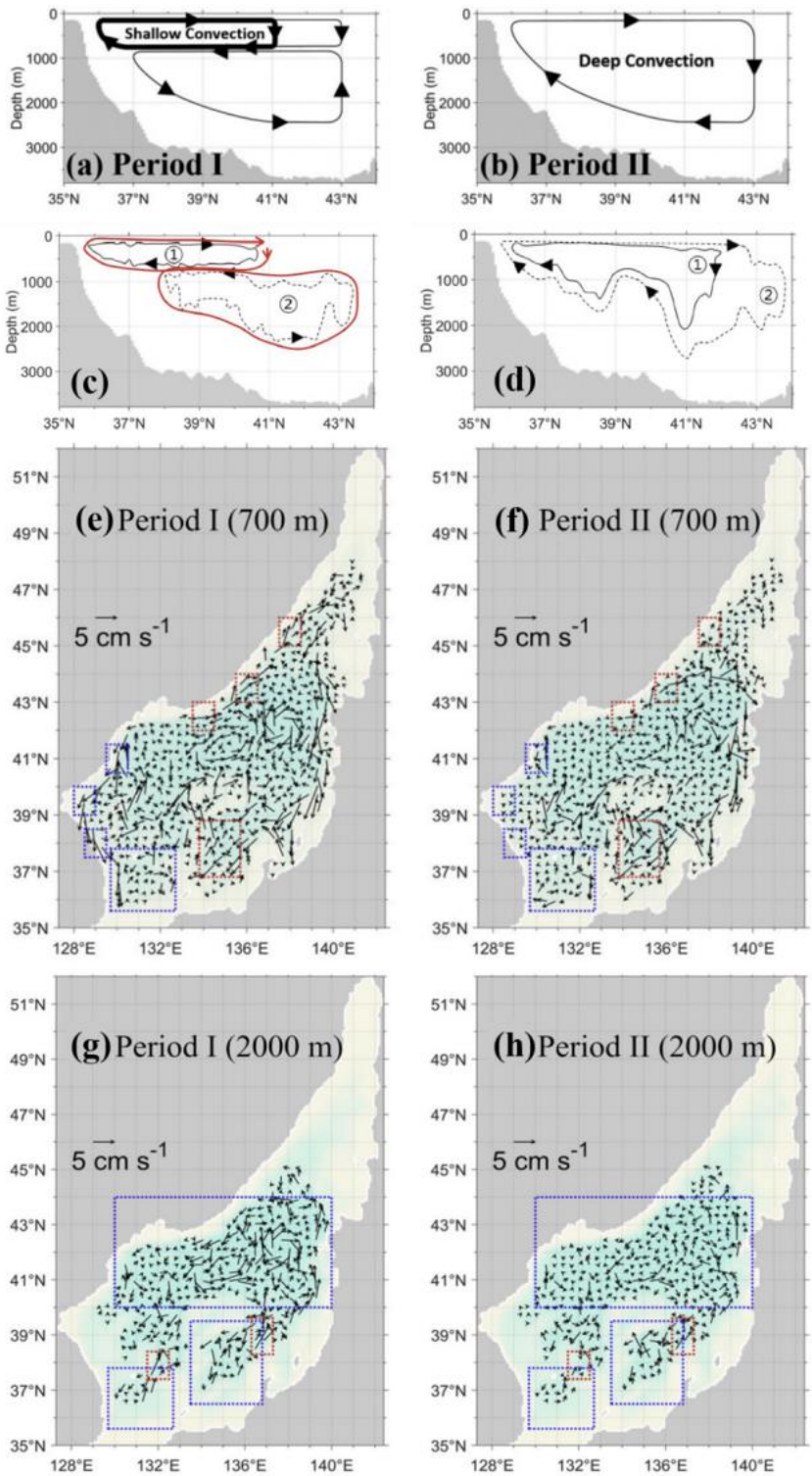

Figure I.7. Schematics of East Sea meridional overturning circulation in the (a) shallow convection period (Period I; dual cell years, late 1990s and early 2010 s) and (b) deep slope convection period (Period II; single cell years, 2000s). (c

) Streamlines of 0.2 Sv (①: solid line) and -0.3 Sv (②: dashed line) for the s hallow convection case of the MOC stream function. Turnover times are ① 8. 68 y, ② 36.76 y, and ①+② 45.44 y. (d) Streamlines of 0.3 Sv (①: solid line) and 0.13 Sv (②: dashed line) for the deep convection case of the meridional overturning stream function. Individual turnover times are ① 26.41 y and ② 3 7.28 y. Horizontal currents at (e, f) intermediate layer (700 m) and (g, h) deep abyssal layer (2000 m), averaged over (left) Period I and (right) Period II. In (e, f), three sequential small blue and red dotted boxes represent the boundary c urrent regions, and large blue and red boxes are UB and YB. Blue dotted boxe s represent JB, UB, and YB anticlockwise from the top, and small red boxes a re deep abyssal currents such as DAC (left box) and East Yamato Basin Abyss al Current (right box) in (g, h). (a, b) and (e-h) are modified from Han et al.(2 020), and (c, d) are modified from Han et al.(2021).

4. 요약 및 전망

동해 심층 해수는 북부 해역 심층사면대류 및 심층외양대류 과정을 통해 생성되며, 북부 해역의 해상풍과도 밀접히 관련된 대마난류 재순환, 해양-대기 열과 담수 교환, 해빙 형성에 따라 그 생성 과정과 분포 및 물리적 특성의 변화를 겪는다. 태평양 내에서 심층 해수 생성이 가장 활발한 반폐쇄성 해역인 동해의 심층에서는 잠재수온이 0–1℃, 염분이 34.0–34.1 로 매우 균질한 해수가 발견되므로 오랜 기간 이를 일본해고유수(동해고유수)로 명명해 왔으나, 1990년대 이후 정밀하고 세밀한 수 온, 염분, 용존산소 구조 측정이 가능해짐에 따라 그 내부에 심해염분최소층과 심해용존산소최소층이 존재하여 단일 해수로 구성되어 있지 않음이 밝혀졌다. 그러므로 동해 심층 해수는 심해염분최소층 상부에 위치하는 중앙수(CW), 심해염분최소층 하부에 위치하여 심해용존산소최소층을 포함하며 해저면 부근의 균질층 상부에 위치하는 심층수(DW), 그리고 심해용존산소최소층 하부에 위치하여 해저면 부근의 균질층에 해당하는 저층수(BW)로 명명된, 적어도 3개 이상의 서로 다른 해수들로 구성되어 있음이 알려졌다.

이들 3가지 심층 해수(CW, DW, BW) 사이의 경계 수심은 항상 일정한 것이 아니라, 지난 수십 년 동안 그 생성 및 순환 과정에 따라 유의한

수준의 변화를 겪었는데, 전 지구적인 온난화와 함께 1928년부터 2015년까지 관측된 심층 해수의 전반적인 잠재수온은 장기적으로 증가했으며, 염분과 용존산소는 장기적으로 감소했다. 그러나 1990년대 중반에는 심층사면대류가 약화하고 심층외양대류 과정이 강화하여 BW 생성보다 CW 생성이 우세한 변화가 관측자료로부터 확인되었으며, 2000/2001년 겨울에는 다시 심층사면대류가 재활성하며 CW 생성보다 BW 생성이 우세했음이 밝혀졌다. 특히 2000년대 이후 BW 생성의 재활성화는 동해 심층 장기 용존산소 감소율의 둔화(1977-1999년 기간에 비해 1995-2015년 기간 동안 약 50% 둔화)와 과거 장기간 깊어지고 있었던 BW 상부의 DW-BW 경계 수심이 최근(1995-2015년) 거의 일정하게 유지되는 특징을 잘 설명하여, 동해 심층이 무산소 환경으로 변화하거나 BW가 다른 해수로 대체되지는 않을 것으로 새롭게 전망 되었다.

동해 북부 해역에서 생성된 심층 해수는 이론적인 지형 효과로부터 예상할 수 있는 것처럼 수심이 얕은 해역을 오른쪽에 두고 등수심선을 따라 수송되며 반시계 방향으로 순환하기 때문에, 일본 분지에서부터 울릉 분지, 야마토 분지, 다시 일본 분 지로 차례대로 수송된다. 그러나 이러한 반시계 방향의 심층 순환, 남북 방향의 해수 수송량, 수평적인 해수의 수렴과 발산(용승과 침강을 동반), 그리고 동해의 자오면 순환은 항상 일정한 것이 아니라 시간에 따라 크게 변화할 수 있다. 특히 2000/2001년 겨울 동해 북서부 해역에서 심층사면대류를 통한 BW 생성이 활성화된 후 반시계 방향의 심층 순환이 강화되었을 가능성 이 현장 관측 연구 결과로부터 제기되었다. 1950년부터 2016년까지 관측된 심층 해수들(CW, DW, BW)의 경계 수심 변화도 1990년대에 약화되었던 심층 순환이 2000년대 이후 다시 강화되었을 가능성을 뒷받침한다. 동해 자오면 순환(ESMOC) 이 1990년대 후반 이중 순환 구조에서 2000년대 단일 순환 구조로, 그리고 2010년대 초반에 다시 이중 순환 구조로 약 10년의 시간 규모를 가지고 유의한 변동을 보임이 최근 수치모델 연구 결과로부터 밝혀졌고, 심층 해수의 순환 주기는 최대 58.59 년으로 화학적 추적자 등을 통해 기존에 추정된 수백 년 규모의 평균체류시간보다 짧을 가능성도 보

였다. 심층사면대류의 활성-재활성은 동해 북부 해역의 대마난류 재순환에 의한 고염수 수송량, 해양-대기 열 교환(냉각-가열)과 담수 교환(증발-강수)에 따른 해표면 밀도 변화, 해빙 형성 시 염분 방출 과정의 적어도 3가지 요인에 영향을 받는 것으로 해석된다.

동해 심층 해수의 물리적 특성과 순환에 대한 선행 연구들은 동해 심층 해수를 구성하는 주요 해수들(CW, DW, BW)의 물리적 특성, 심층 순환과 자오면 순환, 그리고 이들의 시간에 따른 변화를 주로 다루었다 (Figure I.8). 그러나 심층 해수의 물리적 특성 변화와 심층 및 자오면 순환 사이의 연계성, 대양으로부터 유입하고 대양으로 유출하는 상층 해수의 수송을 포함하는 상층 순환과의 연계성은 아직까지 상당 부분 밝혀지지 않았으며, 심화하는 기후위기 조건에서 심층 해수 수송의 경로와 강도 변화를 지배하는 상층 및 중층 순환과 해양-대기 상호작용 과정들에 대한 여러 후속 연구들이 요구된다. 향후 우선적으로 요구되는 후속 연구를 다음과 같이 제시하고자 한다.

1) 동해 북부 해역의 대류 과정(심층사면대류 vs 심층외양대류) 발생 조건과 해양-대기 상호작용 변동성

2) 대류 과정에 따른 심층 순환과 상층 및 중층 순환의 연계성

3) 동해 북부 해역의 대류 과정 변동에 따른 (a) 수층별(상층, 중층, 심층) 순환 강도와 경로 변동성, (b) 심층 해수(CW, DW, BW)의 물리적 특성과 분포 특성의 분지별(JB, UB, YB) 변동성, (c) 자오면 순환(ESMOC)의 구조와 강도 변동성

4) 동해 심층 순환과 자오면 순환 변동이 생지화학적 순환과 생태계에 미치는 영향

지속적인 전 지구적 온난화와 대양의 심층 해수 생성 조건 및 전 지구적 자오면 순환(MOC)의 변화와 유사하게 동해의 심층 해수 생성 조건 및 자오면 순환(ESMOC)도 여러 요인에 의해 지속적인 변화를 겪을 것으로 전망된다. 특히, 2000/2001년 겨울 심층사면대류에 따른 심층 해수 생성의 재활성과 심층 순환 강화는 향후 충분히 다시 발생할 가능성이

있다. 첫째, 해 양-대기 열 교환(가열vs냉각) 관점에서 동해 북부 해역의 러시아 블라디보스토크 겨울철 기온의 최근(1870-2000년) 증가 추세(Kim et al., 2002; Talley et al., 2003)와 해표면 수온의 최근(1982-2018년) 증가 추세(Lee and Park, 2019), 그리고 해상풍과 해표면 열속(heat flux) 장기 변화를 통해 동해 북부 해역의 대류 과정 발생 조건과 해양-대기 상호작용이 어떻게 변동할 지를 조사할 필요가 있겠다. 또, 중요한 대류 과정 발생 조건인 해표면 밀도는 해표면 수온뿐만 아니라 해표면 염분에도 민감하게 좌우되므로 해양-대기 담수 교환(증발vs강수) 관점에서 1990/2010년대보다 1980/2000년대에 강수 대비 더 활발한 증발을 통해 해표면 밀도를 증가시키는 변동성(Yoon et al., 2018)이 10년의 시간 규모로 지속적인 변동을 보일 지 여부 역시 중요 한 조사 대상이 되어야 하겠다. 둘째, 타타르해협에서 겨울철 해빙 생성은 온난화와 함께 1980-2015년 기간 동안 줄곧 감소 했고 그에 따른 염분 방출은 제한될 가능성이 높으나, 타타르해협에서의 해빙 생성에도 뚜렷한 변동을 보여 1980-1995년 기간에 비해 1995-2015년 기간에 더 활발히 해빙 생성이 이루어졌으므로(Yoon et al., 2018) 해빙 변동에 의한 해표면 염분 변화가 대류 과정 발생 조건에 얼마나 주효한 영향을 미치게 될 것인지에 대한 연구가 필요하다. 셋째, 동해로 유입하는 대마난류 수송량의 증가와 함께 대마난류 재순환을 통한 북부 해역으로의 염분 공급 또한 심층사면대류 발생 해역의 해표면 염분 조건을 결정하는 중요한 요소로 작용할 수 있어(Park, 2007), 이에 대한 후속 연구도 이루어질 필요가 있다.

향후 동해 자오면 순환의 지속적인 변화에 동반되어 동해 심층 해수의 물리적 특성 또한 지속적인 변화를 겪을 것으로 전망할 수 있는데, 특히 현재의 추세가 지속된다면 해표면 수온과 심층 해수의 잠재수온은 전반적으로 증가하고(Yoon et al., 2018; Lee and Park, 2019), 염분과 용존산소 농도는 감소할 것을 예상할 수 있다(Dickson et al., 2002; Kwon et al., 2004). 심층 해수의 전반적인 용존산소 농도는 BW 생성과 심층으로의 산소 공급이 제한되면서 유광층에서 생산된 유기물질의 침강에 따른 분해 과정으로 인해 지속 감소할 것으로 전망되지만(Kim et al., 2022b), 2000/2001년

겨울과 같이 심층사면대류가 재활성하면, 심층 해수의 용존산소 농도 감소 추세는 다시 둔화하거나 오히려 증가할 수도 있다. 이처럼 심층 해수의 물리적 특성 미래 변화 방향을 전망하기 어려운 가장 큰 요인은 동해 북부 해역의 대류 과정 발생 조건과 해양-대기 상호작용 변동성에 대한 불확실성이므로 위 1) 주제의 후속 연구가 보다 우선적으로 요구된다고 할 수 있다. 대류 과정에 따른 미래 심층 해수의 생성 변화를 전망할 수 있게 되면 심층 순환과 자오면 순환의 변화가 동반될 것이며 위 2), 3) 주제들의 후속 연구를 통해 조사가 이루어질 수 있다. 마지막으로 동해의 심층 순환과 자오면 순환 변동은 필연적으로 생지화학적 순환과 생태계 변화로 이어지기 때문에 위 4) 주제의 후속 연구를 통해 그 파급 효과를 이해할 필요가 있다.

이러한 후속 연구들을 진행하기 위해서는 새로운 현장 관측 자료와 원격탐사 자료의 수집은 물론 다양한 수치모델 실험도 요구된다. 동해 북부 해역에서 대류 과정 발생 해역의 물리적 특성과 발생 조건에 대한 지속적인 자료 수집이 필요하며, 심층 순환의 주요 경로에서 심층 해류와 심층 해수(CW, DW, BW)의 부피, 열, 염 수송량을 추정할 수 있는 자료도 수집할 필요가 있다. 특히 3개 분지를 연결하는 주요 길목(예: 울릉해저간극)에서 집중적인 현장 관측 자료 수집 노력이 중요하다. 시공간적으로 제한된 현장 관측 자료의 한계를 극복하기 위한 다양한 원격탐사 자료의 수집과 기법 개발은 물론, 동해 북부 대류 과정 발생 해역을 포함하는 주요 영역을 대상으로 하는 다양한 수치모델과 대류 과정의 난류 모수화 개선(Kim et al., 2022a) 및 해빙 접합 모델의 개발 필요성(Park et al., 2006)도 제기된다. 현장 관측, 원격탐사 관측, 수치모델이 가지는 한계를 극복하기 위한 다양한 인공지능 분석 방법의 적극적인 활용 또한 후속 연구에서는 충분히 고려할 필요가 있다.

Category	Reference
Hydrography (physical properties)	Gamo *et al*.(2014) Kim *et al*.(1996), (2004) Kim and Kim(1996) Talley *et al*.(2006) Uda(1934)
Changes of physical properties	Chen *et al*.(1999) Cui and Senjyu(2010) Gamo *et al*.(1986), (2014) Gamo(2011) Jeong *et al*.(2022) Kang *et al*.(2003), (2004) Kim *et al*.(2001), (2004), (2022b) Kim and Kim(1996) Kwon *et al*.(2004) Minami *et al*.(1999) Yoon *et al*.(2018)
Deep (abyssal) circulation	Chang *et al*.(2002), (2004), (2009) Cui and Senjyu(2012) Gamo *et al*.(2014) Kim *et al*.(2002), (2022a) Min and Warner(2005) Noh *et al*.(1999) Postlethwaite *et al*.(2005) Senjyu *et al*.(2005) Talley *et al*. (2003), (2006) Tanaka(2014) Teague *et al*.(2005) Yoon *et al*.(2018)
Meridional Overturning Circulation	Gamo *et al*.(2001) Han *et al*.(2020), (2021) Kang *et al*.(2003), (2004) Park(2007) Senjyu *et al*.(2002)

Figure I.8. Categorization of previous studies on the hydrography, deep (abyssal) circulation, and meridional overturning circulation in the East Sea (Japan Sea)

5. 참고문헌

- Belkin, I.M., 2009. Rapid warming of large marine ecosystems. Prog. Oceanogr., 81(1-4): 207-213.
- Bryden, H.L., H.R. Longworth and S.A. Cunningham, 2005. Slowing of the Atlantic meridional overturning circulation at 25°N. Nature, 438(7068): 655-657.
- Chang, K.I., K. Kim, Y.B. Kim, W.J. Teague, J.C. Lee and J.H. Lee, 2009. Deep flow and transport through the Ulleung Interplain Gap in the southwestern East/Japan Sea. Deep Sea Res. Part I Oceanogr. Res. Pap., 56(1): 61-72.
- Chang, K.I., N.G. Hogg, M.S. Suk, S.K. Byun, Y.G. Kim and K. Kim, 2002. Mean flow and variability in the southwestern East Sea. Deep Sea Res. Part I Oceanogr. Res. Pap., 49(12): 2261-2279.
- Chang, K.I., W.J. Teague, S.J. Lyu, H.T. Perkins, D.K. Lee, D.R. Watts, Y.B. Kim, D.A. Mitchell, C.M. Lee and K. Kim, 2004. Circulation and currents in the southwestern East/Japan Sea: Overview and review. Prog. Oceanogr., 61(2-4): 105-156.
- Chen, C.T.A., A.S. Bychkov, S.L. Wang and G.Y. Pavlova, 1999. An anoxic Sea of Japan by the year 2200?. Mar. Chem., 67(3-4): 249-265.
- Choi, Y.J. and J.H. Yoon, 2010. Structure and seasonal variability of the deep mean circulation of the East Sea (Sea of Japan). J. Oceanogr., 66(3): 349-361.
- Clayson, C.A. and M. Luneva, 2004. Deep convection in the Japan (East) Sea: A modeling perspective. Geophys. Res. Lett., 31(17).
- Cui, Y. and T. Senjyu, 2010. Interdecadal oscillations in the Japan Sea proper water related to the arctic oscillation. J. Oceanogr., 66(3): 337-348.
- Cui, Y. and T. Senjyu, 2012. Has the upper portion of the Japan Sea Proper Water formation really been enhancing?. J. Oceanogr., 68(4): 593-598.
- Dickson, B., I. Yashayaev, J. Meincke, B. Turrell, S. Dye and J. Holfort, 2002. Rapid freshening of the deep North Atlantic Ocean over the past four decades. Nature, 416(6883): 832-837.
- Gamo, T. and Y. Horibe, 1983. Abyssal circulation in the Japan Sea. J. Oceanogr. Soc. Jpn., 39(5): 220-230.
- Gamo, T., 1999. Global warming may have slowed down the deep conveyor belt of a marginal sea of the northwestern Pacific: Japan Sea. Geophys. Res. Lett., 26(20): 3137-3140.

- Gamo, T., 2011. Dissolved oxygen in the bottom water of the Sea of Japan as a sensitive alarm for global climate change. Trends Analyt Chem, 30(8): 1308-1319.
- Gamo, T., N. Momoshima and S. Tolmachyov, 2001. Recent upward shift of the deep convection system in the Japan Sea, as inferred from the geochemical tracers tritium, oxygen, and nutrients. Geophys. Res. Lett., 28(21): 4143-4146.
- Gamo, T., N. Nakayama, N. Takahata, Y. Sano, J. Zhang, E. Yamazaki, S. Taniyasu and N. Yamashita, 2014. The Sea of Japan and its unique chemistry revealed by time-series observations over the last 30 years. Monogr Environ Earth Planets, 2(1): 1-22.
- Gamo, T., Y. Nozaki, H. Sakai, T. Nakai and T. Tsubota, 1986. Spacial and temporal variations of water characteristics in the Japan Sea bottom water. J. Mar. Res., 44(4): 781-793.
- Han, M., Y.K. Cho, H.W. Kang and S. Nam, 2020. Decadal changes in meridional overturning circulation in the East Sea (Sea of Japan). J. Phys. Oceanogr., 50(6): 1773-1791.
- Han, M., Y.S. Chang, H.W. Kang, D.J. Kang and Y.S. Kim, 2021. Turnover time of the East Sea (Sea of Japan) meridional overturning circulation. Front. Mar. Sci., 8.
- Jamet, Q., W.K. Dewar, N. Wienders, B. Deremble, S. Close and T. Penduff, 2020. Locally and remotely forced subtropical AMOC variability: a matter of time scales. J. Clim., 33(12): 5155-5172.
- Jeong, Y., S. Nam, J.I. Kwon, U. Uppara and Y.H. Jo, 2022. Surface Warming Slowdown with Continued Subsurface Warming in the East Sea (Japan Sea) over Recent Decades (2000-2014). Front. Mar. Sci., 173.
- Kang, D.J., J.Y. Kim, T. Lee and K.R. Kim, 2004. Will the East/Japan Sea become an anoxic sea in the next century?. Mar. Chem., 91(1-4): 77-84.
- Kang, D.J., S. Park, Y.G. Kim, K. Kim and K.R. Kim, 2003. A moving-boundary box model (MBBM) for oceans in change: An application to the East/Japan Sea. Geophys. Res. Lett., 30(6).
- Kim, B.-G., Y.-K. Cho and Y. Noh, 2022a. Deep convection along the continental slope in the East/Japan Sea: A large-eddy simulation study. Front. Mar. Sci., 9:824256.
- Kim, H., N. Hirose and K. Takayama, 2022b. Physical and Biological Factors Underlying Long-Term Decline of Dissolved Oxygen Concentration in the East/Japan Sea. Front. Mar. Sci., 9: 851598.

- Kim, K., K.R. Kim, D.H. Min, Y. Volkov, J.H. Yoon and M. Takematsu, 2001. Warming and structural changes in the East (Japan) Sea: a clue to future changes in global oceans?. Geophys. Res. Lett., 28(17): 3293-3296.
- Kim, K., K.R. Kim, Y.G. Kim, Y.K. Cho, D.J. Kang, M. Takematsu and Y. Volkov, 2004. Water masses and decadal variability in the East Sea (Sea of Japan). Prog. Oceanogr., 61(2-4): 157-174.
- Kim, K., K.R. Kim, Y.G. Kim, Y.K. Cho, J.Y. Chung, B.H. Choi, S.K. Byun, G.H. Hong, M. Takematsu, J.H. Yoon, Y. Volkov and M. Danchenkov, 1996. New findings from CREAMS observations: Water masses and eddies in the East Sea. J. Korean Soc. Oceanogr., 31(4): 155-163.
- Kim, K.R. and K. Kim, 1996. What is happening in the East Sea (Japan Sea)?: Recent chemical observations during CREAMS 93-96. J. Korean Soc. Oceanogr., 31(4): 164-172.
- Kim, K.R., G. Kim, K. Kim, V. Lobanov, V. Ponomarev and A. Salyuk, 2002. A sudden bottom-water formation during the severe winter 2000-2001: The case of the East/Japan Sea. Geophys. Res. Lett., 29(8): 75-1–75-4.
- Kim, Y.-B. and G.-T. Yi, 2017. Historical background and its scientific meaning of the Japanese hydrographic survey of the East Sea in 1932. J. Fis. Mar. Sci. Edu., 29(5): 1373-1383.
- Kosugi, N., N. Hirose, T. Toyoda and M. Ishii, 2021. Rapid freshening of Japan Sea Intermediate Water in the 2010s. J Oceanogr., 77(2): 269-281.
- Kumamoto, Y.I., M. Yoneda, Y. Shibata, H. Kume, A. Tanaka, T. Uehiro and K. Shitashima, 1998. Direct observation of the rapid turnover of the Japan Sea bottom water by means of AMS radiocarbon measurement. Geophys. Res. Lett., 25(5): 651-654.
- Kwon, Y.O., K. Kim, Y.G. Kim and K.R. Kim, 2004. Diagnosing long-term trends of the water mass properties in the East Sea (Sea of Japan). Geophys. Res. Lett., 31(20).
- Lee, E.Y. and K.A. Park, 2019. Change in the recent warming trend of sea surface temperature in the East Sea (Sea of Japan) over decades (1982–2018). Remote Sens., 11(22): 2613.
- Levin, L.A. and N. Le Bris, 2015. The deep ocean under climate change. Science, 350(6262): 766-768.

- Lindsey, R. and L. Dahlman, 2020. Climate Change: Ocean Heat Content. Climate. gov, August, 17.
- Marshall, J. and F. Schott, 1999. Open-ocean convection: Observations, theory, and models. Rev. Geophys, 37(1): 1-64.
- Min, D.H. and M.J. Warner, 2005. Basin-wide circulation and ventilation study in the East Sea (Sea of Japan) using chlorofluorocarbon tracers. Deep Sea Res. Part II Top. Stud. Oceanogr., 52(11-13): 1580-1616.
- Minami, H., Y. Kano and K. Ogawa, 1999. Long-term variations of potential temperature and dissolved oxygen of the Japan Sea Proper Water. J Oceanogr., 55(2): 197-205.
- Mooers, C.N., H. Kang, I. Bang and D.P. Snowden, 2006. JES CIRCULATION. Oceanography., 19(3): 86.
- Na, T., J. Hwang, S.Y. Kim, S. Jeong, T. Rho and T. Lee, 2022. Large increase in dissolved organic carbon in the East Sea (Japan Sea) from 1999 to 2019. Front. Mar. Sci., 108.
- Nitani, H., 1972. On the deep and bottom waters in the Japan Sea, in Research in Hydrography and Oceanography, edited by D. Shoji, pp. 151–201, Hydrogr. Dep. of Jpn. Mar. Safety Agency, Tokyo.
- Noh, Y., C.J. Jang and J.W. Kim, 1999. Large eddy simulation of open ocean deep convection with application to the deep water formation in the East Sea (Japan Sea). J. Oceanogr., 55(2): 347-367.
- Pai, S.C., G.C. Gong and K.K. Liu, 1993. Determination of dissolved oxygen in seawater by direct spectrophotometry of total iodine. Mar. Chem., 41(4): 343-351.
- Park, K.A., K. Kim, P.C. Cornillon and J.Y. Chung, 2006. Relationship between satellite-observed cold water along the Primorye coast and sea ice in the East Sea (the Sea of Japan). Geophys. Res. Lett., 33(10).
- Park, Y.G., 2007. The effects of Tsushima Warm Current on the interdecadal variability of the East/Japan Sea thermohaline circulation. Geophys. Res. Lett., 34(6). Postlethwaite, C.F., E.J. Rohling, W.J. Jenkins and C.F. Walker, 2005. A tracer study of ventilation in the Japan/East Sea. Deep Sea Res. Part II Top. Stud. Oceanogr., 52(11-13): 1684-1704.
- Send, U., M. Lankhorst and T. Kanzow, 2011. Observation of decadal change in the Atlantic meridional overturning circulation using 10 years of continuous

transport data. Geophys. Res. Lett., 38(24).
- Senjyu, T. and H. Sudo, 1993. Water characteristics and circulation of the upper portion of the Japan Sea Proper Water. J. Mar. Syst., 4(4): 349-362.
- Senjyu, T. and H. Sudo, 1994. The upper portion of the Japan Sea Proper Water; its source and circulation as deduced from isopycnal analysis. J. Oceanogr., 50(6): 663-690.
- Senjyu, T., 2022. Changes in Mid-Depth Water Mass Ventilation in the Japan Sea Deduced From Long-Term Spatiotemporal Variations of Warming Trends. Front. Mar. Sci.
- Senjyu, T., H.R. Shin, J.H. Yoon, Z. Nagano, H.S. An, S.K. Byun and C.K. Lee, 2005. Deep flow field in the Japan/East Sea as deduced from direct current measurements. Deep Sea Res. Part II Top. Stud. Oceanogr., 52(11-13): 1726-1741.
- Senjyu, T., T. Aramaki, S. Otosaka, O. Togawa, M. Danchenkov, E. Karasev and Y. Volkov, 2002. Renewal of the bottom water after the winter 2000-2001 may spin-up the thermohaline circulation in the Japan Sea. Geophys. Res. Lett., 29(7): 53-1–53-3.
- Shin, J., S. Noh and S. Nam, 2020. Intraseasonal abyssal current variability of bottom-trapped topographic Rossby waves in the Southwestern East Sea (Japan Sea). Front. Mar. Sci., 7: 579680.
- Srokosz, M., M. Baringer, H. Bryden, S. Cunningham, T. Delworth, S. Lozier, J. Marotzke and R. Sutton, 2012. Past, present, and future changes in the Atlantic meridional overturning circulation. Bull Am Meteorol Soc, 93(11): 1663-1676.
- Stouffer, R.J., J. Yin, J.M. Gregory, K.W. Dixon, M.J. Spelman, W. Hurlin, A.J. Weaver, M. Eby, G.M. Flato, H. Hasumi, A. Hu, J.H. Jungclaus, I.V. Kamenkovich, A. Levermann, M. Montoya, S. Murakami, S. Nawrath, A. Oka, W.R. Peltier, D.Y. Robitaille, A. Sokolov, G. Vettoretti and S.L. Weber, 2006. Investigating the causes of the response of the thermohaline circulation to past and future climate changes. J. Clim., 19(8): 1365-1387.
- Sudo, H., 1986. A note on the Japan Sea proper water. Prog. Oceanogr., 17(3-4): 313-336.
- Talley, L., D.H. Min, V. Lobanov, V. Luchin, V. Ponomarev, A. Salyuk, A. Shcherbina, P. Tishchenko and I. Zhabin, 2006. Japan/East Sea water masses and their relation to the sea’s circulation. Oceanography., 19(3): 32-49.

- Talley, L.D., V. Lobanov, V. Ponomarev, A. Salyuk, P. Tishchenko, I. Zhabin and S. Riser, 2003. Deep convection and brine rejection in the Japan Sea. Geophys. Res. Lett., 30(4).
- Tanaka, K., 2014. Formation of bottom water and its variability in the northwestern part of the Sea of Japan. J. Geophys. Res. Oceans, 119(3): 2081-2094.
- Teague, W.J., K.L. Tracey, D.R. Watts, J.W. Book, K.I. Chang, P.J. Hogan, D.A. Mitchell, M.S. Suk, M. Wimbush and J.H. Yoon, 2005. Observed deep circulation in the Ulleung Basin. Deep Sea Res. Part II Top. Stud. Oceanogr., 52(11-13): 1802-1826.
- Tsunogai, S., Y.W. Watanabe, K. Harada, S. Watanabe, S. Saito and M. Nakajima, 1993. Dynamics of the Japan Sea deep water studied with chemical and radiochemical tracers. In Elsevier oceanography series, Vol. 59, Elsevier, pp. 105-119.
- Uda, M., 1934. The results of simultaneous oceanographic investigations in the Japan Sea and its adjacent waters in May and June, 1932. J. Imp. Fish. Exp. Stn., 5: 57-190.
- Worthington, E.L., B.I. Moat, D.A. Smeed, J.V. Mecking, R. Marsh and G.D. McCarthy, 2021. A 30-year reconstruction of the Atlantic meridional overturning circulation shows no decline. Ocean Sci., 17(1): 285-299.
- Yoon, S.T., K.I. Chang, S. Nam, T. Rho, D.J. Kang, T. Lee, K.A. Park, V. Lobanov, D. Kaplunenko, P. Tishchenko and K.R. Kim, 2018. Re-initiation of bottom water formation in the East Sea (Japan Sea) in a warming world. Sci. Rep., 8(1): 1-10.
- Yoshikawa, Y., T. Awaji and K. Akitomo, 1999. Formation and circulation processes of intermediate water in the Japan Sea. J. Phys. Oceanogr., 29(8): 1701-1722.